University of Louisville

ThinkIR: The University of Louisville's Institutional Repository

Electronic Theses and Dissertations

12-2020

Evaluating the effects of PCBs in non-alcoholic fatty liver disease & diabetes and the role of AhR in regulating the hepatic proteome and lipid metabolism.

Jian Jin
University of Louisville

EVALUATING THE EFFECTS OF PCBS IN NON-ALCOHOLIC FATTY LIVER
DISEASE & DIABETES AND THE ROLE OF AHR IN REGULATING THE
HEPATIC PROTEOME AND LIPID METABOLISM

By

Jian Jin

M.D Wenzhou Medical University, 2006

A dissertation

Submitted to the Faculty of the

School of Medicine of the University of Louisville

In Partial Fulfillment of the Requirements

for the Degree of

Doctor of Philosophy in Pharmacology and Toxicology

Department of Pharmacology and Toxicology

University of Louisville

Louisville, KY

December 2020

EVALUATING THE EFFECTS OF PCBS IN NON-ALCOHOLIC FATTY LIVER
DISEASE & DIABETES AND THE ROLE OF AHR IN REGULATING THE
HEPATIC PROTEOME AND LIPID METABOLISM

By

Jian Jin

M.D Wenzhou Medical University, 2006

Dissertation Approved on

10-27-2020

By the following Dissertation Committee

_____
Matthew C. Cave, M.D.

_____
Daniel J. Conklin, Ph.D.

_____
Joshua L. Hood, M.D., Ph.D.

_____
Sriprakash Mokshagundam, M.D.

_____
Jonathan Freedman, Ph.D.

DEDICATION

This dissertation is dedicated to my wife and my boy

Dr. Hanyang Ye

And

Yexin Jin

who have supported me all the way.

ACKNOWLEDGEMENTS

First and foremost, I would like to express my sincere gratitude to my mentor, Dr. Matthew C. Cave, for his support, guidance, patience and encouragement in my research. I would like to thank Dr. Russ Prough for his continuous help and concern. I also feel so grateful to Dr. Banrida Wahlang for she has taught me the methodology to carry out the research and to present the research data as clearly as possible. They made this dissertation possible. My gratitude also goes to our lab manager, Kim Head, for all her support and advice in my research and our lab previous Ph.D. students, Dr. Josiah Hardesty and Dr. Hongxue Shi for their teaching on the methods for the experiments in my project over the years. Then, I want to give my special thanks to my committee members, Drs. Daniel J. Conklin, Joshua L. Hood, Sriprakash Mokshagundam, and Jonathan Freedman, for their comments and assistance in my dissertation.

Additionally, I am extending my heartfelt thanks to my family, including my wife, my son and my parents as well. They have always been my backup force. Lastly, I want to express my thanks to my friends and my colleagues, Monica Jin and Hayley Lu; we are from the same city and the same hospital. We have been supporting and encouraging each other in the last a few years.

ABSTRACT

EVALUATING THE EFFECTS OF PCBS IN NON-ALCOHOLIC FATTY LIVER
DISEASE & DIABETES AND THE ROLE OF AHR IN REGULATING THE
HEPATIC PROTEOME AND LIPID METABOLISM

Jian Jin

October 27, 2020

Polychlorinated biphenyls (PCBs) are persistent organic pollutants

associated with non-alcoholic fatty liver disease (NAFLD) and diabetes.

Based on their ability to activate the aryl hydrocarbon receptor (AhR), PCBs

are subdivided into two classes: dioxin-like (DL) and non- dioxin-like (NDL)

PCBs. This study not only evaluated the chronic effect of DL PCBs (PCB126),

NDL PCBs (Aroclor1260 mainly contains NDL), and the DL/NDL PCB mixture

(PCB126/Aroclor1260 mixture) on liver, but also explored the acute hepatic

effects of DL PCB and potential mechanisms in NAFLD and the role of AhR in

regulating hepatic proteome and lipid metabolism, and whether the process

independent of PCB exposure. Additionally, the acute effects of different

doses of Aroclor1260/PCB126 on pancreatic proteome in female mice model

were evaluated. HFD fed male C57BL/6J mice were treated with same

exposures above for 12 weeks; and chow diet fed male C57BL/6J and AhR$^{-/-}$

mice were exposed to PCB 126 (20 µg/kg) for 2 weeks. Besides, chow

diet fed female C57BL/6J mice were treatd with low dose and high dose Aroclor 1260/PCB 126 mixture for 2 weeks. Chronic exposure experiments revealed Aroclor1260 increased hepatic inflammation and promoted phosphoprotein signaling disruption; PCB126 altered cytoskeletal remodeling, metal homeostasis, and disruption of intermediary/xenobiotic metabolism. Aroclor1260+PCB126 exposure enriched multiple epigenetic processes. AhR$^{-/-}$ mice fed control diet had histological steatosis with higher levels of hepatic free fatty acids and triglycerides. AhR ablation upregulated lipogenic genes *(Cd36, Perilipin-2)* and downregulated lipolytic genes (*Pnpla3*). Pancreatic proteome in acute female mice showed transcription factors related to pancreas function were overconnected with low dose and high dose Aroclor 1260/PCB 126, including NEUROD5, HNF1-beta, HNF4-alpha, E2F1, FOXP3, HNF1-alpha. Processes associated with the insulin signal pathway were enriched by low dose or high dose Aroclor 1260/PCB126, including 'insulin-like growth factor receptor signaling pathway', 'receptor tyrosine kinase signaling pathway', 'signal transduction_insulin signaling. In summary, PCB exposures differentially regulated the hepatic proteome and the histologic severity of diet induced NAFLD. AhR plays a pivotal role in maintenance of lipid metabolism and energy homeostasis and suggested AhR regulated the hepatic proteome and lipid metabolism independent of PCB exposure. Aroclor1260+PCB126 exposure was overconnected transcription factors related to pancreas function and enriched receptor tyrosine kinase signaling pathways, including insulin signaling pathways.

TABLE OF CONTENTS

LIST OF FIGURES

LIST OF TABLES

CHAPTER 1

INTRODUCTION

Polychlorinated biphenyls (PCBs)

 Polychlorinated biphenyls (PCBs) are a group of persistent environmental toxicants that are detected in the serum of 100% American adults (1). PCB exposures are associated with fatty liver disease, diabetes, obesity and hypertension (1-6). PCBs are thermodynamically stable polyhalogenated aromatic hydrocarbons consisting of up to ten chlorine atoms attached to the biphenyl rings. The number of chlorine atoms and their location in the PCB molecule are associated with its physical and chemical properties (Fig, 1.1). PCBs were manufactured from 1929 until these chemicals were banned by the United States Congress in 1979 under the Toxic Substances Control Act (7) and globally by the Stockholm Convention in 2001 (8) due to a variety of toxicities such as causing fatty liver disease, diabetes, obesity, etc. (1-6). PCB congeners have been categorized into two major classes: coplanar and noncoplanar PCBs.

   Coplanar PCB congeners have none or only one chlorine atom attached to the ortho-position of biphenyl rings, called non-ortho and mono-ortho PCBs, respectively. There are 12 coplanar PCBs: PCB 77, PCB 81, PCB 126, and PCB 169 are non-ortho PCBs; and, PCB105, PCB156, PCB114,

PCB157, PCB118, PCB167, PCB123 and PCB189 are mono-ortho PCBs. Coplanar PCBs have dioxin-like toxicity, and they can activate the aryl hydrocarbon receptor (AhR), so they are also called dioxin-like (DL) PCBs. Non-coplanar PCB congeners have two or more chlorine atoms at the ortho-position of biphenyl rings, and do not have dioxin-like properties, thus, these are known as non-dioxin-like (NDL) PCBs.

Aroclor 1260 is a commercial mixture of PCBs containing an average of chlorine content of 60% -- it was manufactured by Monsanto, a well-known PCB manufacturer in Anniston, Alabama in North America. It consists of mainly pentachlorobiphenyls (43.35%) and hexa-chlorobiphenyls (38.54%) and also includes mono-, bi-, tri, tetra-, hexa-, octa- and nona-chlorinated homologs. Minimally chlorinated PCB congeners are easily metabolized and eliminated, and only PCB congeners with high-level chlorination are resistant to metabolism and have bioaccumulated in humans. The PCB profiles in Aroclor 1260 best mimic the PCBs present in human adipose tissue(2) (Fig. 1.2). However, Aroclor1260 contains lower amounts of DL-PCBs, which cannot activate murine and human AhR; PCB126 (20μg/kg) was added in my project to make the PCB mixture (Aroclor1260/PCB126) more environmentally relevant, making a significant contribution by effect, while a small contribution by mass.

PCBs interact with some xenobiotic receptors associated with non-alcoholic fatty liver disease (NAFLD). The receptors include AhR, constitutive androstane receptor (CAR), pregnane xenobiotic receptor (PXR), peroxisome

proliferator-activated receptors (PPARs), and liver-X-receptor(9, 10). AhR is a

transcription factor that regulates gene expression of phase I and phase II

xenobiotic metabolizing enzyme genes (such as the *CYP1A1* gene). AhR is

normally inactive and bound to several co-chaperones and can be activated

by several exogenous ligands such as natural plant flavonoids, polyphenolics

and indoles, but the majority of the identified high-affinity ligands are synthetic

chemicals, including synthetic polycyclic aromatic hydrocarbons and dioxin-

like compounds. Upon binding to ligands such as 2,3,7,8-tetrachlorodibenzo-

p-dioxin (TCDD) or DL-PCBs (PCB126, *etc.*), chaperones dissociate from the

cytosolic AhR complex leading to AhR translocating into the nucleus

and dimerizing with ARNT (AhR nuclear translocator), resulting in changes

in gene transcription. AhR activation regulates the transcription of many

genes, such as the cytochrome P4501A (CYP1A) family.

CAR is a member of the nuclear receptor superfamily and in human is

encoded by the *NR1I3* gene (11). Along with pregnane X receptor (PXR), it

functions as a sensor of xenobiotic substances, CAR regulates expression of

genes associated with all three phases of hepatic metabolism and transport

including phase I monooxygenation, phase II conjugation, and phase III

transporters that include multidrug resistance-associated proteins and organic

anion transporting polypeptides. CAR is expressed primarily in the liver and

intestinal enterocytes.

PXR, also known as the steroid and xenobiotic sensing nuclear receptor

(SXR) or nuclear receptor subfamily 1, group I, member 2 (NR1I2) is a nuclear

receptor that in humans is encoded by the *NR1I2* gene (12, 13). PXR is activated by many endogenous and exogenous chemicals including steroids (progesterone, 17α-hydroxyprogesterone, 17α-hydroxypregnenolone, etc.), antimycotics, bile acids, and many herbal and other compound (e.g., meclizine, paclitaxel) (14). PXR can sense the presence of toxic foreign substances and upregulate the expression of proteins involved in the detoxification and clearance of these substances from the body. Activation of PXR induces expression of target genes of the Cyp3a family, including Cyp3a11 in mice and Cyp3a4 in human. On the other hand, CAR target genes of the Cyp2b10 family, such as Cyp2b10 in mice and Cyp2b6 in human, are induced upon activation.

PCBs have been found in fatty tissues of animals and humans due to their hydrophobic nature and resistance towards metabolism. Several PCBs have been shown to have toxic effects like those caused by 2, 3, 7, 8-tetrachlorodibenzo-*p*-dioxin (TCDD), the most potent congener to activate AhR. To estimate the toxicity of PCBs to human, the World Health Organization (WHO) has set up toxic equivalency factors (TEFs) for AhR ligands (15). TCDD is assigned a TEF of 1 as the prototypical ligand. The TEFs of other chemicals are calculated based on relative effect potency (REP) values compared to that of TCDD. PCB 126, having highest AhR binding affinity of DL-PCBs, has the TEF 0.1 and is the major contributor to the total TEQ from PCBs.

There are two major PCB exposure events occurred in Japan (Yusho,

1968) and in Taiwan (Yucheng, 1979) due to rice oil contamination. The Yusho study showed that the standardized mortality ratios (SMRs) for all types of cancer (SMR = 1.26; 95% CI: 1.03–1.53) and lung cancer (SMR = 1.56; 95% CI: 1.03–2.27) were significantly increased among males, but not among females. Several follow-up studies of the Yucheng events (PCB poisoning) demonstrated increased mortality from chronic liver disease and cirrhosis in men (3, 16), increased rates of DM in females (4) and neurocognitive deficits in elderly women patients (17).

In The Anniston Community Health Survey (ACHS) and ACHS-II study supported by the Agency for Toxic Substances and Disease Registry (ATSDR), the association between PCB exposure and steatohepatitis was observed; a high prevalence of diabetes (27%) was also observed, which was almost 3-times higher than the US prevalence rate (9.3%), and higher blood pressure was observed in high-PCB exposure residents. Another epidemiological study, National Health and Nutrition Examination Survey (NHANES) in the US demonstrated that in NHANES 2003-2004 adult participants, PCBs were associated with unexplained ALT elevation, a proxy marker of NAFLD (18).

Non-alcoholic fatty liver disease

Non-alcoholic fatty liver disease (NAFLD) is the accumulation of excessive fat in liver cells that is not caused by alcohol. NAFLD includes a spectrum of fatty liver diseases, from hepatic steatosis to hepatic steatohepatitis (NASH), fibrosis, cirrhosis, and even hepatocellular carcinoma (HCC) (19). If more

than 5% – 10% of the liver's weight is fat, it is called steatosis, which reflects abnormal processes of synthesis and elimination of triglyceride fat. When steatosis progresses to become associated with inflammation, it is known as steatohepatitis, characterized by liver injury, inflammation, oxidative stress and fibrosis, and elevation in appearance of hepatic enzymes in serum (e.g., ALT, AST) and is seen clinically. In the spectrum of NAFLD, steatosis and steatohepatitis can be reversible, but when it advances to cirrhosis, the progress cannot be reversed and is linked to elevated risk of HCC.

Dramatic modifications in lifestyle in the past century have changed the disease profile in most areas of the world, owing to a growing incidence of noncommunicable disease especially NAFLD, diabetes, obesity, etc. The increased prevalence of NAFLD parallels the worldwide increase of obesity and type 2 diabetes and the estimated global prevalence of NAFLD is currently 24%(16). Different continents have different levels, and the highest rates are from South America (31%) and the Middle East (32%), followed by Asia (27%), the USA (24%) and Europe (23%), whereas is lowest in Africa (14%) (16). 70%-80% of obese and diabetic populations develop NAFLD, 5-10 % of individuals with steatosis progress to NASH, and 30 % of NASH patients develop cirrhosis. Unfortunately, 1-2 % of patients will progress to HCC within 10 years after developing cirrhosis (19).

NAFLD is also associated with increased morbidity and mortality of cardiovascular disease due to abnormal levels of blood lipids. Hypertriglyceridemia is the metabolic comorbidity most commonly associated

with NAFLD. For patients with end stage liver disease, there is no better treatment for end stage liver disease like cirrhosis than liver transplantation. NAFLD has been a heavy burden on public health worldwide. In the USA, estimated annual direct medical costs for NAFLD are about $103 billion (20). The predicament clinicians are facing is that there are still no FDA approved drugs for NAFLD/NASH treatment, and lifestyle modification through body weight loss and physical exercise, is the only way to improve NAFLD/NASH (21).

NAFLD is associated with the dysfunction of glucose and lipid metabolism in the liver and the loss of homeostasis of hepatic lipid metabolism plays an important role in its pathogenesis. The homeostasis of lipid metabolism includes lipid input and output in liver. On the input side, chylomicrons (CM) from dietary fat ingestion and free fatty acids derived mainly from lipolysis can be taken up by the liver via the blood stream. Lipids can be synthesized (*de novo*) from carbohydrates and other precursors. The key proteins involved in the absorption of fatty acid in liver include fatty acid transport proteins (FATPs), plasma membrane fatty acid binding protein (FABP) and fatty acid translocase (CD36/FAT), which are associated with hepatic steatosis (21-23). Three key enzymes (ATP-citrate lyase (Acly), acetyl-CoA carboxylase (ACC) and fatty acid synthase (Fasn)) and some transcription factors like liver X receptor (LXR), sterol regulatory element-binding protein-1c (SREBP-1c), and carbohydrate response element binding protein (ChREBP) regulate the *de novo* lipogenesis (24-26). As a result, free fatty acids are mainly converted

into triglycerides and are stored in hepatocytes. On the output side, lipids can either be transferred into lipoprotein (e.g., very-low-density-lipoprotein (VLDL)) and be secreted into the blood (26), or be utilized in mitochondria by β-oxidation to produce ATP (27). When the total lipid influx rate exceeds efflux rate, excessive lipid deposition arises, resulting in hepatic steatosis. Any factor that affect these steps of lipid metabolism may cause NAFLD.

There are "two-hit" and"multiple parallel hits"hypotheses used to explain the pathogenesis of NAFLD/NASH. One scenario is that fat accumulation, as the first hit, increases susceptibility to a subsequent second hit, which is responsible for liver injury, inflammation and hepatic steatosis. Exposures to occupational and environmental chemicals are the second hit. The toxicant-associated fatty liver disease (TAFLD) and/or toxicant-associated steatohepatitis (TASH) have been used to describe this condition (28). Because the similar histopathology exists between NAFLD/NASH and TAFLD/TASH, the distinction between these will not be considered here. In our previous acute PCB exposure study, different PCBs had different effects on liver and pancreas structure and function, which may be attributed to activation of different 'cross-talking' PCB receptors. PCB 126 phenotypically induced fatty liver disease and novel mechanisms for PCBs in fatty liver disease were identified, like the PNPLA3 gene: environment interaction in fatty liver disease (29).

Diabetes Mellitus (DM)

Diabetes has been a major and rising health concern in the US population and across the world. According to the National Diabetes Statistics Report (2020) of the Centers for Disease Control and Prevention (CDC), 34.2 million people or 10.5% of the US population have diabetes. In 2017, diabetes was the seventh leading cause of death in the United States and the total direct and indirect estimated costs of diagnosed diabetes in the United States in 2017 was $327 billion (30).

As EDCs/MDCs, PCBs increase susceptibility to diabetes. Multiple epidemiological studies and animal experiments have revealed associations between PCBs exposure and DM (31). The studies of Yucheng event showed higher prevalence rate of DM in high PCB exposed females and ACHS-I & II revealed almost 3-times higher morbidity of DM in PCB-exposed residents than the average prevalence in the states (4, 6). Our previous acute study showed the Aroclor 1260/PCB126 co-exposure caused pancreatic histopathology, including acinar cell atrophy, mild steatosis, and fibrosis without ductal changes or immune cell infiltration (29). Several novel mechanisms for PCBs in diabetes were identified, including hepatokines, PCB pancreatopathy and pancreatic islet identity factors in diabetes. Hepatokines, including FGF21, IGF1, and betatrophin, have been involved in the development of NAFLD, diabetes, and metabolic syndrome. FGF21 plays a critical role in regulating obesity, insulin resistance and NAFLD by increasing brown adipose levels and adiponectin secretion. The liver appears

to be both a target and effector organ for PCB-induced endocrine disruption (29).

Proteomics analysis

As a large-scale study analysis of proteins and proteomes, proteomics is able to identify numbers of produced or modified proteins and is widely used both in hepatology and environmental research. In proteomics, proteins generally are detected by using either antibodies (immunoassays) or mass spectrometry. The method of the latter needs to go through detection and separation steps using reverse-phase chromatography. Tandem mass tags (TMT) labeling protocol is a cost-effective and robust method for it reduces the quantity of required reagent and obtains complete labelling, showing its excellent reproducibility.

Overall goal and specific aims

Previously, studies on the effects of PCBs have been focused mostly on single PCB congeners or NDL-PCBs, and the acute study of different PCB exposures (including DL/NDL PCB mixture) effects on liver and pancreas has been completed (29). The chronic effects that the mixture of DL/NDL PCBs have on liver and/or pancreas require elucidation. The mechanisms that DL-PCBs and the mixture of DL/NDL PCBs utilize to induce toxicity remain to be elucidated. AhR overactivation was thought to be associated with DL-PCB-induced hepatotoxicity (32) and activation of AhR could induce hepatic steatosis via the upregulation of fatty acid transport (33). AhR gene deletion

was thought to be protective (34), but Ahr$^{-/-}$ mice (1-3 weeks) developed spontaneous extensive microvesicular lipidosis (35). Therefore, the complex role of the AhR in hepatic lipid metabolism warrants investigation. The overall goal of this dissertation is to evaluate the chronic effects of different PCBs exposure by phenotypes and untargeted proteomics and examine if AhR altered hepatic proteome and lipid metabolism depending on PCB exposure. The specific aims of the project are as follows:

Aim 1: Investigate the chronic exposure effects and potential mechanisms of DL-PCBs and NDL-PCBs, or co-exposures to both in a diet-induced obesity mouse model.

In recent years, review of the publications involved in PCB studies mostly focus on NDL-PCBs, but in real world, humans are exposed to DL-PCBs and NDL-PCBs simultaneously; another issue is whether the combination of DL- and NDL-PCB will cause a synergistic effect for different PCBs involves different mechanisms of action. The purpose of this chronic exposure study was to perform a phenotypic and proteomic analyses to evaluate the difference of chronic effects and potential mechanisms of different PCBs exposure in HFD obese mice.

Aim 2: Evaluate the role of AhR plays in the regulating hepatic proteome and whether this process is independent of PCB exposure or not in an AhR knockout mouse model.

11

From the results of our acute PCB exposure study, as a potent AhR agonist, DL-PCBs (e.g., PCB126) caused hepatic steatosis, while on the flip side, AhR activation also is involved in the processes of lipid metabolism and there appears to be an over-activation of AhR (33) inducing hepatic steatosis. The role that the AhR plays in regulating the hepatic proteome and lipid metabolism and whether these processes depend on PCB exposure needs to be further elucidated. The present study was performed with PCB126 and explored the acute effects in chow diet fed global Ahr$^{-/-}$ mice. Hepatic proteomics analysis was performed, and the results from proteomics were validated by phenotypic analysis and real-time PCR. Another purpose of the study was to explore whether the global AhR ablation will bring about beneficiary or deleterious effects on lipid accumulation.

Aim 3: Investigate the acute exposure effects and potential mechanisms of different doses of DL+NDL PCBs on pancreatic proteome in a female mouse model.

In our previous sex difference mice study (36), the co-exposure of Aroclor1260/PCB126 decreased INS1 gene expression in female mice, while increased pancreas weight/body weight ratio. Some epidemiological studies, like ACHS-I and II showed women with high PCB exposure had higher prevalence of diabetes than men (6). These results suggested that compared with individual PCB congeners, the Aroclor1260/PCB126 mixture were more relevant to diabetes. The female mouse appears to be a susceptible mouse

model. In Aim 3, we used two different doses of Aroclor1260/PCB126

(20mg/kg+20μg/kg and 100mg/kg+100μg/kg) in a female mouse model.
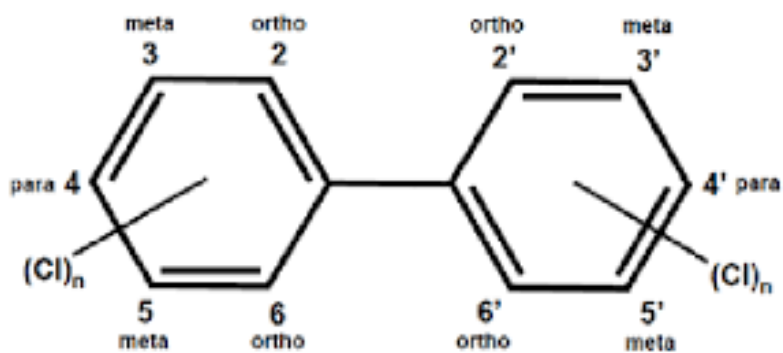
Figure 1.1. Chemical structure of PCBs.

PCBs have the basic chemical formula ($C_{12}H_{10-n}Cl_n$), where n means the number of chlorine atoms, and the number means the positions where a chlorine atom is attached to biphenyl rings.
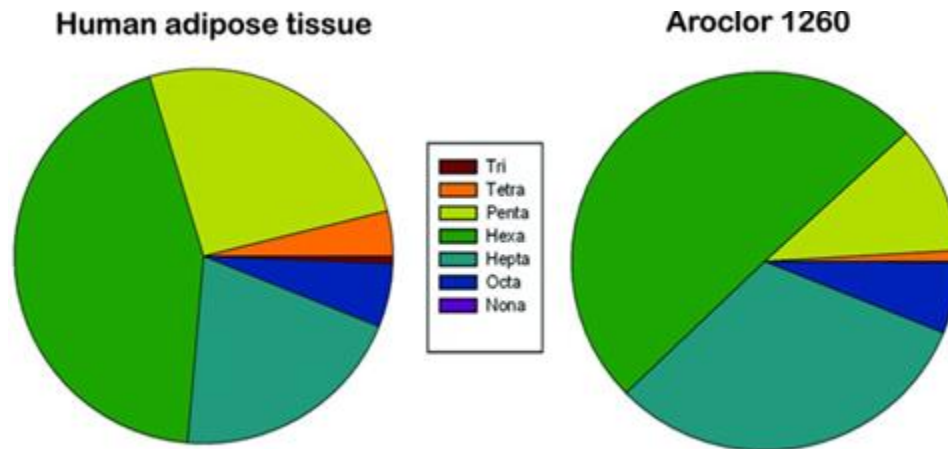
Figure 1.2. Relative PCB Composition in human Adipose tissue and Aroclor 1260

Pie charts depicting the relative abundance of PCB congeners in human adipose tissue and Aroclor 1260. Figure adapted from Wahlang, *et al.*, *Toxicol Sci*, 2014,140 (2): 283-297.

CHAPTER 2

DIOXIN-LIKE AND NON-DIOXIN-LIKE PCBS DIFFERENTIALLY REGULATE
THE HEPATIC PROTEOME AND MODIFY DIET-INDUCED NONALCOHOLIC
FATTY LIVER DISEASE SEVERITY

INTRODUCTION

The pollutants, polychlorinated biphenyls (PCBs), are metabolism-disrupting chemicals associated with nonalcoholic fatty liver disease (NAFLD), obesity, dyslipidemia, diabetes, and cardiovascular disease (37-42). PCBs were produced during the 1930s–1970s for use in multiple industrial applications (43). Although intentional PCB production is banned, their high thermodynamic stability imparting resistance to metabolism and degradation make PCBs persistent organic pollutants. PCBs bioaccumulate in living organisms and exposures increase along trophic levels of the food chain. PCBs have been detected in the serum of 100% American adult participants in the National Health and Nutrition Examination Survey (NHANES) (38). The 209 possible PCB congeners have been generally categorized into two major classes: "coplanar" and "noncoplanar". Coplanar PCBs (no or one chlorine atom in the ortho-position) including PCB126 potently activate the aryl hydrocarbon receptor (AhR), thereby eliciting a dioxin-like (DL) response similar to TCDD, and are known as "DL" PCBs (44). In contrast, noncoplanar PCBs have two or more chlorine atoms at

the ortho-position, conferring a conformation that precludes AhR binding and activation. However, these so-called "non-DL" (NDL) PCBs activate other xenobiotic receptors, such as the constitutive androstane receptor (CAR) and elicit a phenobarbital-like response (44). Commercially, PCBs were sold as mixtures rather than individual congeners. Arclor1260 (60% chlorine by weight) was a first-generation PCB mixture manufactured in Anniston Alabama, by Monsanto. The Anniston Community Health Survey I reported a high prevalence of suspected NAFLD associated with PCB congener exposures in Anniston residents (6). The PCB congeners that constitute Aroclor1260 are ones that have higher molecular weights and are not easily metabolized; therefore, they tend to bioaccumulate in living organisms including humans. In fact, the PCB composition in Aroclor1260 more closely resembles human bioaccumulation patterns than any other single commercially produced Aroclor mixture (45). Because low-dose Aroclor1260 does not activate either the human or murine AhR, Aroclor1260 has previously been used to model NDL PCB exposures (2, 45, 46).

PCB exposures are associated with NAFLD in human cohort studies and either cause or exacerbate diet-induced NAFLD in animal studies (reviewed in (45)). NAFLD is a broad spectrum of progressive liver disorders ranging from fat accumulation (steatosis) to hepatic inflammation (steatohepatitis), fibrosis, cirrhosis, and hepatocellular carcinoma. NAFLD and its more severe form, nonalcoholic steatohepatitis (NASH), can be due to various etiological factors, such as high-caloric intake, lifestyle habits, and more recently, environmental

chemical exposures. Our group coined the term "toxicant-associated steatohepatitis" (TASH) to reflect the steatohepatitis associated with industrial chemical exposures (47,48). However, recent studies have implicated known PCB receptors such as the AhR, CAR, pregnane-xenobiotic receptor (PXR), and epidermal growth factor receptor (EGFR) in PCB-induced TASH (49).

   In the liver, AhR activation by TCDD and PCB126 increased lipid accumulation and led to simple steatosis in short-term, rodent studies (50, 51). CAR, along with PXR, function as sensors of xenobiotic substances and are primarily involved in detoxification and foreign compound metabolism. However, previous studies from our group and others have shown that NDL PCB-mediated CAR and PXR activation also play a fundamental role in regulating hepatic energy metabolism and may contribute to TASH development (49). Like phenobarbital, some PCBs appear to indirectly activate CAR by diminishing EGFR phosphorylation, leading to reduced hepatic phosphoprotein signaling and metabolic disruption in TASH (51-53). Nonetheless, these studies only evaluated the effects of either DL or NDL PCBs in diet-induced obesity, although both classes of PCBs are concurrently present in the human exposome. We recently developed a new PCB exposure model, by spiking the potent AhR agonist, PCB126, into Aroclor1260 (51). This mixture produced different hepatic effects than either Aroclor1260 or PCB126 alone in an acute exposure model (51). Therefore, the objective of the current study is to evaluate the modulation of diet-induced NAFLD by several different types of chronic PCB exposures. Similar to our previous model (51), these

exposures include low-dose Aroclor1260 (representative NDL PCB mixture),

PCB126 (prototypical DL PCB), and Aroclor1260 + PCB126 (NDL + DL PCB

mixture). Untargeted liver proteomics was performed to elucidate potential

mechanisms for observed differences in NAFLD disease severity.

MATERIALS AND METHODS

Animal studies

The related animal protocol was ratified by the University of Louisville Institutional Animal Care and Use Committee. Adult male C57BL/6 mice (8 weeks old) were purchased from Jackson Laboratory and distributed into four equal groups (n = 10). All mice were fed a high-fat diet (HFD, 15.2, 42.7, and 42.0% of total calories from protein, carbohydrate, and fat, respectively, TekLad TD88137) throughout the study period. At 10 weeks of age, ten mice in each group were given either corn oil, Aroclor1260 (20 mg/kg), PCB126 (20 μg/kg), or a mixture of Aroclor1260 (20 mg/kg) plus 0.1% PCB126 (20 μg/kg) via a one-time gavage and followed for 12 weeks (Fig. 2.1). At week 8 post gavage, a glucose tolerance test (GTT) was performed as described previously (36). Dual energy X-ray absorptiometry (DEXA) scanning (Lunar PIXImus densitometer, WI) was performed to measure body fat composition before euthanasia. Whole blood for plasma, liver, and fat tissue samples was harvested after euthanasia.

Definition of PCB doses utilized

The doses of the different PCBs used in the present study were similar to those used in the acute study (29) and were designed to mimic doses relevant to human exposures. For example, Aroclor1260 at 20 mg/kg was designed to reflect serum PCB levels measured in the highest exposed quartile of the ACHS cohort (5), while PCB126 at 20 µg/kg (0.1% of Aroclor1260) was

designed to mimic the percent of serum PCB126 measured in NHANES 2003–

2004, relative to other heavily bioaccumulated PCBs such as PCB153, the

congener with the highest reported serum levels in NHANES 2003–2004 (54).

Histological staining

Liver and pancreas tissues were fixed in 10% neutral buffered formalin for 72

h and embedded in paraffin for routine histological examination. Hematoxylin–

eosin (H&E) staining was performed to identify histopathological changes.

Chloroacetate esterase (CAE) activity, macrophage accumulation, and fibrosis

were evaluated by CAE, immunohistochemical staining, and picro sirius red

staining, respectively, according to the manufacturer's protocols. Micrographic

images were obtained by a high-resolution Olympus digital scanner with an

Olympus digital camera (BX41).

Real-time PCR

Mouse liver and pancreas tissues were homogenized and total RNA was

extracted using RNA-STAT 60 reagent according to the manufacturer's

protocol. The purity and quantity of total RNA were measured with a Nanodrop

spectrometer (ND-1000, Thermo Fisher Scientific, Wilmington, DE) using ND-

1000 V3.8.1 software and cDNA was reverse transcribed from 1 μg RNA using

a one-step cDNA synthesis reagent (QScript cDNA Supermix, QuantaBio,

Beverly, MA). RT-PCR was performed on the CFX384TM Real-Time System

(Bio-Rad, Hercules, CA) using iTaq Universal Probe Supermix and Taqman

probes as described elsewhere (36). The probes sequences were as follows:

AhR (Mm00478932_m1); CAR (Mm00731567_m1), and Cyp4a10

(Mm02601690_gH); peroxisome proliferator-activated receptor alpha (Pparα)

(Mm00440939_m1); Cd36 (Mm01135198_m1); fatty acid-binding protein 1

(Fabp1) (Mm00444340_m1); fatty acid synthase (Fasn) (Mm00662319_m1);

interleukin-6 (Il-6) (Mm00446190_m1); stearoyl coenzyme A desaturase1

(Scd1) (Mm00772290_m1); Pnpla3 (Mm00504420_m1); Car (Nr1i3)

(Mm01283978_m1); Pxr (Nr1i2) (Mm01344139_m1); cytochrome P450s,

including Cyp1a2 (Mm00487224_m1), Cyp2b10 (Mm01972453_s1), Cyp3a11

(Mm007731567-m1), and glyceraldehyde-3-phosphate dehydrogenase

(GAPDH) (Mm99999915_g1). All reactions were run in triplicate. The relative

mRNA expression was calculated using the comparative $2^{-\Delta\Delta Ct}$ method and

normalized against GAPDH mRNA (55).

Measurement of hepatic lipids, plasma lipids, and cytokines

   Hepatic lipids were extracted by a mixture of chloroform and methanol (2:1)

according to a published protocol (56). Triglycerides and free fatty acid

contents were measured using commercial kits with final values normalized to

liver wet weight. Plasma alanine transaminase (ALT), aspartate transaminase

(AST), triglyceride, cholesterol, and lipoproteins were quantified with lipid panel

plus kits on a Piccolo Xpress Chemistry Analyzer (Abbott Laboratories, IL).

Plasma cytokine and adipokine levels were acquired using a customized

Milliplex® MAP mouse adipokine panel on a Luminex® 100 system (Luminex

Corp, Austin, TX).

Proteomics analysis

Proteins were extracted from liver tissue in RIPA buffer supplemented with protease and phosphatase inhibitors using a bead homogenizer and protein amounts were quantitated by BCA assay. Protein lysates (200 μg) were trypsinized using the modified filter-aided sample preparation method (57) and enriched for phosphopeptides by the TiO2–SIMAC–HILIC method (58). Briefly, protein samples were reduced with dithiothreitol, denatured with 8M urea, and alkylated with iodoacetamide followed by centrifugation through a high molecular weight cutoff centrifugal filter (Millipore, 10k MWCO). After overnight digestion with sequencing grade trypsin (Promega), the digested proteins were collected and cleaned with a C18 Proto™ 300 Å Ultra MicroSpin column. Protein digested samples (50μg) were labeled with tandem mass tag (TMT) TMT10plex™ Isobaric Label Reagent Set (Thermo Fisher, Waltham, MA); samples were then concentrated and desalted with Oasis HLB Extraction cartridges (Waters Corporation, Milford, MA) using a modified protocol for extraction of the digested peptides (59). Samples were then subjected to high pH reversed phase separation with fraction concatenation on a Beckman System Gold LC system supplemented with 126 solvent module and 166 detector in tandem with a Bio-Rad Model 2110 Fraction Collector (60). Liquid chromatography/mass spectrometry was used to measure TMT-labeled peptides. Briefly, every high pH reversed phase fraction was dissolved in 50μL solution of the combination of 2% v/v acetonitrile/0.1% v/v formic acid and 1 μL of each fraction was analyzed on

EASYnLC 1000 UHPLC system (Thermo Fisher) and an Orbitrap Elite—ETD

mass spectrometer (Thermo Fisher Scientific, Waltham, MA, USA). Proteome

Discoverer v2.2.0.388 was used to analyze the raw data collected from the

mass spectrometer. Hepatic proteins that had significance abundance were

imported into MetaCore software (Clarivate Analytics, Philadelphia, PA) for

the following analyses: gene ontology (GO), enrichment by protein function

(EPF), and interaction by protein function (IPF).

Statistical analysis and data sharing

Statistical significance was determined by two-way analysis of variance

using GraphPad Prism version 7.02 for Windows (GraphPad Software Inc., La

Jolla, CA, USA). $p < 0.05$ was considered statistically significant. Statistical

analysis for the proteome data was analyzed using the R package as

described previously (61, 62). Given the exploratory nature of the study,

significantly altered proteins were further filtered using an FDR threshold of

0.2 and proteins exhibiting a fold change of $-0.5 < \log_2 FC < 0.5$ were rejected

to rule out false positives. Proteomics data files were deposited in the

MassIVE (http://massive.ucsd.edu/) data repository, Center for Computational

Mass Spectrometry at the University of California, San Diego, and shared on

the ProteomeXchange (www. proteomexchange.org).
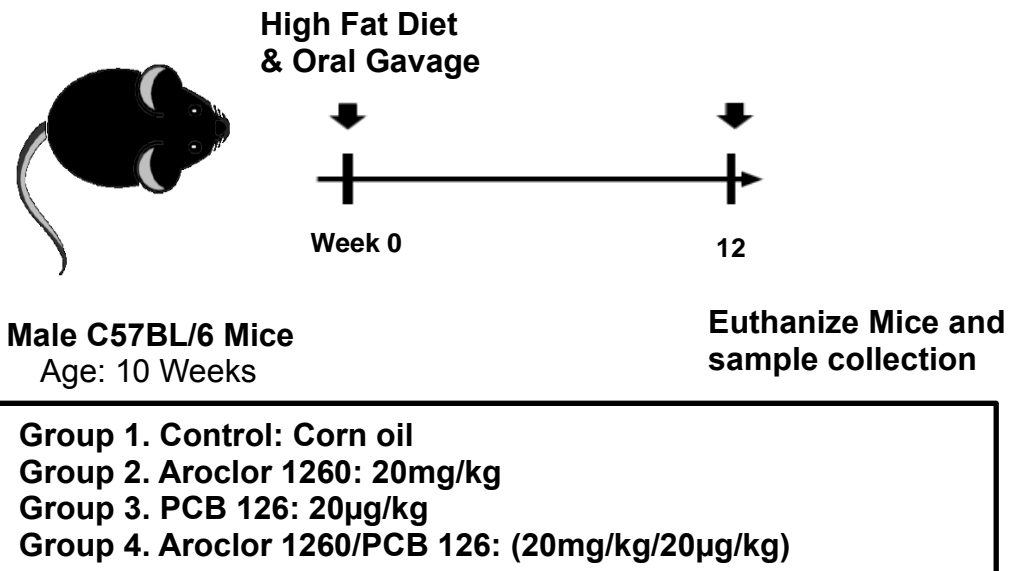
Figure 2.1. Experimental design of chronic PCB exposure study.

Mice were divided into 4 study groups based on the type of exposure. All

animals were fed a high fat diet and received a one-time gavage of their

respective dose at the beginning of the study.

RESULTS

Effects of PCB exposures on body composition, glucose tolerance, and adipokines

Body weight was measured weekly throughout the 12-week study. There was a gradual increase in body weight in all the four groups from week 0 to week 12 (Fig. 2.2A). However, there were no significant differences in the amount of body weight gain between the groups (Fig. 2.2B). Body fat composition was measured using both DEXA scan and by weighing the harvested epididymal fat (white adipose tissue) content. Although there was no significant difference in overall percent fat composition (Fig. 2.2E), Aroclor1260 exposure, however, increased white adipose tissue to body weight ratio (Fig. 2.2C). In addition, neither Aroclor1260 nor PCB126 affected liver weight to body weight ratio (Fig. 2.2D) and pancreas weight to body weight ratio in these mice (Fig. 2.2F). A GTT was performed to examine PCB effects on glucose metabolism; there were no differences between groups for alteration in glucose uptake (Fig. 2.2G). PCB effects on plasma lipids and adipocytokines were evaluated. The Aroclor1260+PCB126 group significantly decreased plasma cholesterol levels via its interacting Aroclor1260 and PCB126 components. PCB126 exposure decreased triglycerides levels in the Aroclor1260+ PCB126 group (Table 1). There was no PCB effect on adipokines including adiponectin, leptin, and resistin (Table 1).

Effects of PCB exposures on hepatic steatosis, inflammation, injury, and fibrosis
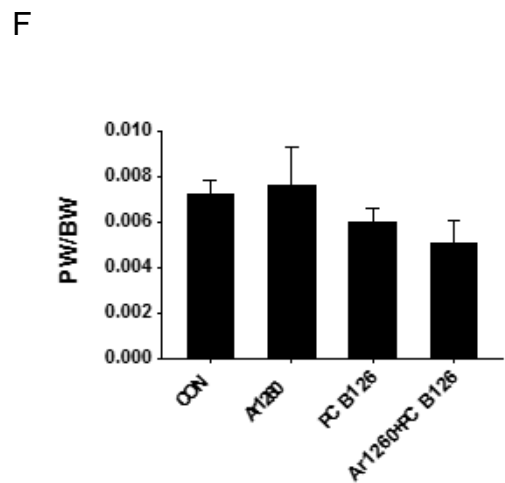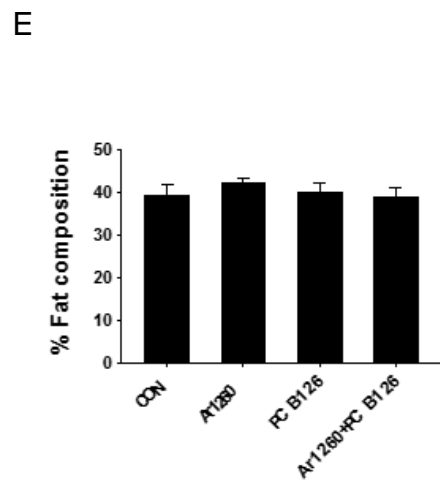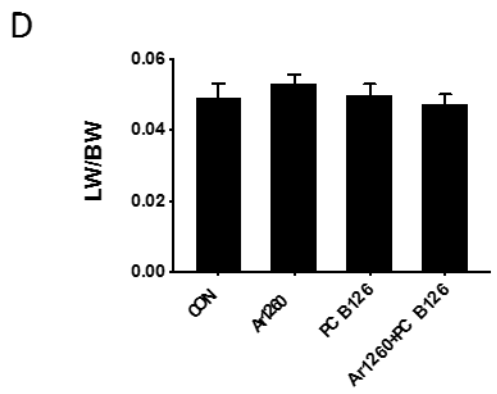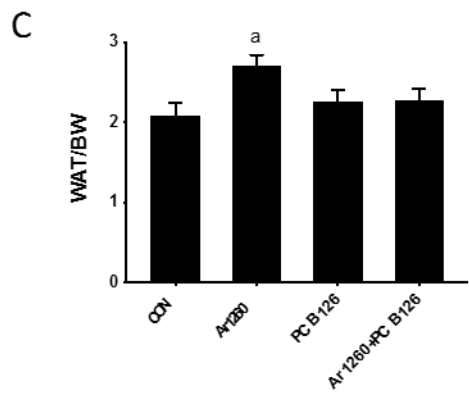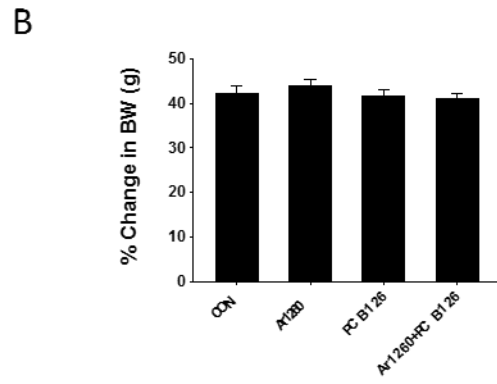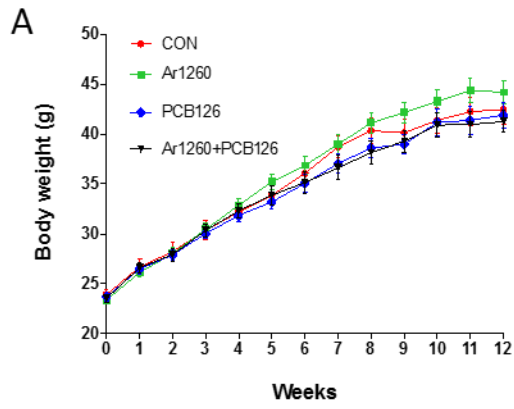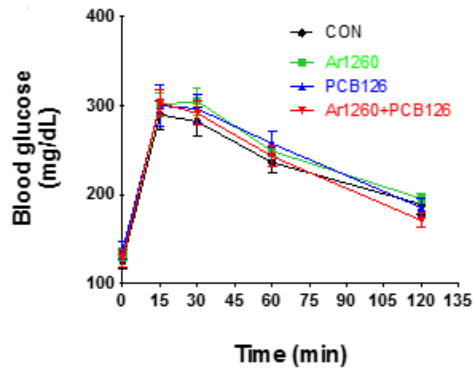
G   H
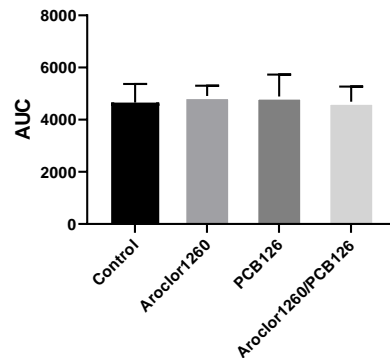
Figure 2.2. Effects of PCB exposures on body composition and glucose metabolism.

(A) Body weight (BW) was measured weekly throughout the 12-week study and (B) % change in body weight relative to the initial body weight taken at the beginning of the study was calculated. (E) Percent fat composition was measured using a dual energy X-ray absorptiometry (DEXA) scan. White adipose tissue (WAT) weight, liver weight (LW) and Pancreas weight (PW) were measured and the (C) WAT/BW, (D) LW/BW and (F) PW/BW ratios were calculated. (G) A glucose tolerance test was performed and blood glucose levels were obtained at baseline and at 15, 30, 60, and 120 minutes. There were no significant differences in (H) AUC (Area under curve) between four groups. Values are mean ± SEM; n=10, $p < 0.05$, a = Aroclor1260 effect, b = PCB126 effect, c = interaction between Aroclor1260 and PCB126.

Table 1. Plasma lipids and adipo-cytokines.

Plasma levels of lipids and adipo-cytokines were measured using either Piccolo Chemistry Analyzer or Luminex Milliplex system. Values are mean ± SD; n=10, p <0.05, a= Aroclor1260 effect, b=PCB126 effect, c=interaction between Aroclor1260 and PCB126. PAI-1: plasminogen activator inhibitor 1.

Analyte	Control	Ar1260	PCB126	Ar1260+PCB126
Triglyceride (mg/dl)	75.2 ± 20.8	78.5 ± 17.2	68.7 ± 14.4	52.1 ± 12[b]
Cholesterol (mg/dl)	124.7 ± 26.2	146.2 ± 30	136.5 ± 18.7	118.6 ± 27.4[c]
PAI-1 (pg/ml)	873.2 ± 262.6	890.2 ± 354.9	675.2 ± 330.1	577.5 ± 205.6
Adiponectin (pg/ml)	81982 ± 4811	84484 ± 3753	86390 ± 3874	83272 ± 6660
Leptin (pg/ml)	6476 ± 2266	8221 ± 1631	6912 ± 3017	8227 ± 4834
Resistin(pg/ml)	1169 ± 233.5	1149 ± 375.6	1091 ± 421.5	955.2 ± 197.3

Hepatic steatosis was using H&E staining of liver sections. All HFD-fed mice developed variable, centrilobular, macrovesicular steatosis and the different PCB exposures did not exacerbate HFD-induced steatosis (Fig. 2.3A). Hepatic lipids were measured and PCB exposures had no effect on either hepatic triglyceride or cholesterol levels (Fig. 2.3H&I). However, hepatic free fatty acid levels were significantly increased by the Aroclor1260 + PCB126 mixture (Fig. 2.3B). Histological analyses for liver inflammation were assessed using CAE and F4/80 staining. CAE staining demonstrated that HFD feeding induced neutrophil infiltration in the liver (Fig. 2.3C); however, Aroclor1260 exposure exacerbated this effect as shown by the number of inflammatory foci counted per field (Fig. 2.3D). Interestingly, the Aroclor1260 + PCB126 group showed a lesser number of inflammatory foci counted per field. Likewise, F4/80 staining demonstrated that the Aroclor1260 group had increased macrophage infiltration compared with any other group (Fig. 2.3E). This observation was consistent with hepatic Cd68 gene expression where in Aroclor1260 increased Cd68 mRNA levels, indicating a hepatic inflammatory state, while this effect was absent with PCB126 exposure (Fig. 2.3F). Commonly used biomarkers of liver injury, namely plasma ALT and AST levels, were measured. Elevated plasma ALT activity levels were only seen with Aroclor1260 exposure, but not with PCB126 (Fig. 2.3G) while PCB126 showed a trend for decreased plasma AST activity levels (Fig. 2.3J). In addition, the Aroclor1260 + PCB126 group showed attenuation of Aroclor1260-elevated plasma ALT levels, suggesting that PCB126 may be protective against liver injury in this model. Fibrosis was

assessed by picro sirius red staining of liver sections to detect collagen deposition (Fig. 2.4). While there were no histological differences between groups, PCB126 decreased the hepatic gene expression of collagen (Col1a2) and actin 2 (Acta2), implicating a suppression of profibrotic gene expression in the liver (Fig. 2.4).

Effects of PCB exposures on the expression of AhR, CAR and their target genes

Known PCB receptor activation such as AhR and CAR activation was examined. PCB126 exposure caused upregulation of cytochrome P450 1a2 (Cyp1a2), an AhR target gene, indicative of AhR activation. In contrast, the Aroclor1260 + PCB126 group showed decreased Cyp1a2 mRNA levels (Fig. 2.5A). With regards to AhR gene expression, PCB126 alone showed a trend for decreased AhR mRNA levels (Fig. 2.5B). For CAR activation, the CAR target gene, Cyp2b10, was measured. The Aroclor1260 group showed upregulated Cyp2b10 mRNA levels, indicative of CAR activation (Fig. 2.5C), while CAR expression was increased in the Aroclor1260 + PCB126 groups (Fig. 2.5D).

Effects of PCB exposures on the hepatic proteome

The various PCB exposures produced distinct hepatic proteomes (Fig. 2.6). A total of 8355 unique proteins and their isoforms were detected, corresponding to 4609 protein groups. Liver protein content was regulated as follows: Aroclor1260 (35 increased and 48 decreased); PCB126 (158 increased and

H **I** **J**
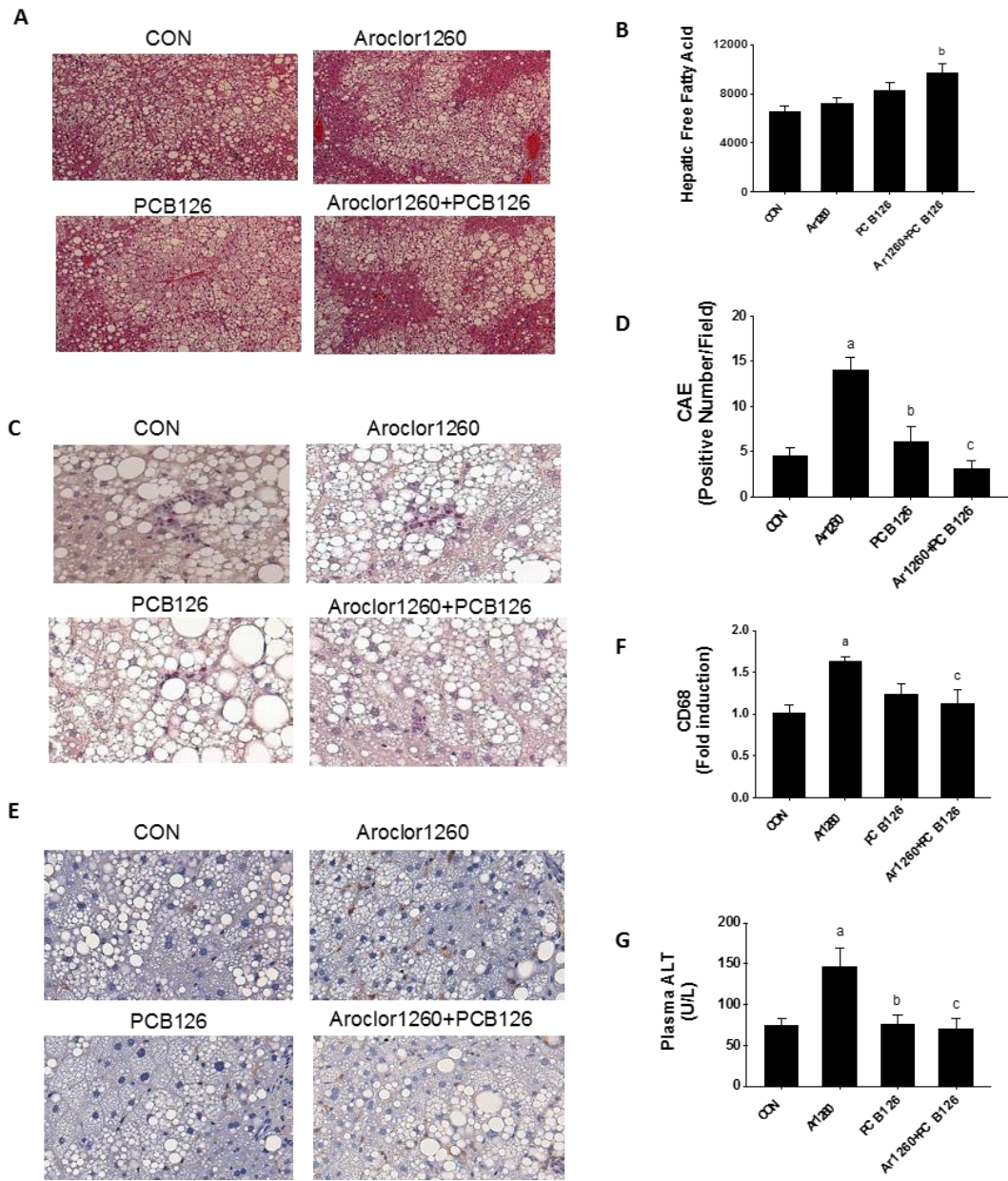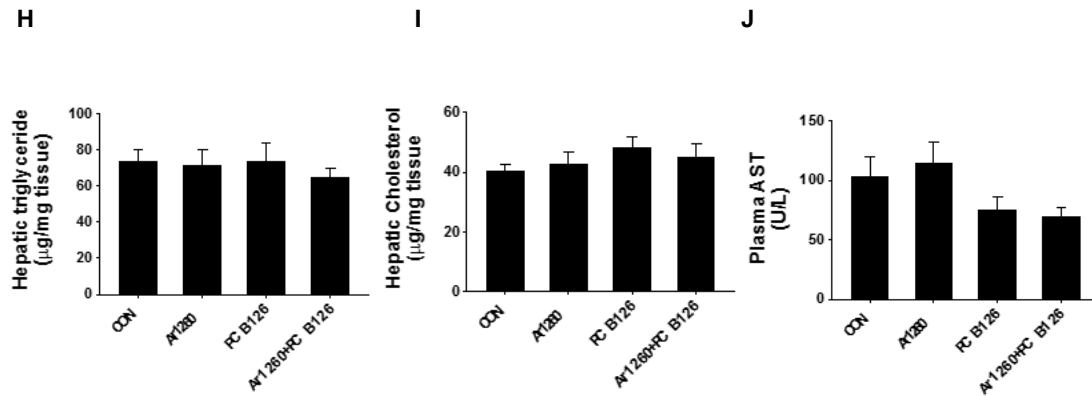
Figure 2.3. Effects of PCB exposures on steatosis and inflammation.

(A) Liver sections were analyzed for steatosis using H&E staining. (B) Hepatic
free fatty acid levels, (H) triglycerides and (I) cholesterol were measured using
colorimetric assays. (C) Liver sections were analyzed for neutrophil infiltration
using CAE staining where red positive cells indicate neutrophil infiltration. (D)
The number of CAE positive cells per microscopic field were counted. (E) Liver
sections were analyzed for macrophage infiltration using F4/80
immunohistochemistry staining and brown positive cells indicate macrophage
accumulation. (F) Hepatic *CD68* mRNA levels were measured using RT-PCR.
(G) Plasma ALT and (J) plasma AST activity levels were measured using the
Piccolo Xpress Chemistry Analyzer. Values are mean ± SD, n=10, $p < 0.05$, a -
Aroclor1260 effect, b - PCB126 effect, c - interaction between Aroclor1260 and
PCB126.
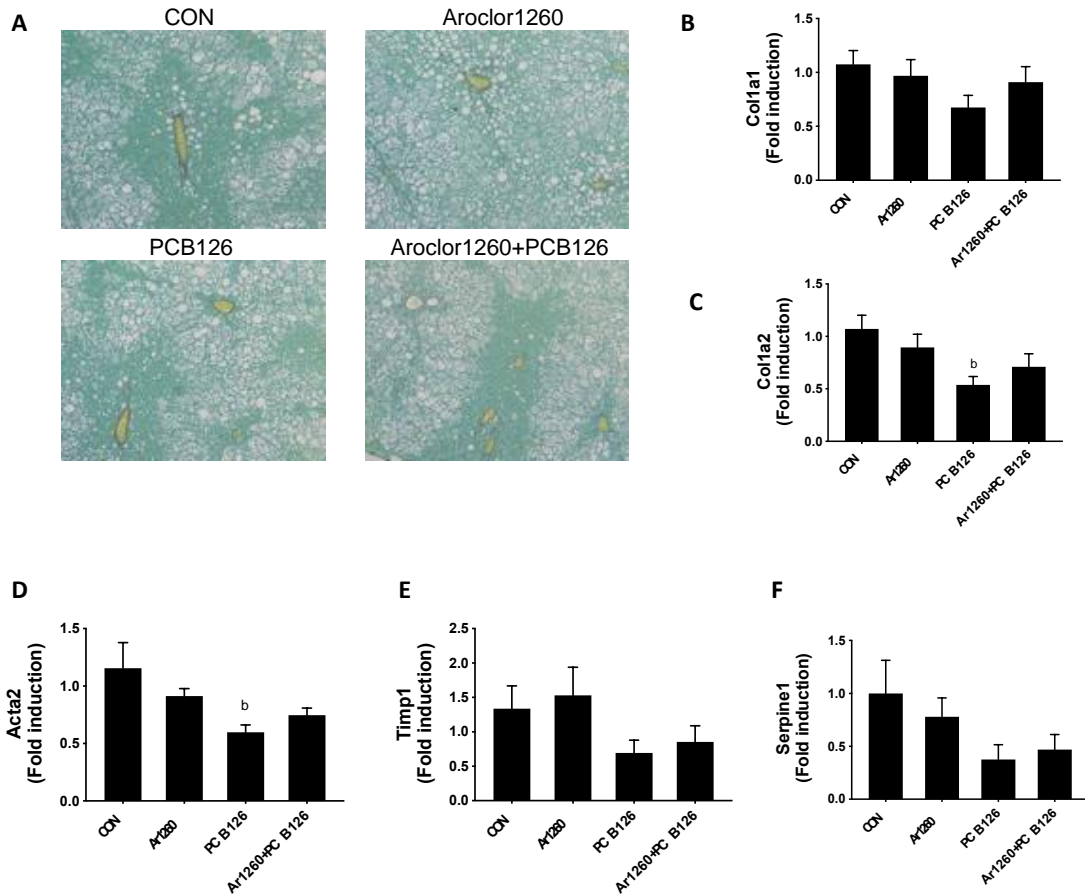
Figure 2.4. Effects of PCB exposures on hepatic fibrosis.

(A) Collagen deposition was analyzed by picro sirius red staining of liver
sections. There were no differences between groups. Hepatic gene expression
of fibrotic markers, namely (B) collagen 1a1 (*Col1a1*), (C) collagen 1a2
(*Col1a2*), (D) actin 2 (*Acta2*), (E) TIMP metallopeptidase inhibitor 1 (*Timp1*),
and (F) plasminogen activator inhibitor 1 (*PAI-1*, *Serpine1*) were measured
using RT-PCR. Values are mean ± SD; n=10, *p* <0.05, b - PCB126 effect.
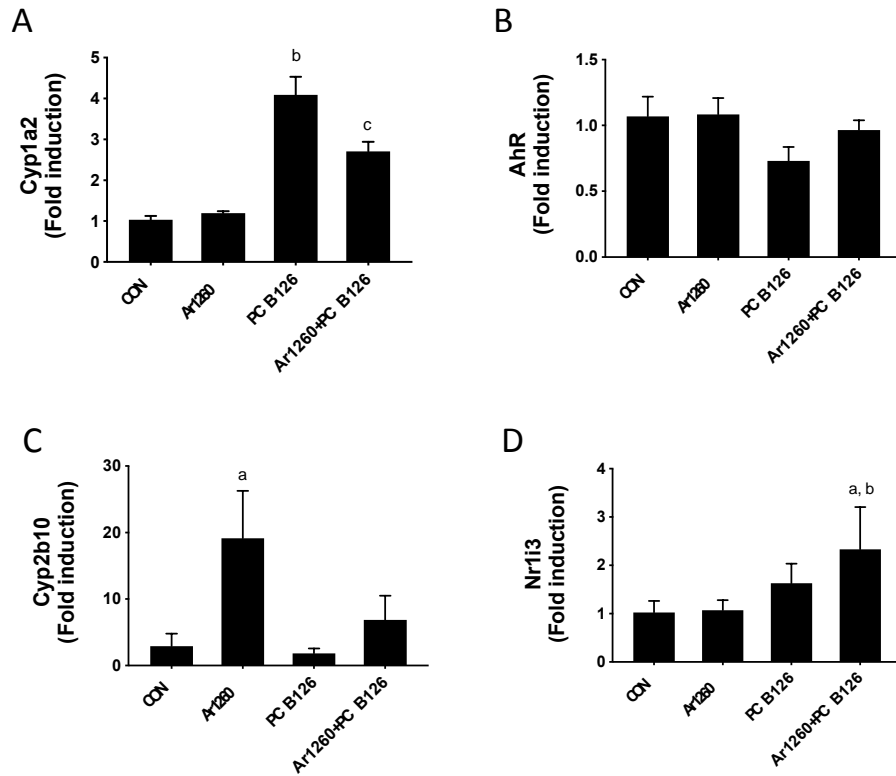
Figure 2.5 Effects of PCB exposures on target gene expression.

Hepatic mRNA expression for the AhR target gene (A) *Cyp1a2* and (B) *AhR*
and the CAR target gene target gene *Cyp2b10* (C) and (D) CAR (*Nr1i3*) were
measured by RT-PCR. Values are mean ± SD; n=10, *p* <0.05, a - Aroclor1260
effect, b - PCB126 effect, c - interaction between Aroclor1260 and PCB126.

238 decreased); and Aroclor1260 + PCB126 (144 increased and 257 decreased) (Fig. 2.6 and Supplemental Table 1). The majority of differentially abundant proteins for each and Aroclor1260 + PCB126 (144 increased and 257 decreased) (Fig. 3.6 and Supplemental Table 1). The majority of differentially abundant proteins for each group were unique to that exposure (range 58.7–63.1%). Of the 401 proteins associated with Aroclor1260 + PCB126 exposure, only 5.9% were also associated with Aroclor1260, while only 33.6% were also associated with PCB126. Only three proteins were changed in all three PCB exposure groups (BET1-like protein and two isoforms of protein-O-linked-mannose-β-1,4-N-acetylglucosaminyltransferase 2). Clearly, the proteomic changes associated with the Aroclor1260 + PCB126 mixture were not the sum of its parts.

EPF analysis was performed to determine the protein classes most impacted by PCBs (Table 2). Enzymes were the most affected class (Aroclor1260, z-score= 3.63; PCB126, z-score = 7.11; Aroclor1260 + PCB126, z-score = 4.89). Consistent with this observation and the RT-PCR data, the enzyme levels of CYP1A1 and CYP1A2 were higher for PCB126 (CYP1A1: 9.09-fold, p = 7.10E−06 and CYP1A2: 5.85-fold, p = 3.10E−08) and, to a lesser degree, for Aroclor1260 + PCB126 (CYP1A2: 2.39-fold, p = 2.39E−08) (Supplemental Table 1). While Aroclor1260 increased hepatocyte injury (by histologic and plasma ALT enzyme activity biomarkers), plasma AST activity was not significantly increased. This could be related to the peculiar proteomic observation that hepatic AST enzyme levels were reduced by PCB exposures (Aroclor1260: 0.64-fold, p = 2.18E−03 and PCB126: 0.68-fold, p = 5.82E−03).

Again, consistent with the liver histology, inflammation-associated enzymes and leukocyte markers were increased with Aroclor1260 (e.g., macrosialin/CD68, 2.26-fold, p = 1.85E−04) and decreased with either PCB126 (e.g., myeloperoxidase: 0.51-fold, p = 1.79E−03; α-defensin 20: 0.48-fold, p = 2.90E−02; and the calprotectin component, protein S100-A8: 0.32-fold, p = 8.05E−03) or Aroclor1260 + PCB126 (e.g., protein S100-A9: 0.62-fold, p = 4.35E−02; neutrophil granule protein: 0.58-fold, p = 1.17E−02; protein jagunal homolog 1: 0.33-fold, p = 1.20E−02; and neutrophil gelatinase-associated lipocalin (0.30-fold, p = 2.41E−02) (Supplemental Table 1). EPF revealed that Aroclor1260 altered protein levels of slightly more transcription factors than expected (z-score =1.67), while the other exposures changed fewer than expected. Several nuclear receptors implicated in steatohepatitis were differentially regulated including peroxisome proliferator-activated receptor alpha (PPARα, Aroclor1260: 0.7-fold, p = 1.97E−03), liver X receptor alpha (PCB126: 1.47-fold, p = 1.81E−02), and V-erbArelated protein 2 (PCB126: 0.69- fold, p = 1.14E−02 and Aroclor1260 + PCB126: 0.63-fold, p = 2.69E−03). Thus, while each PCB exposure was associated with a distinct proteome, EPF demonstrated that these proteomes were consistent with the observed phenotypes.

Enrichment by GO processes (Fig. 2.7) revealed that the distinct proteomes associated with PCB126 and Aroclor1260 + PCB126 exposures were associated with similar top GO processes, although some differences were apparent. However, the top GO processes associated with Aroclor1260 were

unique to that exposure. These findings are again consistent with the histology and phenotyping data. A very limited number of GO processes were enriched by Aroclor1260 including "negative regulation of receptor internalization"; "negative regulation of catabolic process"; aspartate catabolic metabolism; and polyadenylation-dependent RNA catabolic processes (Fig. 2.7). In contrast, hundreds of GO processes were significantly enriched by PCB126 and/or Aroclor1260 + PCB126 (data not shown). Both exposures enriched: (i) cellular, metabolic, and catabolic processes; (ii) protein metabolism processes; (iii) cellular localization and organization processes; and (iv) the PCB126 and/or Aroclor1260 + PCB126 (data not shown). Both exposures enriched: (i) cellular, metabolic, and catabolic processes; (ii) protein metabolism processes; (iii) cellular localization and organization processes; and (iv) the "negative regulation of neurotransmitter (acetylcholine) secretion". These processes, however, were enriched to a greater degree by Aroclor1260 + PCB126. In contrast, while both exposures enriched xenobiotic metabolism processes and lipid metabolism processes, these were enriched to a greater degree by PCB126.

GO processes related to cytoskeletal remodeling/fibrosis and metal homeostasis were enriched by PCB126 only (Fig. 2.7). The abundance of several cytoskeletal-associated proteins were markedly increased by PCB126 including troponin C (120.33-fold, p = 1.30E−03); actin α, skeletal muscle (55.47- fold, p = 7.38E−03); myosin light chain 3 (33.67-fold, p = 1.27E−02); LIM domain-binding protein (15.24-fold, p = 7.88E−03), etc. (Table 3).

However, other cytoskeletal proteins, including type II keratins, were differentially regulated by Aroclor1260 (keratin 5: 0.28-fold, p = 2.12E−03) or Aroclor1260 + PCB126 (keratin 2: 0.30-fold, p = 3.85E−02; keratin 4: 0.62-fold, p = 4.19E−02; and keratin 6a: 1.89-fold, p = 1.34E−02). While the PCB exposures were not associated with fibrosis at the histologic level, PCB126 exposures were associated with reduced expression of several profibrogenic genes at the molecular level. Consistent with this observation, PCB126 was associated with reduced abundance of several proteins associated with liver fibrosis including collagen α-1(IV) chain (0.68-fold, p = 2.26E−02); prolyl 4-hydroxylase subunit alpha-1 (0.66-fold, p = 1.42E−03); and procollagen-lysine, 2-oxoglutarate 5-dioxygenase 3 (0.47-fold, p = 2.28E−02). Multiple proteins associated with metal homeostasis were likewise reduced only by PCB126 including ferritin light chain 1 (0.64-fold, p =1.44E−02), light chain 2 (0.63-fold, p = 1.24E−02), and heavy chain (0.60-fold, p = 6.11E−03), and zinc transporter 4 (0.55-fold, p = 3.09E−02).

Several GO processes related to the epigenetic mechanisms were enriched only by Aroclor1260 + PCB126 (Fig. 2.7). These included "regulation of gene expression, epigenetic", "negative regulation of chromatin silencing", and "histone H3-K27 methylation". Differentially abundant proteins contributing to these observations included reduced histone deacetylase 2 (0.68-fold, p = 1.13E−02); reduced histones H1.2 (0.63-fold, p = 5.98E−04), H1.4 (0.66-fold, p = 8.87E−03), H1.5 (0.67-fold, p = 2.45E−02), and H1t (0.67-fold, p = 1.40E−02); reduced RNA polymerase-associated protein CTR9 homolog (0.60-

fold, p = 7.64E−04); and reduced exportin 5 (0.66-fold, p = 2.07E−02).

However, several other epigenetics proteins were reduced by PCB126 and

Aroclor1260 + PCB126, such as RNA binding protein 3 (PCB126: 0.68-fold, p =

2.64E−03; Aroclor1260 + PCB126: 0.69-fold, p = 2.78E−03); LIM domain-

containing protein 1 (PCB126: 0.66-fold, p = 6.66E−03; Aroclor1260 +

PCB126: 0.63-fold, p = 2.93E−03); and protein arginine methyltransferase 7

(PCB126: 0.64-fold, p = 9.69E−04; Aroclor1260 + PCB126: 0.70-fold, p =

4.74E−03).

   IPF analysis was performed and the top overconnected interactions by z-

score are provided in Fig. 2.8. Seven unique objects, all protein kinases, were

over-connected with Aroclor1260 exposure. These kinases included the

mammalian target of rapamycin (mTOR); the adenylate kinase isoenzyme,

mitochondrial (AK3L1); the alternate mitogen-activated protein kinase, p38γ;

and protein kinase C α (PKCα). PCB126 and/or Aroclor1260 + PCB126

exposures were associated with 18 over-connected objects (Fig. 3.8). Eleven

of these objects were transcription factors and eight of these were common

between the two groups. Shared transcription factors included protein C-ets-1

(ETS1), SRY-box transcription factor 17 (SOX17), and GA binding protein

transcription factor subunit α (GABPα); glucocorticoid receptor; zinc finger

protein x-linked (ZFX); neuroblastoma MYC oncogene (N-Myc); and acute

myeloid leukemia 1 (AML1). The z-scores were all higher with the Aroclor1260

+ PCB126 exposure. Unique transcription factors overconnected by PCB126

included zinc finger protein, FOG family member 1 (ZFPM1), and CAR, while

cellular oncogene FOS (c-FOS) was uniquely over-connected by Aroclor1260 + PCB126. PCB126 exposure was uniquely over-connected with the bradykinin precursor, kininogen 1, and thrombin. Aroclor1260 + PCB126 was uniquely overconnected with two enzymes associated with steatohepatitis and liver cancer, protein arginine methyltransferase 1 (PRMT1), and hypoxia-associated factor (SART1) (63, 64).

Effects of PCB exposures on hepatic intermediary metabolism and plasma profile

Proteomics analysis revealed that PCBs played a role indictating intermediary metabolism such as lipid and protein processes. To further validate these findings, hepatic expression of genes involved in a variety of metabolic processes, including lipogenesis, lipid transport and mobilization, fatty acid β-oxidation, and glucose and protein metabolism were measured. The expression of genes related to lipogenesis, namely, fatty acid synthase (Fasn), sterol regulatory element-binding protein 1 (Srebf1), stearoyl-CoA desaturase-1 (Scd1), and peroxisome proliferator-activated receptor gamma (Pparg) were measured by RT-PCR. PCB exposure did not alter Fasn or Srebf1 mRNA levels although the PCB126 group demonstrated a trend for decreased Fasn and Srebf1 mRNA levels (Fig. 2.9H&I), consistent with previous findings (65, 66). Similarly, Aroclor1260 + PCB126 exposure decreased Scd1 mRNA levels (Fig. 2.9A), consistent with protein abundance data (0.70-fold, $p = 1.35E{-}02$, Table 3) and a prior study (51). The same group also showed increased Pparg gene expression (Fig. 2.9B). With regards to lipid transport, the hepatic mRNA levels

of Cd36 and fatty acid binding protein 1 (Fabp1) were determined. Both Aroclor1260 and PCB126 contributed to the upregulated Cd36 expression in the Aroclor1260 + PCB126 mixture (Fig. 2.9C). There was no significant difference for Fabp1 mRNA levels between groups (Fig. 2.9J). In terms of lipid breakdown, the mRNA levels of Pparα, a transcription factor that regulates fatty acid β-oxidation, the Aroclor1260 + PCB126 group decreased Pparα levels (Fig. 2.9D). These results differed from the proteomics data that showed decreased protein abundance only for Aroclor1260. PCB126 exposure also decreased the expression of the lipolytic gene, patatin-like phospholipase domain-containing protein 3 (Pnpla3, Fig. 2.9E). In addition, the gene expression of phosphoenolpyruvate carboxykinase 1 (Pck1), a gluconeogenic gene, was measured and found to be decreased with PCB126 exposure (Fig. 2.9F). Proteomics data demonstrated that PCB126 disrupted the coordination of glycolysis and gluconeogenesis by simultaneously downregulating abundance of hexokinase-3 (0.52-fold, p = 2.53E−03), phosphofructokinase (0.61-fold, p = 6.53E−03), and glucose-6-phosphatase (0.51-fold, p = 1.33E−02). The gene expression of albumin (Alb), a biomarker for protein metabolism, was increased in the Aroclor1260 + PCB126 group (Fig. 2.9G). Overall, these results confirm that PCBs differentially altered hepatic intermediary metabolic processes.
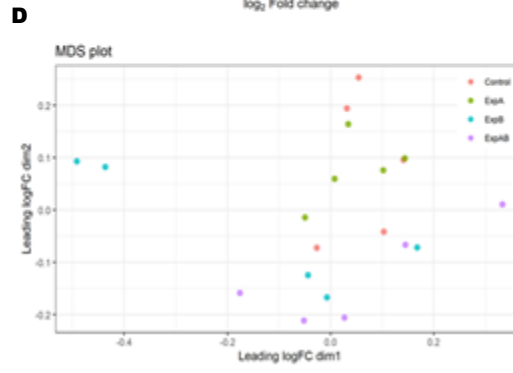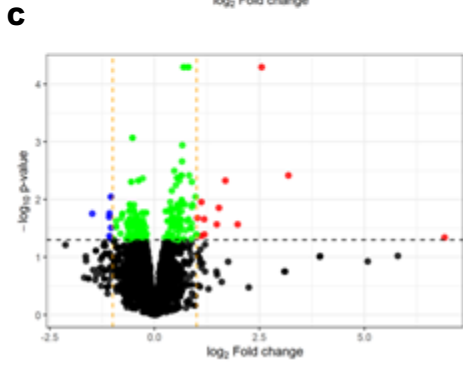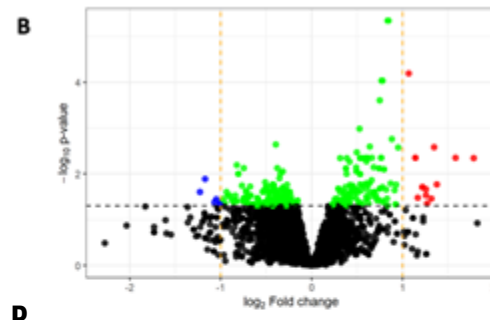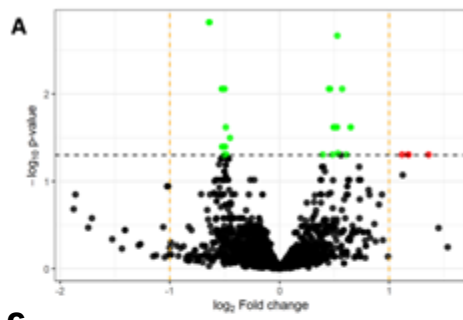
Differentially Abundant Proteins	Aroclor1260	PCB126	Aroclor1260/PCB126
Altered	83	396	401
Increased	35	158	144
Decreased	48	238	257
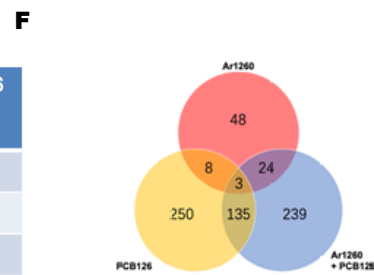
Figure 2.6. Effects of PCB exposures on the hepatic proteome.

Alterations in hepatic proteins are depicted by volcano plots showing significance (y-axis) versus protein fold change (x-axis) for (A) Aroclor1260, (B) PCB126 and (C) Aroclor1260+PCB126. Black denotes unaltered proteins, green denotes significantly altered proteins, red denotes significantly altered protein with ($\log_2$FC >1), blue denotes significantly altered protein with ($\log_2$FC <-1). (D) A multi-dimensional scatter (MDS) plot depicting the pattern for protein alterations in the different groups. ExpA - Aroclor1260, ExpB - PCB126, ExpC - Aroclor1260+PCB126. (E) The number of proteins and their isoforms that were altered for the different exposure groups. (F) Venn diagram showing the number of overlapping proteins between the three exposure groups.

Table 2. Enrichment by protein function analysis

Enrichment by protein function analysis was performed by MetaCore software using the hepatic proteomics data. For a given protein class, a positive *z*-score indicates that more proteins in that class were altered than expected. Likewise, a negative *z*-score means that fewer proteins in the class were altered than expected.

Protein Class	PCB Exposure		
	Ar1260	**PCB126**	**Ar1260+PCB 126**
Ligands		-0.687	-1.99
Phosphatases		1.55	0.892
Proteases	-0.238	0.541	0.117
Kinases	0.512	0.243	-0.535
Transcription Factors	1.67	-1.36	-1.97
Receptors	-0.767	-1.39	-0.940
Enzymes	3.63	7.11	4.89
Other	-2.53	-3.98	-1.47
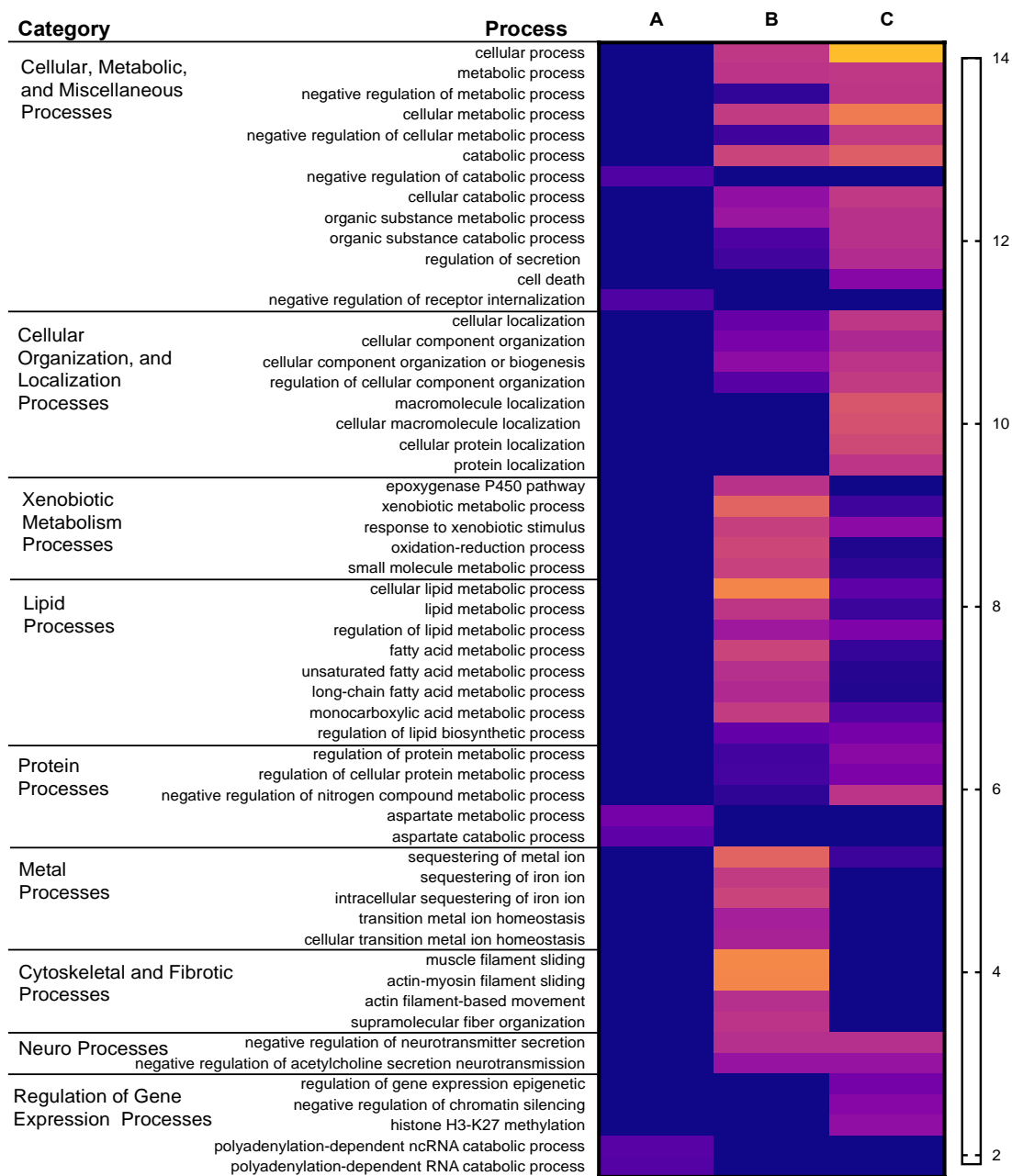
Figure 2.7. Heatmap of PCB effects on gene ontology (GO) processes.

Heatmap showing different processes that were altered by PCB exposures according to the -log(p-value). The processes were obtained by GO analysis enrichment of the different proteins altered by PCB exposures using MetaCore. A - Aroclor1260, B - PCB126, C - Aroclor1260+PCB126.
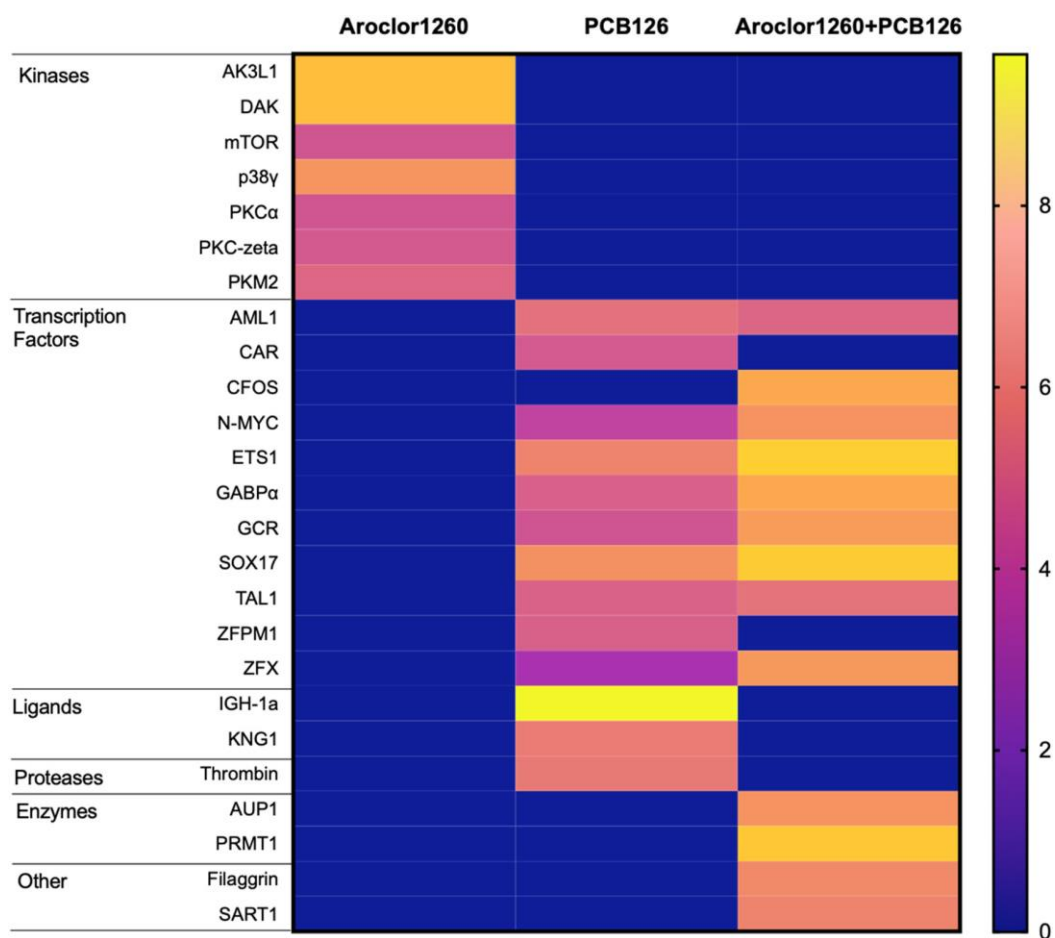
Figure 2.8. Effects of PCB exposures on protein function.

Heatmap showing different classes of proteins, for the three exposure groups, obtained from the Interaction by Protein Function analysis using MetaCore Software and their corresponding *z*-scores. A - Aroclor1260, B - PCB126, C - Aroclor1260+PCB126.

J
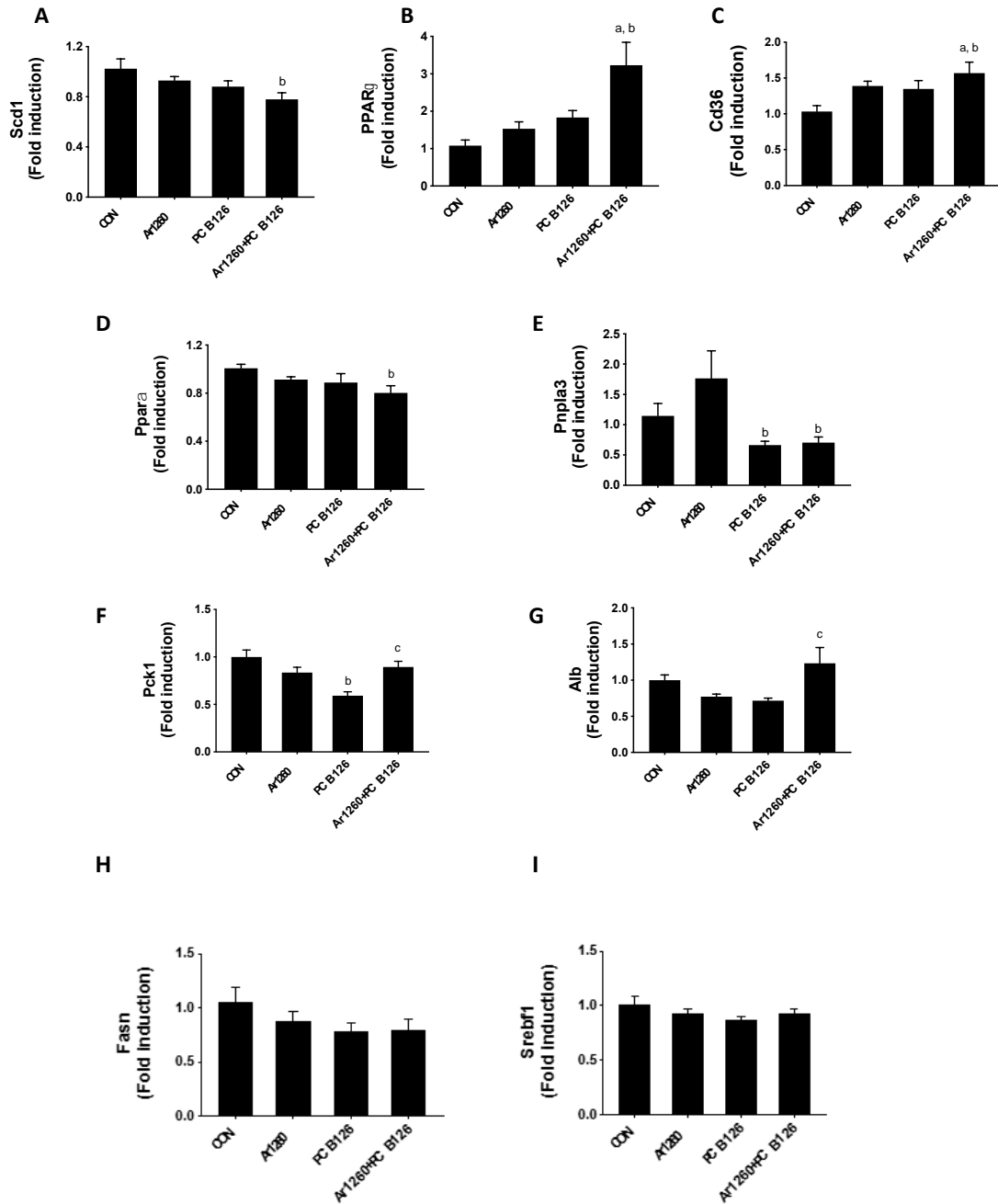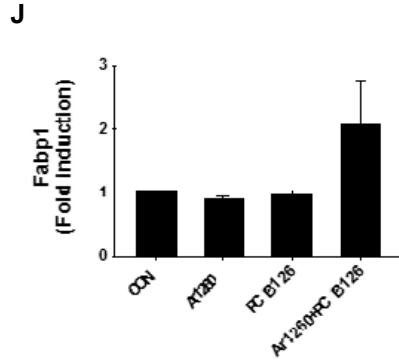
Figure 2.9. Effects of PCB exposures on genes involved in hepatic energy metabolism.

Hepatic mRNA levels of genes involved in hepatic energy metabolism inlcuding (A) Scd1, (B) Pparg, (C) Cd36, (D) Pparα, (E) Pnpla3, (F) Pck1, (G) Alb, (H) Fasn, (I) Srebf1, and (J) Fabp1 were measured by RT-PCR. Values are mean ± SD; n=10, p <0.05, a - Aroclor1260 effect, b - PCB126 effect, c - interaction between Aroclor1260 and PCB126.

DISCUSSION

PCBs, including both DL and NDL congeners, are metabolism-disrupting chemicals (37). PCBs exposures are associated with obesity-related diseases including diabetes, dyslipidemia, cardiovascular disease, and NAFLD. PCB-related NAFLD mechanisms was recently reviewed (49). In animal models fed a healthy diet, DL, but not NDL PCBs, caused hepatic steatosis and NAFLD. In contrast, NDL PCBs exposures compromised the liver, thereby increasing the histologic severity of HFD-induced NAFLD. The NDL PCB exposures variably increased diet-induced hepatic steatosis, inflammation, and fibrosis while interacting with PCB receptors including PXR, CAR, and the EGFR (2, 46, 48, 51-53, 67). While humans have simultaneous exposures to both PCB classes, no previously published studies in the literature have systematically evaluated the disease modifying effects of DL PCBs, NDL PCBs, and the more environmentally relevant combination of DL + NDL PCBs in a chronic exposure model of HFD-induced NAFLD. Few to no published data exist on either DL or DL + NDL PCBs in such a model.

Our recently published acute PCB exposure study demonstrated that Aroclor1260, PCB126, and Aroclor1260 + PCB126 exposures differentially affected histology and disease mechanisms in liver and related organs in male mice fed a healthy diet (29). Based on the direction of these results, environmental relevance, and knowledge gaps in the literature, the objective of the current study was to elucidate the effects and potential mechanisms of these different PCB exposures in a diet-induced obesity mouse model of NAFLD.

The combination of the phenotyping, histologic, and molecular biomarkers demonstrated the following differential PCB effects on metabolic conditions related to HFD-induced obesity. Consistent with prior studies (65), Aroclor1260 increased liver inflammation/ injury and the white adipose tissue to body weight ratio. PCB126 decreased liver inflammation and fibrosis at the molecular level. PCB126 alone did not increase hepatic free fatty acids and hepatic triglycerides, as reported previously (29). These differences are likely related to differences in duration of exposure or diet. Aroclor1260 + PCB126 modulated lipid metabolism such as hepatic free fatty acids were increased, while the plasma cholesterol/triglycerides were decreased, and it decreased liver inflammation. The lipid effects were mediated predominantly by the PCB126 component of this mixture as previously reported (29). Therefore, PCB126 and co-exposure attenuated Aroclor1260-induced hepatic inflammation despite worsening the disruption of intermediary and xenobiotic metabolism. None of the exposures affected glucose tolerance or adipokines. AhR activation was highest with PCB126 alone; increased to a lesser degree with Aroclor1260 + PCB126; and absent with Aroclor1260, consistent with Shi et al. (29). The effects on CAR were complex. Cyp2b10 gene expression was increased by Ar1260; IPF demonstrated enriched CAR interactions with PCB126; and Aroclor1260 + PCB126 induced Nr1i3 gene expression. PCBs induced Cyp2b10 gene expression to a lower degree in HFD-fed mice compared with mice fed a low fat diet (29).

Proteomics was performed to elucidate potential mechanisms for the

observed differences in metabolic phenotype and TASH severity, which were greatest for Aroclor1260 versus the more similar PCB126 and Aroclor1260 + PCB126 exposure groups. The large number of differentially abundant proteins between the PCB exposure groups was surprising. For example, 99.58% of these proteins were not conserved across all three treatment groups. PCB126 and Aroclor1260 + PCB126 altered many more proteins than Aroclor1260. However, 79.06% of the proteins altered by either of the latter two treatments were not common to both groups. Despite these differences, PCB126 and Arclor1260 + PCB126 shared many top GO processes consistent with the observed similarities in liver histologic phenotype. The observed alterations in cholinergic neurotransmission associated with these exposures is novel and could be mechanistic. For example, human neonates exposed to PCBs display a number of hematologic and immunologic disturbances in neuronal signaling, immune regulation via the AhR and other receptors (68, 69). In addition, these exposures alter many normal medical biomarkers used in clinical medicine, such as cholesterol levels, AST enzyme levels, etc.

While a number of new putative PCB targets and modes of action in TASH were identified, others were reassuringly consistent with known targets. Aroclor1260 exposure was associated with the "negative regulation of receptor internalization" GO process and overconnected interactions with protein kinases including mTOR, AK3L1, p38γ, and PKCα. These findings could be consistent

with the decreased EGF-stimulated EGFR internalization with consequent phosphoprotein signaling disruption previously reported for Aroclor1260-

associated TASH (36, 51-53, 67). These studies reported decreased protein kinase B (Akt)/mTOR and extracellular signal-regulated kinases (ERK) signaling. AK3L1 is a downstream EGFR target that regulates glycolysis, thereby adding a new link between signaling disruption and intermediary metabolism (70). Intriguingly, p38γ and PKCα regulate both EGF-dependent ERK signaling (71-73) and NASH (74, 75). The potential mechanistic roles of these kinases warrant future investigation in Aroclor1260-associated TASH.

The observed alterations in GO processes related to hepatic metal hemostasis and cytoskeleton for PCB126 could be mechanistic. PCB126-induced metal dysregulation has been described previously (76, 77). However, the specific effector proteins identified by the present study (e.g., hepcidin, ferritin, zinc transporter 4, etc.) and the hepcidin-regulating transcription factor, ZFPM1(78) , warrant future investigation. Several cytoskeleton proteins were the most upregulated proteins by PCB126. The other exposures were associated with altered abundance of keratins 2, 4, 5, or 6a. Cellular localization analysis of a previous hepatic proteomics experiment from our group demonstrated that cytoskeletal-associated proteins were the top enriched cellular location for liver proteins differentially regulated by Aroclor1260 in mice fed a control diet, but this decreased in HFD-fed mice (51). Circulating epithelial cell-derived keratin18 was associated with PCB-related TASH in ACHS (6). Ethanol-associated alterations of the hepatocyte cytoskeleton may influence the progression of alcohol-related steatohepatitis (79). Therefore, the potential mechanistic role of PCB-induced cytoskeletal changes in TASH warrants future investigation. If the observed

reduction in hepatic AST protein abundance is confirmed in humans, the utility of circulating AST enzyme activity as a biomarker for PCB-related liver toxicity in environmental epidemiology studies would be reduced. Several GO processes uniquely enriched with Aroclor1260 + PCB126 co-exposure were discovered, including the epigenetic regulation of gene expression and the localization of macromolecules including proteins.

IPF analysis of the PCB126 and Aroclor1260 + PCB126 exposure groups revealed overconnected interactions with several transcription factors regulating myriad processes involved in the resolution and repair of liver injury including inflammation, stellate cell plasticity and fibrosis, stem cells, proliferation, differentiation, metabolism, and transformation. These transcription factors are new targets for PCB hepatotoxicity in NASH and include ETS1 (80, 81), SOX17 (82, 83), GABPα (80, 84), c-FOS (85), ZFX (86), N-Myc (87), and AML1 (81). While tumors were not observed in the present study, the identification of oncogenes is not surprising because PCB126 has previously been associated with liver cancer. Although Cyp1a2 message and protein were induced by PCB126 and Aroclor1260 + PCB126, MetaCore analyses provided no evidence to support the potential AhR-dependence in any of the identified GO processes. Moreover, IPF analysis did not identify AhR as an overconnected transcription factor. While this could simply be a limitation of the software package, future studies are required to determine the AhR-dependence of PCB-related TASH.

Aroclor1260 and PCB126 did not result in either additive hepatotoxicity or additive differential protein abundances in this chronic, diet-induced NAFLD

model. Hepatic protein abundance is a function of protein synthesis, degradation and transport into and out of the liver. Epigenetics-related GO processes were enriched in the Aroclor1260 + PCB126 exposure group, and this may have influenced the synthesis rates of specific hepatic proteins. The abundance of multiple epigenetics-related proteins was reduced including histone deacetylase 2; histones H1.2, H1.4, H1.5, and H1t; RNA polymerase-associated protein CTR9 homolog; RNA binding protein 3; and LIM domain-containing protein 1 and protein arginine methyltransferase 7). The proteins are involved in numerous epigenetics processes including histone acetylation, methylation, and microRNAs. IPF demonstrated overconnected interactions with the methyltransferase, PRMT1, and the several transcription factors associated with the epigenetic regulation of gene expression such as ETS1 and GABPα (80).

The abundance of other proteins involved in epigenetics and the regulation of gene expression was altered in the other treatment groups (e.g., the noncanonical poly(A) RNA polymerase PAPD5, Table 3) in Aroclor1260). Future studies are required to establish the mechanistic importance of epigenetic mechanisms in the genesis, progression, and potential heritability of PCB-related liver diseases.

Although perhaps the most comprehensive analysis of different chronic PCB exposures in an animal model of NAFLD, the present study is not without its limitations. Most notably, while proteins regulating metal homeostasis and epigenetics were implicated, direct measurement of hepatic metals and epigenetic signatures was not performed. While we previously published a

proteomics analyses in the HFD plus Aroclor1260 TASH model (51), the present experiment utilized a different, and potentially more sensitive, proteomics technique (TMT labeling) as well as different analytic procedures. This may limit the comparability of results between studies, and as a result, the MetaCore outcomes may vary. Sex differences were previously reported for Aroclor1260-induced TASH (36), with female mice being more susceptible. Because male mice were utilized in the present study, potential sex differences for PCB126 and Aroclor1260 + PCB126 exposures in TASH remain unknown. While Aroclor1260 + PCB126 exposures were associated with a pancreatic pathology resembling diabetic exocrine pancreatopathy in an acute model (51), the present study did not evaluate pancreatic endpoints because GTT was unchanged.

In conclusion, the present study demonstrated the complexity of the hepatic effects of PCB mixtures. DL PCBs, NDL PCBs, and a more environmentally relevant mixture of both types of PCBs differentially modulated the hepatic proteome and the severity of diet-induced NAFLD. Aroclor1260 increased hepatic inflammation and phosphoprotein signaling disruption consistent with prior research. PCB126 decreased hepatic inflammation and fibrosis at the molecular level. Mechanisms including altered cytoskeletal remodeling, metal homeostasis, and disruption of intermediary and xenobiotic metabolism were implicated in PCB126's mode of action, and all have been previously reported. Neither the histologic nor the proteomic effects of Aroclor1260 and PCB126 were additive in the co-exposure model. PCB126 attenuated Aroclor1260-induced hepatic inflammation but increased hepatic free fatty acids while reducing

plasma lipids. The overwhelming majority of differentially regulated hepatic proteins associated with Aroclor1260 + PCB126 exposure were not associated with either Aroclor1260 or PCB1260 exposure. Likewise, most proteins associated with either Aroclor1260 or PCB126 exposures were not associated with co-exposure to both. Despite this, many of the top GO processes and overconnected interactions by protein function were common to the PCB126 and Aroclor1260 + PCB126 exposure groups. These conserved processes were broadly related to metabolism and cellular organization and localization. A complex web of overconnected transcription factors broadly regulating metabolism; liver injury and inflammation; and liver repair was identified. Aroclor1260 + PCB126 exposure was strongly associated with multiple epigenetic processes, and these could potentially explain the observed nonadditive effects of the exposures on the hepatic proteome. When compared with our recently published acute study investigating the same PCB exposures, the modifying effect on diet (and possibly duration) on PCB-induced hepatotoxicity is also demonstrated. More data including translational research are required on potential modes of PCB action in NAFLD including phosphoprotein signaling disruption; abnormal metal homeostasis; cytoskeletal remodeling; and transcriptional reprogramming by epigenetic mechanisms. Likewise, potential sex differences and the AhR-dependence of PCB126's NAFLD modifying effects warrant future investigation.

CHAPTER 3

AHR PLAYS A PIVOTAL ROLE IN REGULATING HEPATIC PROTEOME

AND LIPID METABOLISM

INTRODUCTION

As a highly stable chemical, polychlorinated biphenyls (PCBs) were used in

industrial and commercial applications, such as coolant fluids, transformers

and they were commercially produced Both contraction of HIK and PE have been

normalized to length. in the United States from 1929 to 1979. Although the

production of PCBs is banned by the US government, 1.3 million tons of PCBs

were produced, consisting of 130 individual congeners, which has an

association with a variety of conditions, especially like non-alcoholic fatty liver

disease (NAFLD), diabetes and hypertension. According to the National

Health and Nutrition Examination Survey (NHANES), PCBs can be detected in

the serum of 100% American adults (38).

PCBs have been categorized into two major classes: coplanar and

noncoplanar PCBs. The former have none or only one chlorine atom attached

to the ortho-position of biphenyl rings, called non-ortho and mono-ortho PCBs,

respectively. Coplanar PCBs like PCB 126 can activate the aryl hydrocarbon

receptor (AhR), and they are also called dioxin-like (DL) PCBs, causing a

response similar to TCDD. Non-coplanar PCB congeners, known as non-dioxin-like (NDL) PCBs, have two or more chlorine atoms at the ortho-position, and do not have dioxin-like properties, which can activate the constitutive androstane receptor (CAR) (44). Aroclor 1260 is a commercial mixture of PCBs manufactured by Monsanto, a well-known PCB manufacturer in Anniston, Alabama, containing an average chlorine content of 60%. Mostly, it contains NDL-PCB, and the PCB profiles in Aroclor 1260 best mimic the PCBs present in human adipose tissue (45). Although Aroclor 1260 contains small amounts of DL-PCBs, it cannot activate human or murine AhR (2, 45).

PCBs are found to be associated with NAFLD either in human studies and in animal studies, and NAFLD is a progressive condition with a broad spectrum ranging from simple steatosis, non-alcoholic steatohepatitis (NASH), liver cirrhosis, hepatocellular carcinoma (HCC) with multiple pathogenic factors such as fat accumulation, occupational and environmental chemicals. In 2019, we firstly raised the term of the toxicant-associated fatty liver disease (TAFLD) and/or toxicant-associated steatohepatitis (TASH) to describe this condition (29). Apart from AhR, our group found PCB receptors involved with CAR, pregnane-xenobiotic receptor (PXR), and epidermal growth factor receptor (EGFR) in TASH in the last a few years.

As a ligand-binding activated transcription factor, the AhR regulates a variety of physiological and pathological function (88). The activation of AhR induces the transcription of many genes, such as the cytochrome P4501A (*CYP1A*) family involved in carcinogenesis. The high-affinity binding agonists for AhR

include 2,3,7,8-tetrachlorodibenzo-p-dioxin (TCDD), 1,2-benzo[a]pyrene (BA) and DL-PCBs. While, low-affinity binding agonists for AhR are flavonoids and indoles, endogenous bilirubin and tryptophan metabolites, and products of the microflora (89). Apart from regulation of immunity, stem cell maintenance and cellular differentiation (89), AhR activation also is involved in the processes of glucose and lipid metabolism. Over-activation of AhR (33) or constitutively activated AhR (90) induces hepatic steatosis via upregulation of fatty acid transport genes, such as *CD36/FAT*. Alteration of hepatic fatty acid composition (91) and decreased fatty acid oxidation (92) contribute to AhR ligand-induced liver toxicity and steatosis. Some publications showed AhR deficiency has a protective effect against high fat diet-induced obesity, and mitigates hepatic steatosis (34, 93). On the other hand, liver-specific AhR knockout mice are susceptible to HFD-induced hepatic steatosis, inflammation and injury (94), suggesting AhR activation protects against fatty liver disease. There is also a report that Ahr$^{-/-}$ mice developed spontaneous microvesicular lipidosis (35). The exact role of AhR activation plays in regulating hepatic proteome and lipid metabolism needs to be elucidated.

MATERIALS AND METHODS

Animal studies

The related animal protocol was approved by the University of Louisville Institutional Animal Care and Use Committee. Adult male C57BL/6 mice and Ahr$^{-/-}$ mice (8-9 weeks old) were purchased from Taconic Biosciences Laboratory and distributed into four equal groups (n=10): WT Vehicle group, WT PCB 126 group, Ahr$^{-/-}$ Vehicle group and Ahr$^{-/-}$ PCB126 group. All mice were fed a control synthetic diet (20.0 %, 69.8 %, and 10.2 % of total calories come from protein, carbohydrate, and fat, TekLad TD 06416). At 10 weeks of age, 10 mice in each group were given either corn oil, or PCB126 (20 μg/kg) via a one-time gavage and followed for 2 weeks (Fig. 3.1). Dual energy X-ray absorptiometry (DEXA) scanning (Lunar PIXImus densitometer, WI) was performed to analyze body fat composition before euthanasia. Whole blood for plasma, liver, and fat tissue samples were collected after euthanasia.

Histological staining

Liver tissues were fixed in 10% Neutral Buffered Formalin for 72 hours and embedded in paraffin for routine histological examination. Hematoxylin-eosin (H&E) staining was performed to identify histopathological changes. Oil Red O stain was used to evaluate lipid accumulation according to the manufacturer's protocols. Micrographic images were acquired by a high-resolution Olympus digital scanner with an Olympus digital camera (BX41).

Real-time PCR

Mouse liver tissues were homogenized and total RNA was extracted using

RNA-STAT 60 according to the manufacturer's protocol. The purity and quantity of total RNA were assessed with a Nanodrop spectrometer (ND-1000, Thermo Fisher Scientific, Wilmington, DE) using ND-1000 V3.8.1 software and cDNA was reverse transcribed from 1 ug RNA with a one-step cDNA synthesis reagent (QScript cDNA Supermix, QuantaBio, Beverly, MA). Then RT-PCR was performed on the CFX384™ Real-Time System (Biorad, Hercules, CA) using iTaq Universal probe Supermix and Taqman probes as described previously (36). All reactions were run triplicately. The relative mRNA expression was calculated using the comparative $2^{-\triangle\triangle Ct}$ method and normalized against GAPDH mRNA.

Measurement of hepatic lipids, plasma lipids and cytokines

The liver tissues were rinsed in 1× phosphate buffered saline (PBS) and homogenized in 50 mM NaCl solution. Hepatic lipids were extracted by a mixed solution of chloroform and methanol (2:1) according to a published protocol (56). Hepatic triglycerides and free fatty acid contents were assessed using commercial kits with final values normalized to liver weight. Plasma alanine transaminase (ALT), aspartate transaminase (AST), cholesterol, triglyceride, high-density lipoprotein (HDL), low-density lipoprotein (LDL), very low-density lipoprotein (VLDL), and non-HDL cholesterol (nHDLc) levels were determined with lipid panel plus kits on a Piccolo Xpress Chemistry Analyzer (Abbott Laboratories, IL). Plasma cytokine and adipokine levels were evaluated using a customized Milliplex® MAP mouse adipokine Panel on a Luminex® 100 system (Luminex Corp, Austin, TX).

Proteomics Analysis

Proteins were extracted from liver tissues in RIPA buffer with protease and phosphatase inhibitors using a bead homogenizer and protein amounts were measured by BCA assay. Protein lysates (200 μg) were trypsinized using the modified Filter-Aided Sample Preparation (FASP) method (57) and enriched for phosphopeptides by the method of TiO2-SIMAC-HILIC (TiSH) (58). Firstly, protein samples were reduced by dithiothreitol, denatured by 8M urea and alkylated by iodoacetamide, then they were centrifuged through a high molecular weight cutoff centrifugal filter (Millipore, 10k MWCO). Next, after overnight digestion with sequencing grade Trypsin (Promega), the digested proteins were collected and cleaned with a C18 Proto™ 300 Å Ultra MicroSpin column. Digested protein samples (50 μg) were labeled with tandem mass tag (TMT) TMT10plex™ Isobaric Label Reagent Set (Thermo Fisher, Waltham, MA), then were concentrated and desalted with Oasis HLB Extraction cartridges (Waters Corporation, Milford, MA) using a modified protocol for extraction of the digested peptides (59). Then samples were separated by high pH reversed phase separation with fraction concatenation on a Beckman System Gold LC system supplemented with 126 solvent module and 166 detector in tandem with a BioRad Model 2110 Fraction Collector (60). Liquid Chromatography/Mass Spectrometry (LC/MS) was used to measure TMT-Labeled peptides. Briefly, every high pH reversed phase fraction was dissolved in 50 μL solution of the combination of 2% v/v acetonitrile/ 0.1% v/v formic acid and 1 μL of each fraction was analyzed on EASY-nLC 1000 UHPLC system (Thermo Fisher) and an Orbitrap Elite – ETD mass spectrometer (Thermo Fisher Scientific, Waltham, MA,

USA). The raw data from the mass spectrometer were analyzed by Proteome Discoverer v2.2.0.388.

Statistical analysis and data sharing

Statistical evaluation was performed by two-way analysis of variance (ANOVA) using GraphPad Prism version 7.02 for Windows (GraphPad Software Inc., La Jolla, CA, USA). P <0.05 was considered statistically significant. Statistical analysis for the proteome data was carried out using the R package as described previously (62). Significantly altered proteins were further filtered with an FDR threshold of 0.2 and proteins exhibiting a fold change of -0.5<$\log_2$FC< 0.5 were rejected to eliminate false positives. Hepatic proteins that had significance abundance were imported into MetaCore software (Clarivate Analytics, Philadelphia, PA) for the further analyses: gene ontology (GO process), enrichment by protein function (EPF), and interaction by protein function (IPF). Proteomics data files were deposited with MassIVE (http://massive.ucsd.edu/) data repository, Center for Computational Mass Spectrometry at the University of California, San Diego and shared with the ProteomeXchange (www.proteomexchange.org).

**Control Diet
& Oral Gavage**

Week 0

2

**Male C57BL/6 Mice/ Ahr$^{-/-}$Mice
Age: 10 weeks**

**Euthanize Mice and
sample collection**

1. WT Vehicle: corn oil	**2. WT PCB 126: 20µg/kg**
3. Ahr$^{-/-}$ Vehicle: corn oil	**4. Ahr$^{-/-}$ PCB 126: 20µg/kg**

Figure 3.1. Experimental Design of acute AhR knockout study.

Mice were divided into 4 study groups based on the type of exposure. All animals were fed a chow diet and received a one-time gavage of their respective dose at the beginning of the study.

65

RESULTS

Effects of PCB126 exposure and Ahr^{-/-} on body composition, glucose tolerance, plasma lipids

Body fat composition was measured using Dexascan and white adipocyte tissue weight was evaluated by weighing the harvested epididymal fat. Body weight was measured weekly throughout the 2-week study. There was a gradual increase in body weight in PCB126-free groups from Week 0 to Week 2, while the weight of PCB 126 exposure mice groups did not change significantly, suggesting PCB126 had an effect of decreasing body weight, which was showed in percentage change in body weight (Fig. 3.2A, 2B & 2C). Compared to wildtype (WT) mice, Ahr^{-/-} mice had lower body weight, lower liver weight/body weight ratio, decreased lean body mass percentage and higher body fat composition. (Fig. 3. 2C, 2D, 2E & 2F). Additionally, Ahr^{-/-} mice also showed higher pancreas weight/body weight ratio (Fig. 3.2G). These results showed AhR deprivation caused or deteriorated lipid accumulation. A glucose tolerance test was performed to evaluate whether PCB126 or AhR gene knockout affects glucose metabolism; GTT curve and AUC graph showed PCB126 exposure groups had significant lower AUC, suggesting PCB126 improves glucose uptake (Fig. 3.2I & 2J). PCB126 exposure and Ahr^{-/-} effects on plasma lipids were also evaluated. Although there was no significant differences in plasma LDL-c between groups (Fig. 3.2N), AhR gene deletion caused a trend to decrease plasma VLDL (p=0.06) (Fig. 3.2O), meanwhile, Ahr^{-/-} mice groups had significantly decreased plasma cholesterol, HDL-c, and

glucose levels (Fig. 3.2K, L & M). Apart from these above, AhR gene ablation had the effect of lowering the plasma triglyceride in Ahr$^{-/-}$ mice. (Fig. 3.2P).

Effects of PCB126 exposure and Ahr$^{-/-}$ on hepatic steatosis, associated hepatic gene expression, hepatic lipids and liver enzymes

Hepatic steatosis was evaluated by H&E stain of liver sections. WT PCB126 group developed small droplet macrovesicular steatosis, while Ahr$^{-/-}$ Vehicle and Ahr$^{-/-}$ PCB126 groups both showed severe centrilobular, large droplet macrovesicular steatosis. No significant difference was found between these two groups in the severity of steatosis by H&E stain (Fig. 3.3A). To confirm the results further from H&E stain, Oil Red O stain was performed. WT PCB126 group developed a few lipid droplets (Red spots), while Ahr$^{-/-}$ Vehicle and Ahr$^{-/-}$ PCB126-exposed groups demonstrated much more larger lipid droplets (Fig. 3.3B). The expression of hepatic genes related to lipid metabolism like *Cd36*, *Pnpla3* and *Perilipin-2* were evaluated by RT-PCR. Both PCB126 exposure and Ahr$^{-/-}$ increased the expression levels of *Cd36*, promoting hepatic lipid uptake (Fig. 4.3E), while global AhR deletion decreased the expression of *Pnpla3*, essential for lipid hydrolysis (Fig. 3.3F). Apart from these genes above, the mRNA expression levels of *Perilipin-2*, which relates to the formation of lipid droplets, was upregulated by Ahr$^{-/-}$ (Fig. 3.3G). Additionally, the mRNA expression level of tyrosine aminotransferase (Tat) gene, a target gene of Glucocorticoid receptor (GCR) was evaluated by RT-PCR. Ahr$^{-/-}$ also increased the expression of Tat gene, meanwhile, there was a trend that PCB126 also upregulated Tat mRNA expression (p=0.06) (Fig. 3.3H). Hepatic lipids were

measured biochemically to further evaluate hepatic steatosis. Both $Ahr^{-/-}$ and PCB126 increased the hepatic triglyceride (Fig. 3.3J). Meanwhile whole AhR ablation increased hepatic free fatty acids. (Fig. 3.3K). There was a trend for PCB126 to increase hepatic cholesterol level (p=0.05) (Fig. 3.3I). As for liver enzymes, $Ahr^{-/-}$ significantly increased plasma ALT and AST levels, showing whole AhR gene deletion caused hepatic injury (Fig. 3.3C & D).

Effects of PCB exposure and $Ahr^{-/-}$ on hepatic expression of AhR, Pxr, Car and their target genes

The activation of AhR, Pxr, Car and their target genes was assessed by RT-PCR. As expected, compared to WT Vehicle group, $Ahr^{-/-}$ groups showed totally inhibited AhR mRNA expression ($2^{-\Delta\Delta Ct}$ value from 1.02 in WT Vehicle group to 0 in $Ahr^{-/-}$ Vehicle and $Ahr^{-/-}$ PCB126 group, both p<0.01), suggesting the AhR knockout was achieved (Fig. 3.4A). As for the target genes of AhR: Cyp1a1 and Cyp1a2, AhR ablation had the effect on downregulating the mRNA expression of both genes (both p<0.01). (Fig. 4.4B & C). Although AhR mRNA level was not significantly increased, Cyp1a1 and Cyp1a2 were upregulated significantly by PCB126 (2615.6-fold & 10.6-fold), indicative of AhR activation (Fig. 3.4B & C). With regards to Pxr gene and its target gene (Cyp3a11) expression, AhR gene depletion showed the effect of upregulating Pxr and Cyp3a11 mRNA expression (p=0.01 and p<0.01) (Fig. 3.4D &E); compared to WT Vehicle, the expression of Pxr in $Ahr^{-/-}$ Vehicle and $Ahr^{-/-}$ PCB126 group increased by 1.39 (p=0.07) and 1.51 fold (p=0.01), while the expression of Cyp3a11 in $Ahr^{-/-}$ Vehicle and $Ahr^{-/-}$ PCB126 group upregulated by 4.32 fold and 4.73 fold (both p<0.01), indicative of Pxr

activation. Meanwhile PCB126 also showed a trend to increase Pxr gene expression (p=0.05) (Fig. 3.4F & G). Both Ahr$^{-/-}$ Vehicle and Ahr$^{-/-}$ PCB126-exposed groups had increased Cyp2b10 (the target gene of Car) mRNA levels (35.29-fold, *p*=0.00 and 44.44-fold, *p*=0.01 respectively vs WT Vehicle), consistent with Car activation, despite the decreased level of Car mRNA expression (Fig. 3.4F & G).

Effects of PCB126 exposure and Ahr$^{-/-}$ on plasma adipo-cytokines

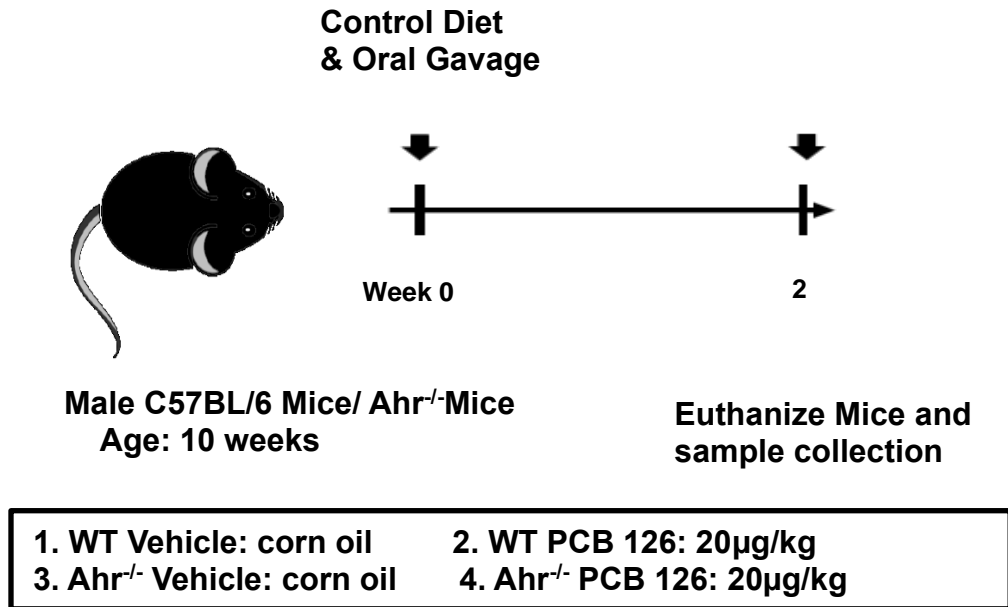Plasma adipo-cytokine levels were determined using a customized Milliplex® MAP mouse adipokine Panel on a Luminex® 100 system (Luminex Corp, Austin, TX). AhR ablation had effect of decreasing the level of IL-6 (Fig. 3.5A), Ahr$^{-/-}$ Vehicle showed a lower IL-6 level than WT Vehicle, while there was no significant difference of PAI-1 and MCP-1 levels between the groups (Fig. 3.5C & F). Meanwhile, AhR knockout decreased the levels of plasma insulin and resistin (Fig. 3.5B & E), but increased the level of leptin (Fig. 3.5D), suggesting the improvement of insulin resistance.

Effects of PCB126 exposure and Ahr$^{-/-}$ on hepatokine expression

Protective hepatokines (e.g. Fgf21, Igf1, and betatrophin) were measured by RT PCR. AhR gene deletion resulted in increasing Fgf21 expression, while both Ahr$^{-/-}$ and PCB126 exposure decreased the expression of *betatrophin*. With respect to Igf1, PCB126 slightly increased the expression, but there was a trend for Ahr$^{-/-}$ mice to downregulate the Igf1 expression (*p*=0.07) (Fig. 3.6A, B&C).
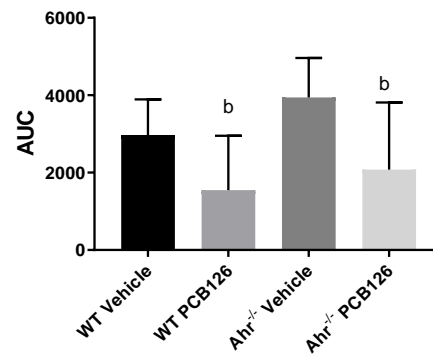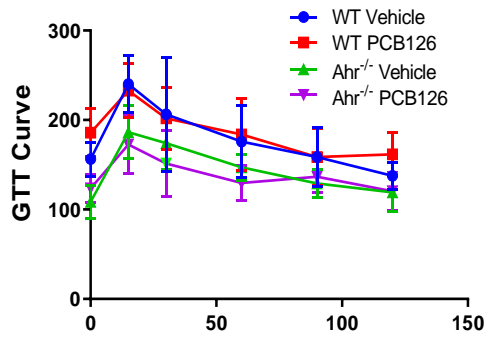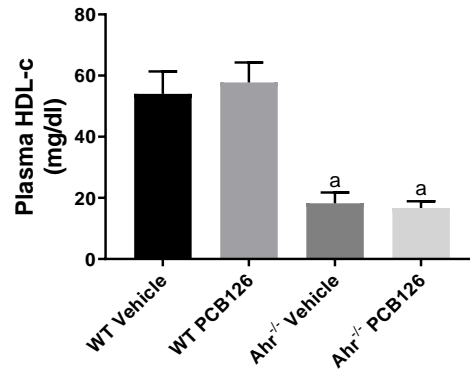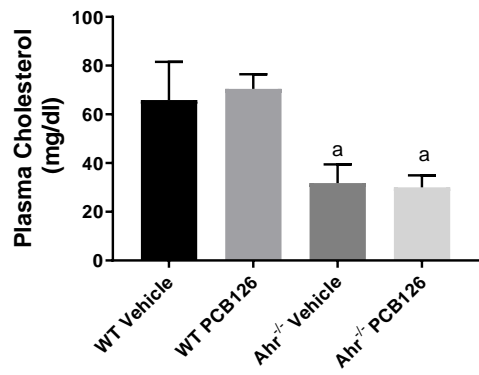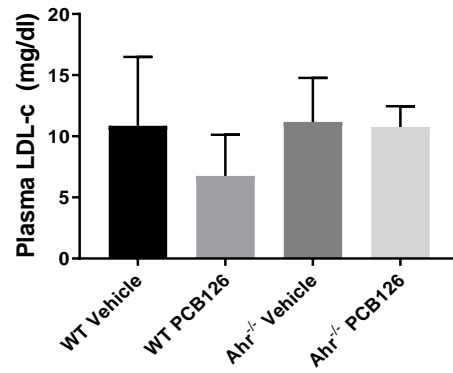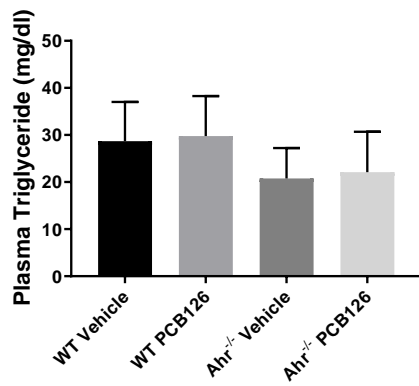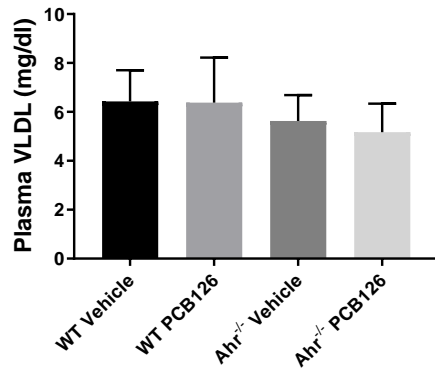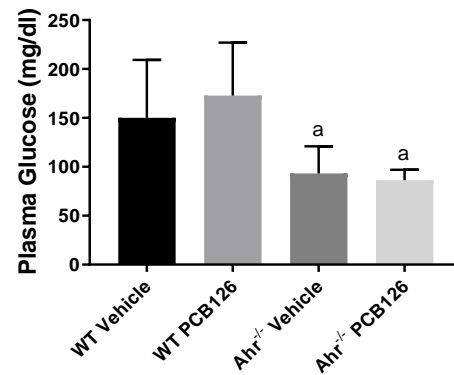
70

I

J

K

L

M

N

O

P

<div align="center">

***p*-value**

</div>

Outcome	Ahr⁻/⁻	PCB126	Interaction	WT (PCB126 vs. Vehicle)	Ahr⁻/⁻ (PCB126 vs. Vehicle)	Vehicle (Ahr⁻/⁻ vs. WT)	PCB126 (Ahr⁻/⁻ vs. WT)
% Change in BW	0.26	**0.01**	0.13	0.75	**0.01**	0.99	0.25
Body weight	**<0.01**	0.81	0.41	0.87	0.97	**0.00**	**<0.01**
Fat Composition	**<0.01**	0.73	0.68	>0.99	0.95	**0.00**	**0.01**
LW/BW	**<0.01**	0.66	0.67	>0.99	0.92	**<0.01**	**<0.01**
% Lean Body Mass	**<0.01**	0.78	0.64	0.95	1.00	**0.00**	**0.01**
PW/BW	**<0.01**	0.24	0.77	0.71	0.92	**<0.01**	**<0.01**
WATW/BW	**0.02**	0.48	0.54	>0.99	0.80	0.56	0.15
AUC	0.16	**0.00**	0.45	0.23	>0.99	**<0.01**	**<0.01**
Plasma Cholesterol	**<0.01**	0.66	0.31	0.73	0.98	**<0.01**	**<0.01**
Plasma HDL-c	**<0.01**	0.60	0.20	0.55	0.95	**<0.01**	**<0.01**
Plasma TG	**0.01**	0.65	0.96	0.99	0.98	0.16	0.20
LDL-c	0.21	0.19	0.28	0.23	1.00	1.00	0.39
VLDL	0.06	0.63	0.70	1.00	0.93	0.68	0.39
Plasma Glucose	**<0.01**	0.56	0.28	0.65	0.98	**0.02**	**0.00**

Figure 3.2. Effects of PCB126 exposure and Ahr$^{-/-}$ on body composition, glucose tolerance, plasma lipids.

(A, C) Body weight was measured weekly throughout the 2-week study. AhR$^{-/-}$ mice had a significant lower body weight than WT mice. (B) % change in body weight relative to the initial body weight taken at the beginning of the study was calculated. (D) the body fat composition was measured by calculating the white adipose tissue weight to body weight ratio. Liver weight (LW) and White adipose tissue (WAT) weight were measured, and WATW/BW was calculated by the epididymal fat weight divide body weight. (E & G) The liver and pancreas were weighed and their respective weights relative to body weight were calculated. (F) % lean body mass was calculated by lean body mass divide body fat weight. Lean body mass= Body weight – body weight * % body fat percentage. A glucose tolerance test was performed after the second PCB gavage and blood glucose levels were measured; (I) GTT curve was made and (J) AUC (Area Under the Curve) of four groups was calculated. （K）Plasma cholesterol, (L) Plasma HDL-c, (M) Plasma triglyceride, (N) Plasma LDL-c, (O) Plasma VLDL, and (P) Plasma glucose were measured by Piccolo Xpress chemical analyzer. Values are mean ± SD. Values for $p < 0.05$ are in bold, a – Ahr$^{-/-}$ effect, b – PCB126 effect, c – interaction between Ahr$^{-/-}$ effect and PCB126 exposure.

A

WT Vehicle

WT PCB126

Ahr$^{-/-}$ Vehicle

Ahr$^{-/-}$ PCB126

B

WT Vehicle

WT PCB126

Ahr$^{-/-}$ Vehicle

Ahr$^{-/-}$ PCB126

| | **p-value** | | | | | | |
Outcome	Ahr^{-/-}	PCB126	Interaction	WT (PCB126 vs. Vehicle)	Ahr^{-/-} (PCB126 vs. Vehicle)	Vehicle (Ahr^{-/-} vs. WT)	PCB126 (Ahr^{-/-} vs. WT)
Plasma ALT	**0.00**	0.66	0.96	0.99	0.98	**0.03**	**0.02**
Plasma AST	**<0.01**	0.63	0.84	1.00	0.96	**<0.01**	**<0.01**
Cd36	**<0.01**	**0.03**	0.53	0.24	0.63	**<0.01**	**<0.01**
Pnpla3	**0.03**	0.26	0.29	0.43	>0.99	0.10	0.83
Perilipin-2	**<0.01**	0.63	0.34	0.99	0.72	0.08	**0.00**
Tat	**0.00**	0.06	0.71	0.38	0.65	**0.02**	0.10
Liver Cholesterol	0.35	0.05	0.64	0.71	0.30	0.99	0.75
Liver TG	**<0.01**	**0.04**	0.09	1.00	**0.04**	**<0.01**	**<0.01**
Liver FFA	**0.00**	0.23	0.70	0.64	0.94	0.05	0.22

Figure 3.3. Effects of PCB126 exposure and Ahr^{-/-} on hepatic steatosis, expression of genes related to lipid metabolism, hepatic lipids and liver enzymes.

Hepatic steatosis was evaluated using (A) hematoxylin-eosin (H&E) staining of liver sections and hepatic lipids (G-H). (B) Oil Red O stain was performed to confirm the existence of neutral triglyceride and lipids on frozen sections. (C) Plasma ALT and (D) Plasma AST were measured to indicate hepatic injury using Piccolo Xpress chemical analyzer. (E) *Cd36*, (F) *Pnpla3*, (G) *Perilipin-2*, and (H) *Tat* mRNA expression levels were evaluated by RT-PCR. (I) Hepatic cholesterol, (J) Hepatic triglyceride, (K) Hepatic free fatty acid and were analyzed. Values are mean ± SD. Values for $p < 0.05$ are in bold, a - Ahr^{-/-} effect, b – PCB126 effect, c – interaction between Ahr^{-/-} effect and PCB126 exposure.

A AhR (Fold induction)

B Cyp1a1 (Fold Induction)

C Cyp1a2 (Fold Induction)

D Pxr (Fold induction)

E Cyp3a11 (Fold Induction)

F Car (Fold induction)

G Cyp2b10 (Fold induction)
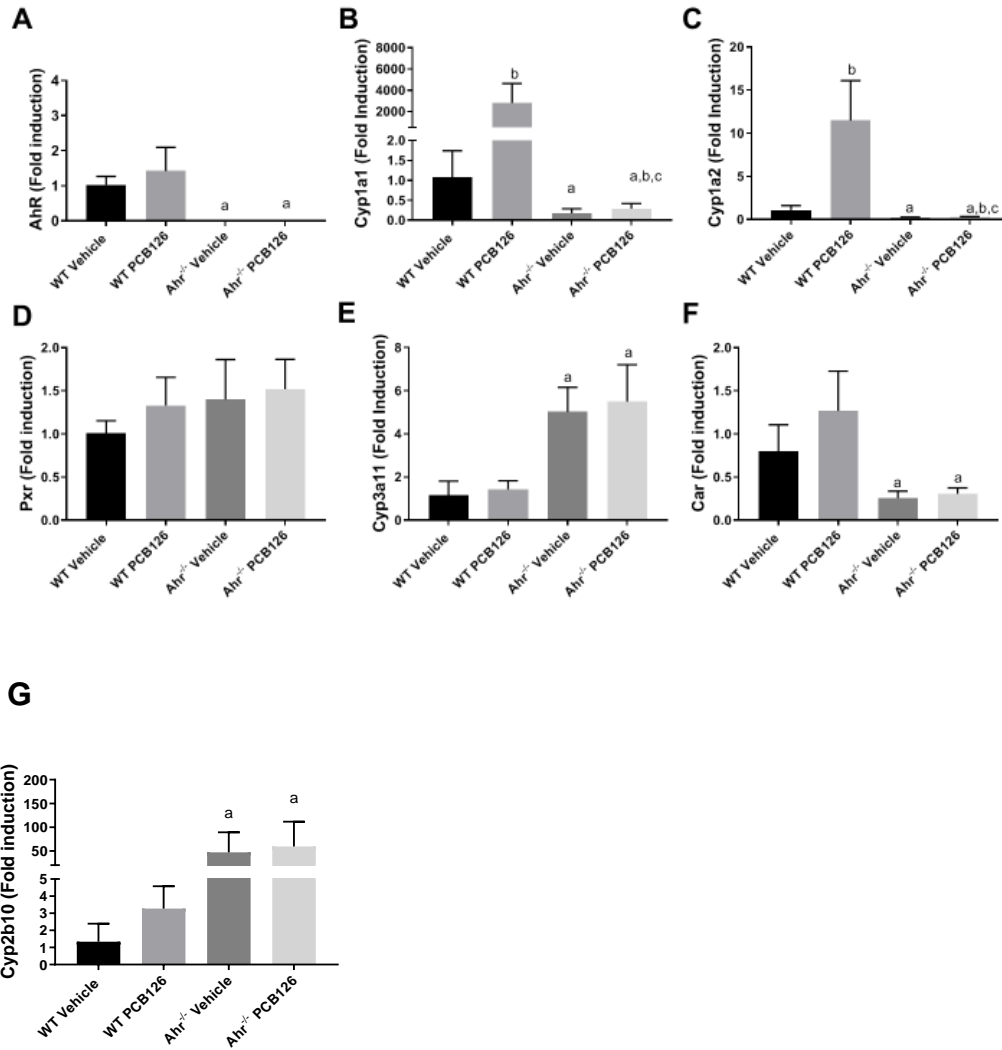
p-value

Outcome	Ahr$^{-/-}$	PCB126	Interaction	WT (PCB126 vs. Vehicle)	Ahr$^{-/-}$ (PCB126 vs. Vehicle)	Vehicle (Ahr$^{-/-}$ vs. WT)	PCB126 (Ahr$^{-/-}$ vs. WT)
AhR	**<0.01**	0.17	0.17	0.23	>0.99	**<0.01**	**<0.01**
Cyp1a1	**<0.01**	**<0.01**	**<0.01**	**<0.01**	>0.99	>0.99	**<0.01**
Cyp1a2	**<0.01**	**<0.01**	**<0.01**	**<0.01**	>0.99	0.82	**<0.01**
Pxr	**0.01**	0.05	0.36	0.19	0.86	0.07	0.62
Cyp3a11	**<0.01**	0.30	0.77	0.95	0.77	**<0.01**	**<0.01**
Car	**<0.01**	**0.01**	**0.02**	**0.00**	0.98	**0.00**	**<0.01**
Cyp2b10	**<0.01**	0.97	0.85	1.00	1.00	**0.00**	0.01

Figure 3.4. Effects of PCB126 exposure and Ahr$^{-/-}$ on hepatic expression of AhR, Pxr, Car and their target genes.

The expression of AhR, Pxr, Car and their target genes were assessed by RT-PCR. (A) Hepatic AhR mRNA expression & the expression of its target genes: (B) *Cyp1a1*, (C) *Cyp1a2.* (D) Hepatic Pxr mRNA expression and the expression of its target gene: (E) *Cyp3a11*. (F) Car mRNA expression and the expression of its target gene: (G) *Cyp2b10*. Values are mean ± SD. Values for $p < 0.05$ are in bold, a - Ahr$^{-/-}$ effect, b – PCB126 effect, c – interaction between Ahr$^{-/-}$ effect and PCB126 exposure.
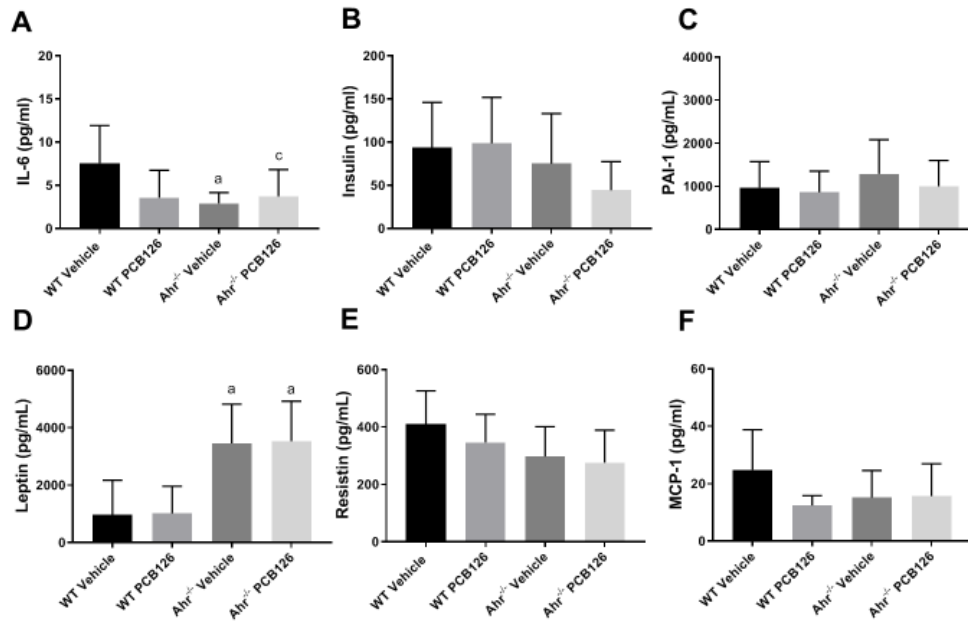
p-value

Outcome	Ahr$^{-/-}$	PCB 126	Interaction	WT (PCB126 vs.Vehicle)	Ahr$^{-/-}$ (PCB126 vs.Vehicle)	Vehicle (Ahr$^{-/-}$ vs.WT)	PCB126 (Ahr$^{-/-}$ vs.WT)
IL-6	**0.04**	0.14	**0.03**	0.06	0.95	**0.02**	1.00
Insulin	**0.01**	0.64	0.41	1.00	0.79	0.56	0.08
PAI-1	0.27	0.34	0.67	0.98	0.74	0.70	0.96
Leptin	**<0.01**	0.89	0.97	1.00	1.00	**0.00**	**0.00**
Resistin	**0.01**	0.22	0.53	0.56	0.97	0.10	0.50
MCP-1	0.34	0.08	0.06	0.06	1.00	0.17	0.90

Figure 3.5. Effects of PCB126 exposure and Ahr$^{-/-}$ on plasma adipo-cytokines.

Plasma adipo-cytokine levels were measured using a customized Milliplex®
MAP mouse adipokine Panel on a Luminex® 100 system (Luminex Corp,
Austin, TX), including IL-6 (A), Insulin (B), PAI-1 (C), Leptin (D), Resistin (E),
MCP-1 (F). Values are mean ± SD. Values for $p < 0.05$ are in bold, a - Ahr$^{-/-}$

effect, b – PCB126 effect, c – interaction between Ahr$^{-/-}$ effect and PCB126

exposure.

A
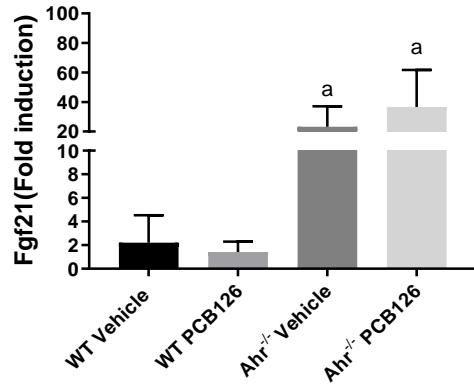
B
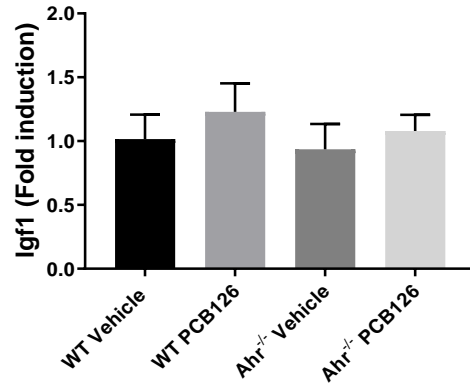
C
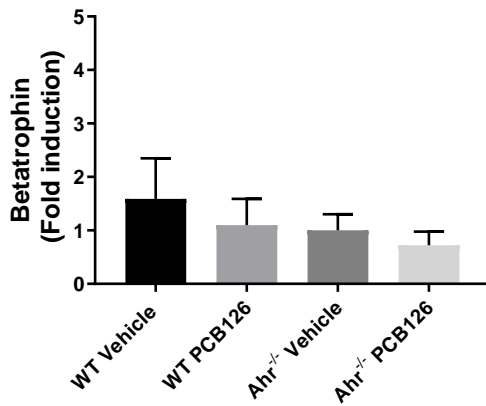
p-value

Outcome	Ahr$^{-/-}$	PCB126	Interaction	WT (PCB126 vs.Vehicle)	Ahr$^{-/-}$ (PCB126 vs.Vehicle)	Vehicle (Ahr$^{-/-}$ vs.WT)	PCB126 (Ahr$^{-/-}$ vs.WT)
Fgf21	**<0.01**	0.19	0.14	1.00	0.19	**0.01**	**<0.01**
Igf1	0.07	**0.01**	0.57	0.09	0.32	0.77	0.34
Betatrophin	**0.00**	**0.02**	0.50	0.17	0.53	0.06	0.30

Figure 3.6. Effects of PCB126 exposure and Ahr$^{-/-}$ on hepatokines expression.

Hepatic mRNA levels of Fgf21 (A), Igf1 (B), and betatrophin (C) were evaluated by RT-PCR. Values are mean ± SD. Values for $p < 0.05$ are in bold, a - Ahr$^{-/-}$ effect, b – PCB126 effect, c – interaction between Ahr$^{-/-}$ effect and PCB126 exposure.

Effects of PCB126 exposure and Ahr^{-/-} on the hepatic proteome

PCB126 exposure and AhR gene knockout produced distinct hepatic

proteomes. 5,075 unique proteins and their isoforms were detected, and

alterations in hepatic proteins were demonstrated by Volcano plots showing

significance (y-axis) versus protein fold change (x-axis) for comparisons

between these four groups. The graphs were denoted as follows: (A) B vs A:

WT PCB126 group vs WT Vehicle group, (B) C vs A: Ahr$^{-/-}$ Vehicle group vs

WT Vehicle group, (C) D vs A: Ahr$^{-/-}$ PCB126 group vs WT Vehicle group, (D)

D vs B: Ahr$^{-/-}$ PCB126 group vs WT PCB126 group & (E) D vs C: Ahr$^{-/-}$ PCB126

group vs Ahr$^{-/-}$ Vehicle group. Black denotes unaltered proteins, green denotes

significantly altered proteins, red denotes significantly upregulated protein with

($\log_2 FC \geq 1$), blue denotes significantly downregulated protein with ($\log_2 FC \leq -1$).

(F) A multi-dimensional scatter (MDS) plot depicting the pattern for protein

alterations in the different groups (Fig. 3.7A-F). The differentially abundant

hepatic proteins were listed at Table 4. The comparisons of hepatic abundance

proteins content between groups were regulated as follows: WT PCB126 group

vs WT Vehicle group (5 increased and 3 decreased), Ahr$^{-/-}$ Vehicle group vs

WT Vehicle group (279 increased and 61 decreased), Ahr$^{-/-}$ PCB126 group vs

WT Vehicle group (209 increased and 92 decreased), Ahr$^{-/-}$ PCB126 group vs

WT PCB126 group (185 increased and 77 decreased) and Ahr$^{-/-}$ PCB126

group vs Ahr$^{-/-}$ Vehicle group (0 increased and 0 decreased) (Fig. 3.7G). A

Venn diagram showed the number of overlapping proteins in different groups

compared with A (WT Vehicle group) (Fig. 3.7H).

PCB126 caused much less proteomic changes which are shown in Graph A (8 proteins) and Graph E (0 protein) than AhR deprivation in Graph B (301 proteins) and Graph C (262 proteins) (Fig. 3.7G). Notably, there were no alterations of proteins in Ahr$^{-/-}$ PCB126 group vs Ahr$^{-/-}$ Vehicle group, suggesting that without AhR gene involvement, PCB126 did not cause significant differentially abundance hepatic protein changes. 3 proteins were altered in all comparisons of groups except Ahr$^{-/-}$ PCB126 vs Ahr$^{-/-}$ Vehicle group , namely, cytochrome P450 1A2, Isoform 2 of cytochrome P450 2C50, and Fatty acid-binding protein 5, showing these proteins were affected by both AhR ablation and PCB126 exposure (Supplemental Table 2). Of the 340 abundant proteins in mice not exposed to PCB126 (Ahr$^{-/-}$ Vehicle vs WT Vehicle) regulated by AhR gene deletion, 91 proteins were unique (26.8%); of the 262 altered proteins in PCB126-exposed mice (Ahr$^{-/-}$ PCB126 vs WT PCB126) related to AhR deprivation, only 46 proteins were exclusive (17.6%).

EPF analysis was performed to evaluate the protein classes most impacted by PCB126 exposure or AhR gene deletion (Table 4). Enzymes were the most affected class (WT PCB126 vs WT Vehicle: z-score=6.423; Ahr$^{-/-}$ Vehicle vs WT Vehicle : z-score=17.84; Ahr$^{-/-}$ PCB126B vs WT PCB126: z-score=15.52). This ending was consistent with the results of abundance proteins which showed 6/8 proteins in WT PCB126 vs WT Vehicle regulated by PCB126 were enzymes and most of the proteins in other comparisons altered by AhR gene knockout also belong to enzymes (Supplemental Table 2). AhR knockout increased hepatic steatosis and injury (by histologic and plasma ALT and AST

enzyme activity biomarkers). The abundance proteins in the comparisons of

Ahr$^{-/-}$ Vehicle vs WT Vehicle and Ahr$^{-/-}$ PCB126 vs WT PCB126 related to AhR

ablation, indicating hepatic steatosis, hepatic injury and inflammation, were

upregulated. These proteins included Glutathione S-transferase A1 (Ahr$^{-/-}$

Vehicle vs WT Vehicle: Log$_2$FC=4.97, p=9.68E-09; Ahr$^{-/-}$ PCB126 vs WT

PCB126: Log$_2$FC=5.13, p=8.00E-08), Glutathione S-transferase Mu3 (Ahr$^{-/-}$

Vehicle vs WT Vehicle: Log$_2$FC=3.76, p=7.63E-09; Ahr$^{-/-}$ PCB126 vs WT

PCB126: Log$_2$FC=3.21, p=8.00E-08), Glutathione S-transferase A4 (Ahr$^{-/-}$

Vehicle vs WT Vehicle: Log$_2$FC=3.06, p=1.03E-08; Ahr$^{-/-}$ PCB126 vs WT

PCB126: Log$_2$FC=2.17, p=1.34E-06), Annexin A5 (Ahr$^{-/-}$ Vehicle vs WT

Vehicle: Log$_2$FC=2.35, p=9.70E-09; Ahr$^{-/-}$ PCB126 vs WT PCB126:

Log$_2$FC=2.10, p=5.83E-08), Protein S100-A11 (Ahr$^{-/-}$ Vehicle vs WT Vehicle:

Log$_2$FC=2.29, p=3.13E-07; Ahr$^{-/-}$ PCB126 vs WT PCB126: Log$_2$FC=2.45,

p=1.70E-07), Perilipin-2 (Ahr$^{-/-}$ Vehicle vs WT Vehicle: Log$_2$FC=2.24, p=1.18E-

03; Ahr$^{-/-}$ PCB126 vs WT PCB126: Log$_2$FC=1.97, p=3.88E-03), Glutathione S-

transferase Mu 1 (Ahr$^{-/-}$ Vehicle vs WT Vehicle: Log$_2$FC=2.23, p=5.45E-08; Ahr^{-}

$^{/-}$ PCB126 vs WT PCB126: Log$_2$FC=1.66, p=3.09E- 06), Long-chain-fatty-acid-

CoA ligase 4 (Ahr$^{-/-}$ Vehicle vs WT Vehicle: Log$_2$FC=1.87, p=3.20E-05; Ahr$^{-/-}$

PCB126 vs WT PCB126: Log$_2$FC=2.12, p=9.24E-06), Isoform Short of Long-

chain-fatty-acid-CoA ligase 4 (Ahr$^{-/-}$ Vehicle vs WT Vehicle: Log$_2$FC=1.87,

p=3.20E-05; Ahr$^{-/-}$ PCB126 vs WT PCB126: Log$_2$FC=2.12, p=9.24E-06),

Apolipoprotein A-IV (Ahr$^{-/-}$ Vehicle vs WT Vehicle: Log$_2$FC=1.51, p=3.65E-06;

Ahr$^{-/-}$ PCB126 vs WT PCB126: Log$_2$FC=2.22, p=3.15E-08), Integrin beta-2

(Ahr$^{-/-}$ Vehicle vs WT Vehicle: Log$_2$FC=1.11, *p*=9.66E-04; Ahr$^{-/-}$ PCB126 vs WT PCB126: Log$_2$FC=1.32, *p*=2.17E-04). Consistent with the results that AhR null mice displayed decreased plasma glucose levels and plasma insulin levels. The effect of AhR ablation in Ahr$^{-/-}$ Vehicle vs WT Vehicle and Ahr$^{-/-}$ PCB126 vs WT PCB126, was to decrease the levels of proteins promoting insulin resistance and glycogenolysis like glycogen phosphorylase, brain form (Ahr$^{-/-}$ Vehicle vs WT Vehicle: Log$_2$FC=3.00, *p*=1.21E-08, Ahr$^{-/-}$ PCB126 vs WT PCB126: Log$_2$FC=2.43, *p*=3.01E-07), and glycogen phosphorylase, liver form (Ahr$^{-/-}$ Vehicle vs WT Vehicle: Log$_2$ FC= -1.09, *p*=7.20E-04, Ahr$^{-/-}$ PCB126 vs WT PCB126: Log$_2$FC=-1.51, *p*=3.11E-05). The liver form of glycogen phosphorylase serves the glycemic demands of the body in general, while the brain form of glycogen phosphorylase supplies just the brain, AhR gene ablation caused an increase in glucose supply for brain, while decreased glucose supply level for the body, in general.

Enrichment by GO processes (Fig. 3.8) revealed that the proteomes associated with AhR gene deletion shared similar top GO processes with those related to PCB126 exposure, although Ahr$^{-/-}$ caused a much higher degree of enrichment. These top GO processes mostly involved in two classes of processes: Lipid processes and Xenobiotic metabolism processes. Lipid processes, included "Fatty acid metabolic process", "Long-chain fatty acid metabolic process", "Cellular lipid metabolic process", "Monocarboxylic acid metabolic process", "Lipid metabolic process", "Carboxylic acid metabolic process" and "Monocarboxylic acid biosynthetic process", and xenobiotic

metabolism processes incorporated "epoxygenase P450 pathway", "small molecule metabolic process", "arachidonic acid metabolic process", "oxidation-reduction process", "omega-hydroxylase P450 pathway", "oxidation-reduction process", "oxoacid metabolic process", "organic acid metabolic process", "drug metabolic process", "organic acid biosynthetic process" and "generation of precursor metabolites and energy". Compared to PCB126 effect in the comparison of WT PCB126 vs WT Vehicle, the effect of ablated AhR in Ahr$^{-/-}$ Vehicle vs WT Vehicle and Ahr$^{-/-}$ PCB126 vs WT PCB126, enriched lipid processes to a much greater extent mostly (-Log$_{10}$ (p-value): 6.510-45.110), consistent with the histology and phenotyping data. The abundance of 8 proteins was altered in WT PCB126 vs WT Vehicle; 3 of which belonged to P450 enzymes were increased, and 1 protein (Acyl-coenzyme A thioesterase 1) related to lipid metabolism was upregulated to promote free fatty acid production (Log$_2$FC=2.05, p=1.79E-02) (Supplemental Table 2), while Ahr$^{-/-}$ resulted in severe large droplet macrovesicular steatosis. The abundance of lipid processes-associated proteins were increased significantly by AhR ablation in Ahr$^{-/-}$ Vehicle vs WT Vehicle and/or Ahr$^{-/-}$ PCB126 vs WT PCB126, including: Acyl-coenzyme A thioesterase 1 (Ahr$^{-/-}$ Vehicle vs WT Vehicle: Log$_2$FC=2.97, p=2.57E-06), Acyl-coenzyme A thioesterase 2, mitochondrial (Ahr$^{-/-}$ Vehicle vs WT Vehicle: Log$_2$FC=2.90, p=7.77E-12, Ahr$^{-/-}$ PCB126 vs WT PCB126: Log$_2$FC=1.99, p=2.74E-09), Perilipin-2 (Ahr$^{-/-}$ Vehicle vs WT Vehicle: Log$_2$FC=2.24, p=1.18E-03, Ahr$^{-/-}$ PCB126 vs WT PCB126: Log$_2$FC=1.97, p=3.88E-03), Acyl-coenzyme A thioesterase 4 (Ahr$^{-/-}$ Vehicle vs WT Vehicle:

$Log_2FC=2.24$, p=1.18E-03, Ahr$^{-/-}$ PCB126 vs WT PCB126: Log_2FC=1.97, p=3.88E-03), Acyl-CoA desaturase 2 (Ahr$^{-/-}$ Vehicle vs WT Vehicle: Log_2FC=1.87, p=3.41E-02), Acyl-CoA desaturase 3 (Ahr$^{-/-}$ Vehicle vs WT Vehicle: Log_2FC=1.87, p=3.41E-02), Long-chain-fatty-acid--CoA ligase 4 (Ahr$^{-/-}$ Vehicle vs WT Vehicle: Log2FC=1.87, p=3.20E-03, Ahr$^{-/-}$ PCB126 vs WT PCB126: Log_2FC=2.12, p=9.24E-06), Isoform Short of Long-chain-fatty-acid--CoA ligase 4 (Ahr$^{-/-}$ Vehicle vs WT Vehicle: Log_2FC=1.87, p=3.20E-03, Ahr$^{-/-}$ PCB126 vs WT PCB126: Log_2FC=2.12, p=9.24E-06), Acyl-coenzyme A thioesterase 10, mitochondrial (Ahr$^{-/-}$ Vehicle vs WT Vehicle: Log_2FC=1.71, p=3.67E-07, Ahr$^{-/-}$ PCB126 vs WT PCB126: Log_2FC=1.56, p=1.59E-06), Acyl-coenzyme A thioesterase 9, mitochondrial (Ahr$^{-/-}$ Vehicle vs WT Vehicle: Log_2FC=1.71, p=3.67E-07, Ahr$^{-/-}$ PCB126 vs WT PCB126: Log_2FC=1.56, p=1.59E-06), Acyl-CoA desaturase 1 (Ahr$^{-/-}$ Vehicle vs WT Vehicle: Log_2FC=1.62, p=2.87E-02), and Elongation of very long chain fatty acids protein 2 (Ahr$^{-/-}$ Vehicle vs WT Vehicle: Log_2FC=1.57, p=8.38E-04, Ahr$^{-/-}$ PCB126 vs WT PCB126: Log_2FC=1.34, p=3.58E-03). Apart from lipid processes, PCB126 exposure enriched xenobiotic metabolism processes, especially "epoxygenase P450 pathway" and "omega-hydroxylase P450 pathway", showing that the P450 pathway played a vital role in the effect of PCB126 as expected. Unlike PCB126 exposure, AhR ablation in Ahr$^{-/-}$ Vehicle vs WT Vehicle and Ahr$^{-/-}$ PCB126 vs WT PCB126 enriched other xenobiotic processes greatly except the two processes above, like "oxidation-reduction process" (Ahr$^{-/-}$ Vehicle vs WT Vehicle: -Log_{10} (p-value)= 53.42, Ahr$^{-/-}$ PCB126

vs WT PCB126: -Log_{10} (p-value)= 26.75), "oxoacid metabolic process" ($\text{Ahr}^{-/-}$

Vehicle vs WT Vehicle: -Log_{10} (p-value)= 42.94, $\text{Ahr}^{-/-}$ PCB126 vs WT PCB126:

-Log_{10} (p-value)= 44.58), "organic acid metabolic process" ($\text{Ahr}^{-/-}$ Vehicle vs WT

Vehicle: -Log_{10} (p-value)= 42.94, B vs D: -Log_{10} (p-value)= 44.58), "drug

metabolic process" ($\text{Ahr}^{-/-}$ Vehicle vs WT Vehicle: -Log_{10} (p-value)= 42.94, $\text{Ahr}^{-/-}$

PCB126 vs WT PCB126: -Log_{10} (p-value)= 44.58), etc. (Fig. 4.8) Consistently,

differentially abundant proteins contributing to these processes included

upregulated objects: Glutathione S-transferase A1 ($\text{Ahr}^{-/-}$ Vehicle vs WT

Vehicle: Log_2FC=4.97, p=9.68E-08, $\text{Ahr}^{-/-}$ PCB126 vs WT PCB126:

Log_2FC=5.13, p=8.00E-08), Glutathione S-transferase Mu 3 ($\text{Ahr}^{-/-}$ Vehicle vs

WT Vehicle: Log_2FC=3.76, p=7.63E-09, $\text{Ahr}^{-/-}$ PCB126 vs WT PCB126:

Log_2FC=3.21, p=8.00E-08), Aldehyde dehydrogenase family 1 member A3

($\text{Ahr}^{-/-}$ Vehicle vs WT Vehicle: Log_2FC=3.56, p=4.50E-09, $\text{Ahr}^{-/-}$ PCB126 vs WT

PCB126: Log_2FC=3.50, p=8.05E-09), Aldehyde dehydrogenase X,

mitochondrial ($\text{Ahr}^{-/-}$ Vehicle vs WT Vehicle: Log2FC=3.06, p=1.03E-08, $\text{Ahr}^{-/-}$

PCB126 vs WT PCB126: Log_2FC=2.17, p=1.34E-06), Glutathione S-

transferase A4 ($\text{Ahr}^{-/-}$ Vehicle vs WT Vehicle: Log_2FC=3.06, p=1.03E-08, $\text{Ahr}^{-/-}$

PCB126 vs WT PCB126: Log_2FC=2.17, p=1.34E-06), transferase Mu1 ($\text{Ahr}^{-/-}$

Vehicle vs WT Vehicle: Log_2FC=2.23, p=5.45E-08, $\text{Ahr}^{-/-}$ PCB126 vs WT

PCB126: Log_2FC=1.66, p=3.09E-06), NADH dehydrogenase [ubiquinone] 1

beta subcomplex subunit 9 ($\text{Ahr}^{-/-}$ Vehicle vs WT Vehicle: Log_2FC=1.38,

p=1.88E-02), NADH dehydrogenase [ubiquinone] 1 beta subcomplex subunit

5, mitochondrial ($\text{Ahr}^{-/-}$ Vehicle vs WT Vehicle: Log_2FC=1.31, p=1.97E-02),

Aldehyde dehydrogenase, and cytosolic 1 (Ahr$^{-/-}$ Vehicle vs WT Vehicle: Log$_2$FC=1.26, p=2.77E-06). Notably, the process "Steroid metabolic process" was greatly enriched by AhR KO in Ahr$^{-/-}$ Vehicle vs WT Vehicle and B vs D (Ahr$^{-/-}$ Vehicle vs WT Vehicle: -Log$_{10}$ (p-value)= 12.34, Ahr$^{-/-}$ PCB126 vs WT PCB126: -Log$_{10}$ (p-value)= 26.75), the abundance of proteins associated with steroid metabolism included upregulated: 17-beta-hydroxysteroid dehydrogenase type 6 (Ahr$^{-/-}$ Vehicle vs WT Vehicle: Log$_2$FC=3.02, p=3.51E-08, Ahr$^{-/-}$ PCB126 vs WT PCB126: Log$_2$FC=2.24, p=2.18E-06), 17-beta-hydroxysteroid dehydrogenase 13 (Ahr$^{-/-}$ Vehicle vs WT Vehicle: Log$_2$FC=3.02, p=2.68E-09, Ahr$^{-/-}$ PCB126 vs WT PCB126: Log$_2$FC=2.29, p=1.71E-07), and Isoform 2 of 17-beta-hydroxysteroid dehydrogenase 13 (Ahr$^{-/-}$ Vehicle vs WT Vehicle: Log$_2$FC=2.94, p=1.86E-09, Ahr$^{-/-}$ PCB126 vs WT PCB126: Log$_2$FC=2.35, p=5.83E-08), downregulated: 3 beta-hydroxysteroid dehydrogenase type 5 (Ahr$^{-/-}$ Vehicle vs WT Vehicle: Log$_2$FC=-4.28, p=9.00E-12, Ahr$^{-/-}$ PCB126 vs WT PCB126: Log$_2$FC=-4.59, p=3.47E-12). All of these enzymes were essential in the synthesis of glucocorticoid and other steroid hormones (Supplemental Table 2). In particular, there was no significant alteration of protein abundance in Ahr$^{-/-}$ PCB126 vs Ahr$^{-/-}$ Vehicle representing the effect of PCB126 in AhR null mice, resulting in no processes being enriched in Ahr$^{-/-}$ PCB126 vs Ahr$^{-/-}$ Vehicle.

IPF analysis was performed and the top over-connected interactions by z-score, are provided in Fig. 4.9. Eight unique objects, 5 enzymes and 3 other proteins, were over-connected with PCB126 exposure in A vs B. 5 enzymes

included: Acyl-CoA desaturase 3 (SCD3), NADH-cytochrome b5 reductase 3 (CYB5R3), NAD(P)H steroid dehydrogenase-like (NSDHL), UDP-glucuronosyltransferase 1-4 (UGT1A4) and DEU-B, the other 3 proteins were visinin-like protein 3 (VILIP3). Ahr$^{-/-}$ Vehicle vs WT Vehicle for AhR knockout effect in PCB126-free mice and Ahr$^{-/-}$ PCB126 vs WTPCB126 for AhR ablation effect in PCB126 exposed mice shared 23 over-connected objects, their only difference was that NADH- dehydrogenase [ubiquinone] 1 beta subcomplex subunit 11, mitochondrial (NDUFB11) was not overconnected in Ahr$^{-/-}$ PCB126 vs WT PCB126 (Fig. 4.9). 23 objects included 10 transcription factors, 1 receptor, two proteases, two enzymes, seven other objects. Shared transcription factors included: Zinc finger protein 125 (Zfp125), Liver X receptor-alpha (LXR-alpha), Glucocorticoid receptor (GCR), Sterol regulatory element-binding protein 1 (nuclear) (SREBP1 (nuclear)), Peroxisome proliferator-activated receptor-alpha (PPAR-alpha), Thyroid hormone receptor beta (TR-beta), cellular oncogene FOS (c-FOS), cAMP‑responsive element‑binding protein H (CREB-H), Specificity protein 1 (SP1), and LIM domain only protein 7 (LMO7); the receptor was Insulin receptor, and two proteases were Coagulation factor XIII A, and Matrix metalloproteinase-2 (MMP-2); two common enzymes were DEAD-box helicase 19B (DDX19B) and Transglutaminase 2 (TGM2); seven other objects were microRNA-132-5p (miR-132-5p), Complement receptor 1 (Cr1), Alpha-synuclein, Diaphanous-related formin-1 (DIA1), Glucose transporter 4 (GLUT4), Transient receptor potential cation channel subfamily M (melastatin) member 8 (TRPM8) and

Enamelin. No significant alterations of abundance proteins were found in Ahr^{-/-}

PCB126 group vs Ahr^{-/-} Vehicle group, accordingly, there was no

overconnected objects in this comparison in IPF analysis. The common top

overconnected objects shared by all three comparisons were Zinc finger

protein 125 (Zfp125), Liver X receptor-alpha (LXR-alpha), Peroxisome

proliferator-activated receptor-alpha (PPAR-alpha), Insulin receptor and miR-

132-5p; the former 3 transcription factors were associated with lipid

metabolism, showing both PCB 126 and AhR deletion had effect on lipid

metabolism.

**Effects of PCB126 exposure and Ahr^{-/-} on the microRNAs (miRNAs) in the
IPF analysis**

   In the IPF analysis from proteomic data, totally 9 miRNAs were

overconnected by PCB126 exposure and Ahr^{-/-}, listed at Table 4. Of these 9

miRNAs, 7 miRNAs were over-connected with PCB126 exposure, which were

miR-122-5p, miR-132-5p, miR-142-5p, miR-150- 5p, miR- 221-3p, miR-222-3p

and miR-223-3p; meanwhile, 4 miRNAs overconnected with Ahr^{-/-} were miR-

122-5p, miR-132-5p, miR-192-3p and miR-544-3p. With respect to the over-

connection with the combination of PCB126 exposure and Ahr^{-/-}, only 3

miRNAs were included, namely, miR-122-5p, miR-132-5p and miR-544-3p.
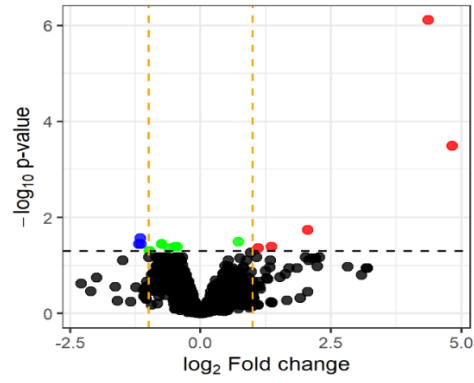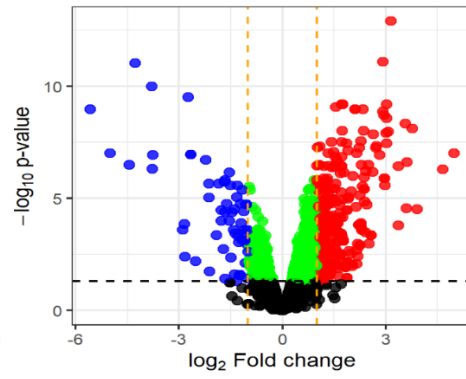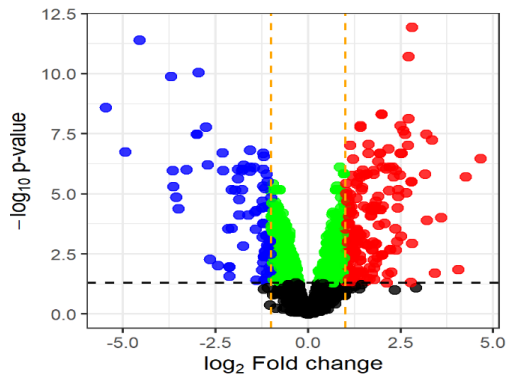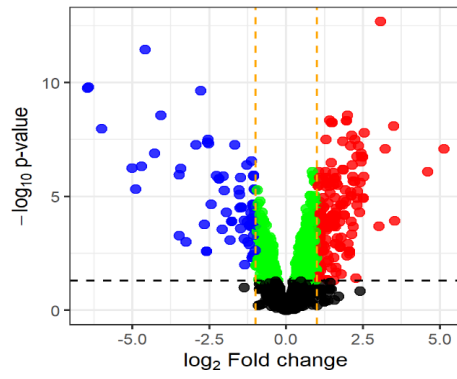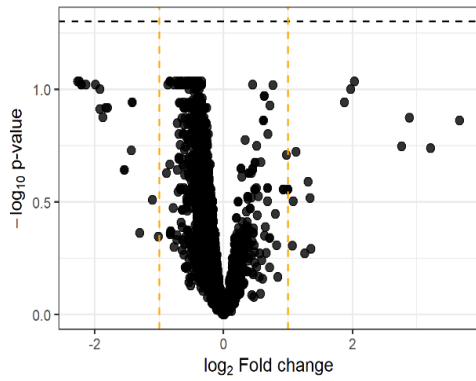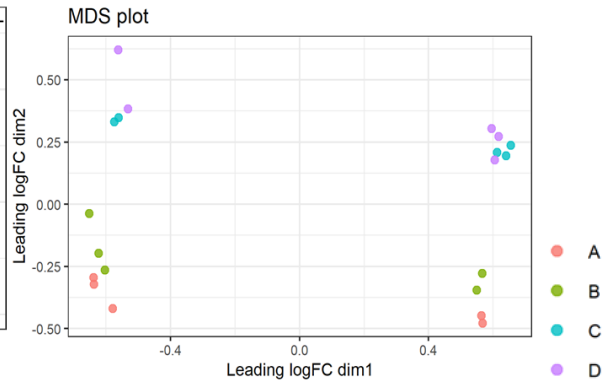
Differentially abundant Proteins	WT Vehicle vs WT PCB126	WT Vehicle vs Ahr$^{-/-}$ Vehicle	WT PCB126 vs Ahr$^{-/-}$ PCB126	Ahr$^{-/-}$ Vehicle vs Ahr$^{-/-}$ PCB126
Altered	8	340	262	0
Increase(Log$_2$FC≥1)	5	279	185	0
Decrease(Log$_2$FC≤-1)	3	61	77	0
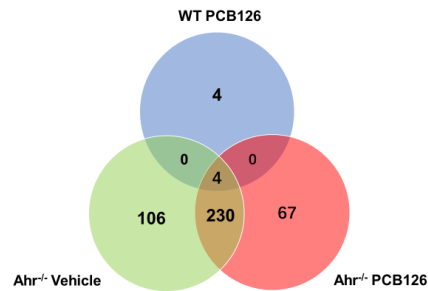
Figure 3.7. Effects of PCB126 exposure and Ahr$^{-/-}$ on the hepatic proteome.

Alterations in hepatic proteins were demonstrated by volcano plots showing significance (y-axis) versus protein fold change (x-axis) for comparisons between these four groups, which are (A) WT PCB126 vs WT Vehicle , (B) Ahr$^{-/-}$ Vehicle vs WT Vehicle, (C) Ahr$^{-/-}$ PCB126 vs WT Vehicle, (D) Ahr$^{-/-}$ PCB126 vs WT PCB126 & (E) Ahr$^{-/-}$ PCB126 vs Ahr$^{-/-}$ Vehicle. Black denotes unaltered proteins, green denotes significantly altered proteins, red denotes significantly altered protein with (log$_2$FC≥0.5), blue denotes significantly altered protein with (log$_2$FC≤-0.5). (F) A multi-dimensional scatter (MDS) plot depicting the pattern for protein alterations in the different groups. A – WT Vehicle, B – WT PCB126, C – Ahr$^{-/-}$ Vehicle, D – Ahr$^{-/-}$ PCB126. (G) The number of proteins and their isoforms that were altered for the four comparisons between different groups (The data was adjusted by FDR=0.2). (H) Venn diagram showing the number of overlapping proteins in different groups relative to WT Vehicle group.

	WT PCB126 vs WT Vehicle	Ahr⁻/⁻ Vehicle vs WT Vehicle	Ahr⁻/⁻ PCB126 vs WT PCB126	Ahr⁻/⁻ PCB126 vs Ahr⁻/⁻ Vehicle
Fatty acid metabolic process	6.60	28.76	26.44	
long-chain fatty acid metabolic process	6.58	6.51	17.14	
cellular lipid metabolic process	5.88	23.33	19.53	
monocarboxylic acid metabolic process	5.61	45.11	43.03	
lipid metabolic process	5.23	30.86	30.91	
carboxylic acid metabolic process	4.56	42.44	43.60	
monocarboxylic acid biosynthetic process	2.50	25.93	25.28	
epoxygenase P450 pathway	6.29	2.52	6.28	
small molecule metabolic process	5.74	41.06	45.81	
arachidonic acid metabolic process	5.26	5.19	8.02	
omega-hydroxylase P450 pathway	5.18	3.48	5.41	
oxidation-reduction process	3.12	53.42	26.75	
oxoacid metabolic process	4.38	42.94	44.58	
organic acid metabolic process	4.32	42.05	45.68	
drug metabolic process	2.73	22.35	30.46	
organic acid biosynthetic process	2.08	24.52	25.88	
generation of precursor metabolites and energy	1.73	35.21	12.64	
cofactor metabolic process	6.01	15.94	20.86	
catabolic process	3.98	21.54	26.55	
steroid metabolic process	2.06	12.34	22.34	X

Figure 3.8. Effects of PCB126 exposure and Ahr⁻/⁻ on gene ontology (GO) processes.

Heatmap showing different processes that were altered by PCB exposures and Ahr⁻/⁻ according to the -log(p-value). The processes were obtained by GO analysis enrichment of the different proteins altered by PCB exposures and/or AhR knockout using MetaCore. No processes were obtained from the comparison of Ahr⁻/⁻ PCB126 vs Ahr⁻/⁻ Vehicle due to no significant protein abundance alteration.
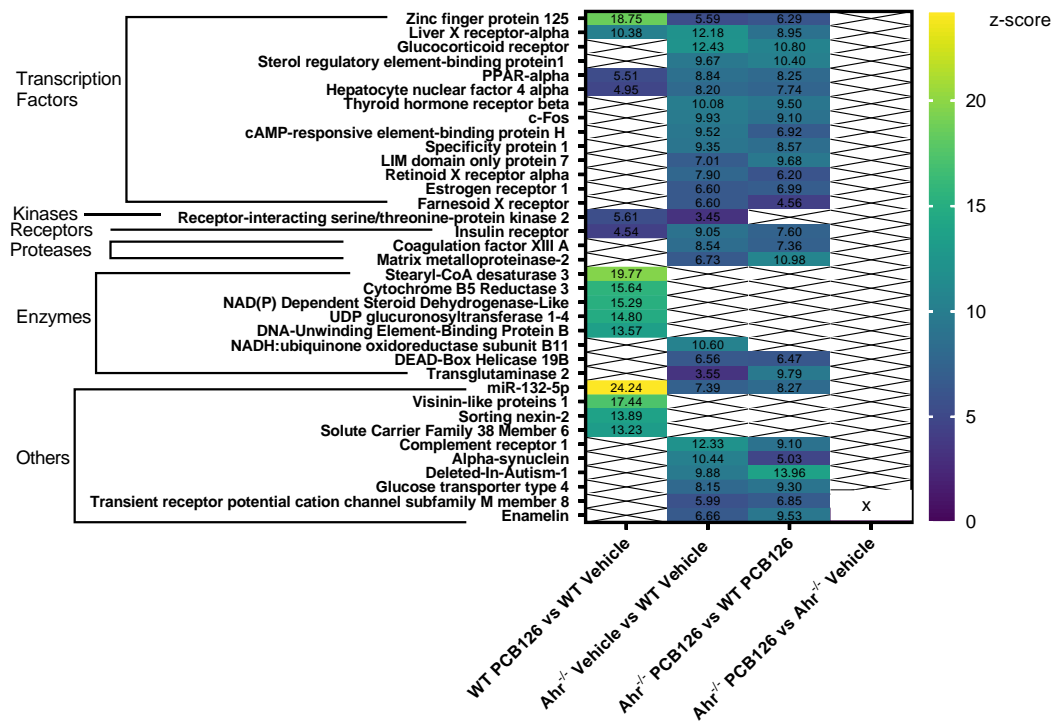
Fig. 3.9. Effects of PCB exposures and Ahr^{-/-} on protein function.

Heatmap showing different classes of proteins, for the different groups, obtained from the Interaction by Protein Function analysis using MetaCore and their corresponding *z* scores. No overconnected proteins were found in Ahr^{-/-} PCB126 vs Ahr^{-/-} Vehicle.

Table 3. Enrichment by protein function analysis

Enrichment by protein function analysis was performed by MetaCore software using the hepatic proteomics data. For a given protein class, a positive *z*-score indicates that more proteins in that class were altered than expected. Likewise, a negative *z*-score means that fewer proteins in the class were altered than expected.

Protein Class	WT PCB126 vs WT Vehicle	Ahr$^{-/-}$ Vehicle vs WT Vehicle	Ahr$^{-/-}$ PCB126 vs WT PCB126
Ligands		1.87	2.60
Phosphatases		0.90	-0.05
Proteases		-0.67	-1.05
Kinases		-0.90	-0.40
Transcription Factors			
Receptors		-2.91	-2.57
Enzymes	6.42	17.84	15.52
Other	-3.31	-9.24	-8.07

Table 4. Over-connected miRNAs and their z-scores in IPF analysis

Seven miRNAs were over-connected with PCB126 exposure in IPF analysis, including miR-122-5p, miR-132-5p, miR-142-5p, miR-150-5p, miR-221-3p, miR-222-3p and miR-223-3p; while only 4 miRNAs were over-connected with Ahr$^{-/-}$, namely, miR-122-5p, miR-132-5p, miR-192-3p and miR-544-3p; and three miRNAs, such as miR-122-5p, miR-132-5p and miR-544-3p were over-connected with the combination of PCB126 exposure and AhR gene ablation.

Overconnected miRs	z-score		
	WT PCB126 Vs WT Vehicle	Ahr$^{-/-}$ Vehicle vs WT Vehicle	Ahr$^{-/-}$ PCB126 vs WT PCB126
miR-122-5p	3.62	4.45	5.30
miR-132-5p	24.24	7.39	8.27
miR-142-3p	4.77		
miR-150-5p	5.53		
miR-221-3p	4.60		
miR-222-3p	3.33		
miR-223-3p	5.19		
miR-192-3p		9.16	
miR-544-3p		8.13	6.75

DISCUSSION

Polychlorinated biphenyls, as endocrine, metabolism and signaling disrupting chemicals, are associated with nonalcoholic steatohepatitis and diabetes (37). PCB-induced NAFLD mechanisms were not fully elucidated, but there have been some findings found, such as a "two-hit" hypothesis was proposed that NAFLD pathogenesis consists of two "hits". The first "hit" causes lipid accumulation in the hepatocytes, while the second "hit" including high fat diet, insulin resistance (IR), proinflammatory cytokines, organelle dysfunction, oxidative stress, altered organokines like fibroblast growth factor 21 (FGF-21), leptin, adiponectin, and alteration in gut microbiome, deteriorate hepatic injury. The PCB126 dose used in this present study was 20μg/kg, the same as our previous acute study and this dose was enough for the activation of AhR target genes, like Cyp1a1 and Cyp1a2.

The aryl hydrocarbon receptor (AhR) is a ligand-activated transcriptional factor that regulates a variety of physiological and pathological function (88). The high-affinity ligands for AhR include 2,3,7,8-tetrachlorodibenzo-p-dioxin (TCDD), and DL PCBs (e.g. PCB126). Many studies have demonstrated that AhR plays a critical role in regulation of metabolic disease, including fatty liver disease. Excessive activation of AhR or activation of AhR induced hepatic steatosis characterized by the accumulation of triglycerides (33), and the effect of AhR is likely through the combined upregulation of CD36 and fatty acid transport proteins (FATPs), resulting in suppression of fatty acid oxidation, inhibition of hepatic export of triglycerides, enhancement of peripheral fat

mobilization, and increased hepatic oxidative stress (90). In a 12-week study,

Banrida Wahlang et al. found that PCB126 (4.9 mg/kg) induced hepatic

steatosis in control diet-fed mice (66). Yulang Chi et. al administered PCB126

by continuous 6- week gavage (total dose of 300µg/kg) in adult female mice,

not only causing hepatic steatosis histologically, but increasing the mRNA

expression of lipogenetic genes including Srebf1, Fasn, Scd1, Cd36, PPARg at

the genetic level (95). A 2-week study showed the gavage of PCB126

(1.5mg/kg) resulted in a significant lipid accumulation and increased the

hepatic triglyceride (TG) level (96). In the 12-day and 28-day studies performed

by Gopi S. Gadupudi et al., PCB126 (1.63 mg/kg) induced hepatic steatosis by

intraperitoneal injection (IP) in rats fed a defined AIN-93 diet (92, 97). In our

previous acute PCB exposure study, two weeks of exposure to PCB126

(20µg/kg) induced mild hepatic steatosis due to increased hepatic lipid import

and associated hypolipidemia (29). The publications above showed that

PCB126 did cause hepatic steatosis, while in the present study did not show

PCB126 had significant hepatic lipotoxicity in wild type mice. The inconsistency

may be due to these reasons below: (1) the difference in exposure time of

PCB126: the time length of most studies above were more than 4 weeks, while

the present study only lasted 2 weeks; (2) different doses of PCB126: most

studies administer the doses of PCB126 ranging from 50µg/kg to 4.9mg/kg, far

more higher the one of my study. (3) different administration routes of PCB126:

some studies administered PCB126 by intraperitoneal injection (ip), having

higher efficacy by avoiding the first-pass effect compared with oral gavage. (4)

different species: some studies used male Sprague Dawley rats as models, compared to C57BL/6 mice, having a higher body mass. Whether the effects of DL-PCBs are AhR dependent or not and what exact role AhR plays in the regulation of hepatic proteome and lipid metabolism needs to be elucidated. AhR deficiency enhances insulin sensitivity and reduces PPARα pathway activity (93), as well as protects against high fat diet (HFD)-induced obesity, hepatic steatosis, insulin resistance and inflammation (34). However, liver-specific AhR knockout mice are susceptible to HFD-induced hepatic steatosis, inflammation and injury (94), suggesting AhR activation protects against fatty liver disease. Whole Ahr$^{-/-}$ mice showed early growth defects, hepatic defects, reduced liver weight, spontaneous microvesicular fatty accumulation and fibrosis, also suggesting the role of AhR in protecting against hepatic lipidosis (35).

The combination of the phenotype, histology and molecular biomarkers showed a variety of PCB126 effects on metabolism. Similar to our previous study (29), PCB126 activated AhR target genes, namely, Cyp1a1 and Cyp1a2. It also activated Car mRNA expression; PCB126 decreased percent change in body weight (showing the wasting syndrome), and caused mild lipidosis in H&E stain and Oil red O stain, although neither hepatic TG nor FFA were increased on biochemical measurement. Meanwhile, PCB126 increased liver triglyceride, and demonstrated a trend to upregulate the liver cholesterol (p=0.05), suggesting lipid accumulation in liver. Proteomics was performed to explore potential mechanisms for the differences in phenotype between different

groups. WT PCB126 vs WT Vehicle reflecting the PCB126 effect in WT mice had 8 altered abundance proteins, mostly belonging to enzymes, consistent with the results of EPF. Two enzymes, namely, Cyp1A1 and Cyp1A2, were increased as expected; another upregulated enzyme: Acyl-coenzyme A thioesterase 1 facilitated fatty acid production. Consistent with the results from abundance protein analysis, IPF in WT PCB126 vs WT Vehicle revealed over-connected interactions with 3 transcription factors, namely, Zfp125, LXR-alpha, PPAR-alpha, regulating lipid metabolism. GO processes analysis demonstrated top processes enriched by PCB126 in WT PCB126 vs WT Vehicle were associated with lipid metabolism and xenobiotic metabolism. The results from hepatic proteome in WT PCB126 vs WT Vehicle were consistent with the phenotype and other biomarkers. An important finding was the fact of alterations of hepatic differentially abundant proteins in Ahr$^{-/-}$ PCB126 vs Ahr$^{-/-}$ Vehicle group, meaning in Ahr$^{-/-}$ mice, PCB126 did not cause significant protein changes. This demonstrated that the effects of PCB126 on protein abundance were AhR dependent.

In the present study, the differentially abundant proteins analysis showed Cyp1A1 was downregulated by AhR ablation in PCB126 exposed mice (Log$_2$FC=-4.90, p=4.66E-06), while Cyp1A2 decreased in Ahr$^{-/-}$ Vehicle vs WT Vehicle (Log$_2$FC=-1.91, p=4.33E-04) and Ahr$^{-/-}$ PCB126 vs Ahr$^{-/-}$ Vehicle (Log$_2$FC=-6.43, p=1.58E-10) (Supplemental Table 2). The RT-PCR showed not only AhR mRNA expression was totally inhibited by AhR ablation (2$^{-\Delta\Delta Ct}$ value close to 0), but the expression of their target genes Cyp1a1 and Cyp1a2 were

significantly downregulated by AhR gene deletion (both p<0.01). Meanwhile, in

the table of abundant proteins, Cyp3a11 was upregulated by AhR deletion in

$Ahr^{-/-}$ Vehicle vs WT Vehicle (Log_2FC=3.61, p=2.33E-07) and $Ahr^{-/-}$ PCB126 vs

$Ahr^{-/-}$ Vehicle (Log_2FC=2.38, p=4.83E-05). With regard to RT-PCR, *Cyp3a11*,

the target gene of Pxr, was increased by global AhR knockout ($Ahr^{-/-}$ Vehicle:

4.33-fold, $Ahr^{-/-}$ PCB126: 4.74-fold relative to WT Vehicle, both p<0.01).

PCB126 did not cause NAFLD in the present study due to no increased hepatic

lipids by biochemical analysis. In hepatic differentially abundant proteins

analysis in hepatic proteome, AhR knockout altered much more proteins than

PCB126 exposure ($Ahr^{-/-}$ Vehicle vs WT Vehicle: 340 proteins, $Ahr^{-/-}$ PCB126 vs

$Ahr^{-/-}$ Vehicle: 262 proteins). In hepatic differentially abundant proteins table

(Supplemental Table 2), AhR deletion upregulated at least 12 proteins involved

in lipid accumulation, including Acyl-coenzyme A thioesterase 1, Acyl-

coenzyme A thioesterase 2, mitochondrial, Perilipin-2, Acyl-coenzyme A

thioesterase 4, Acyl-CoA desaturase 2, Acyl-CoA desaturase 3, Long-chain-

fatty-acid--CoA ligase 4, Isoform Short of Long-chain-fatty-acid--CoA ligase 4,

Acyl-coenzyme A thioesterase 10, mitochondrial, Acyl-coenzyme A

thioesterase 9, mitochondrial, Acyl-CoA desaturase 1, and Elongation of very

long chain fatty acids protein 2 (Supplemental table 2). Hepatic lipid

accumulation originates from an imbalance between lipid acquisition and lipid

disposal, which is determined by four major pathways: hepatic lipid uptake, de

novo lipogenesis (DNL), oxidation of fatty acids (FAO), and lipid export in

VLDL; increased levels of Acyl-coenzyme A thioesterases promote production

of free fatty acids; upregulated Acyl-CoA desaturases, Elongation of very long

fatty acids protein 2, Long-chain-fatty-acid--CoA ligase 4, and its isoform

induce synthesis of triglycerides; these regulation above lead to promoted

hepatic lipid uptake and DNL, resulting in liver fat accumulation. Consistently,

enriched top processes related to lipid metabolism in GO process analysis in

$Ahr^{-/-}$ Vehicle vs WT Vehicle and $Ahr^{-/-}$ PCB126 vs WT PCB126, were listed as

follows: "Fatty acid metabolic process", "Long-chain fatty acid metabolic

process", "Cellular lipid metabolic process", "Monocarboxylic acid metabolic

process", "Lipid metabolic process", "Carboxylic acid metabolic process" and

"Monocarboxylic acid biosynthetic process", most of them were associated with

synthesis and processing of fatty acids (Fig. 4.8). IPF analysis of $Ahr^{-/-}$ effect in

$Ahr^{-/-}$ Vehicle vs WT Vehicle and $Ahr^{-/-}$ PCB126 vs WT PCB126 revealed

several overconnected transcription factors involved in lipid steatosis, like

Zfp125 (causes lipidosis by reducing liver secretion of triglycerides), LXR-

alpha, SREBP1 (nuclear), PPAR-alpha, c-Fos; notably, LXRα activates the

transcription factor SREBP-1c, resulting in lipogenesis and c-Fos, as a new

target of NASH, induces hepatic PPARγ signaling and lipid accumulation (Fig.

4.9). RT-PCR results further validated the results of phenotype s and hepatic

proteomes, which showed $Ahr^{-/-}$ increased Cd36 expression, facilitating the

fatty acid transport, and upregulated perilipin-2 gene expression, promoting

lipid droplets formation, meanwhile, $Ahr^{-/-}$ decreased Pnpla3 gene expression,

downregulating lipolysis. All these alterations in gene expression caused the

overall effect of lipid accumulation. The results from the phenotype, histology,

biomarker and RT-PCR, were consistent with the results from hepatic proteome. AhR ablation increased liver triglyceride, liver FFA, while decreased liver weight/body weight ratio, plasma triglyceride, plasma cholesterol, plasma HDL-c, and plasma VLDL in a trend (p=0.06). Meanwhile, in H&E stain and Oil Red O stain, AhR null mice showed conspicuous lipid steatosis. RT-PCR for genes involved in lipid metabolism demonstrated that AhR knockout increased *Cd36* gene expression, related to lipid uptake, and decreased *Pnpla3* expression (associated with lipolysis). Combined with all the results, AhR gene deletion did not bring about the beneficiary effect on lipid metabolism, on the contrary, caused significant lipidosis, the mechanism of global AhR knockout-induced NAFLD is that AhR deletion promoted the production of fatty acid, increasing hepatic lipid uptake, promoting formation of lipid droplets and downregulated lipolysis. This also suggested a potential role of AhR in the negative regulation of the expression of these genes involved in hepatic steatosis. In the present study, the effects of PCB126 were not all AhR-dependent. However, its effects on the hepatic proteome were AhR dependent.

In IPF analysis, notably, GCR was over-connected with Ahr^{-/-} (Ahr^{-/-} Vehicle vs WT Vehicle: z-score=12.43, Ahr^{-/-} PCB126 vs WT PCB126: z-score=10.80); whether GCR expression was upregulated or downregulated needs to be elucidated, then the expression level of Tat gene, the target gene of GCR was measured, and it showed Tat gene expression was increased by Ahr^{-/-} indicating Tat gene and GCR activation. As cytoplasmic protein complexes, GR and AhR bind their respective ligands, on the flip side, AhR and GR have

potentially complex receptor cross-talk, showing AhR-mediated responses include effects on GR expression, and vice versa (98), although their exact interaction pattern needs to be elucidated. Moreover, global AhR knockout affected the steroid hormone which was shown in the GO process analysis in Ahr$^{-/-}$ Vehicle vs WT Vehicle and Ahr$^{-/-}$ PCB126 vs WT PCB126; check through the hepatic differentially abundance proteins, 3 important enzymes regulating the steroid hormone synthesis were altered, including 17-beta-hydroxysteroid dehydrogenase type 6, 17-beta-hydroxysteroid dehydrogenase 13, Isoform 2 of 17-beta-hydroxysteroid dehydrogenase 13, 3 beta-hydroxysteroid dehydrogenase type 5 (Supplemental table 2). Upregulated 17-beta-hydroxysteroid dehydrogenases (17β-HSD) and its isoform and decreased 3 beta-hydroxysteroid dehydrogenase (3β-HSD) promoted the production of sex hormone and decreased the production of glucocorticoid; IPF analysis in Ahr$^{-/-}$ Vehicle vs WT Vehicle and Ahr$^{-/-}$ PCB126 vs WT PCB126, showed overconnected transcription factor: GCR (glucocorticoid receptor). These results suggest AhR$^{-/-}$ affected the enzymes in the steroidogenesis and showed actual impacting of GCR. Another possible mechanism for overconnected GCR is that GCR was affected by the existence of hepatic lipidosis which may be accompanied by inflammation, and GCR regulated annexins to reduce inflammation (99).

With respect to glucose metabolism, AhR ablation lowered plasma glucose, plasma insulin and resistin level, increased plasma leptin concentration, indicating the effect of AhR knockout on decreasing insulin resistance. In

hepatic differentially abundant proteins analysis, several altered proteins

regulating glucose homeostasis by AhR deletion in $Ahr^{-/-}$ Vehicle vs WT

Vehicle and $Ahr^{-/-}$ PCB126 vs WT PCB126, were found as follows: like

Glycogen phosphorylase, brain form, and Glycogen phosphorylase, liver form;

the liver form of glycogen phosphorylase serves the glycemic demands of the

body in general while the brain form of glycogen phosphorylase supply just

brain, so here, AhR KO caused the increase of glucose supply for brain, but

decreased the blood glucose level for the body. Additionally, IPF analysis

showed two over-connected proteins associated with glucose homeostasis,

which are insulin receptor ($Ahr^{-/-}$ Vehicle vs WT Vehicle: z-score=9.049, $Ahr^{-/-}$

PCB126 vs WT PCB126: z-score=7.595), and glucose transporter 4 (GLUT4)

($Ahr^{-/-}$ Vehicle vs WT Vehicle: z-score=8.153, $Ahr^{-/-}$ PCB126 vs WT PCB126: z-

score=9.295); insulin receptor stimulates glycogen synthesis and promotes the

degradation of insulin; unlike GLUT2 mostly expresses in liver to uptake

glucose for glycolysis and glycogenesis, GLUT4 mostly expresses in adipose

tissues and striated muscle to uptake glucose to promote fat accumulation and

muscle contraction. Overconnected insulin receptor and GLUT4 facilitated the

transport and utilization of glucose and conversion of glucose into fat and

decreased the glucose level. Combined with the results from phenotype,

plasma glucose level, plasma insulin and resistin level, hepatic proteome etc.,

AhR gene ablation had a potential beneficiary effect on glucose metabolism,

improving insulin resistance on molecular level and generally lowering the

glucose level.

MicroRNAs (miRNAs) are small non-coding RNAs that maintain cellular homeostasis and potentially modulate responses to environmental exposures. In the present animal study, totally seven over-connected miRNAs were shown with PCB126 exposure in IPF analysis, including miR-122-5p, miR-132-5p, miR-142-5p, miR-150-5p, miR-221-3p, miR-222-3p and miR-223-3p; while only 4 miRNAs were over-connected with Ahr$^{-/-}$, namely, miR-122-5p, miR-132-5p, miR-192-3p and miR-544-3p; and three miRNAs, such as miR-122-5p, miR-132-5p and miR-544-3p were over-connected with the combination of PCB126 exposure and AhR gene ablation. This suggested different treatments may have their different targets of alteration in miRNAs, like Ahr$^{-/-}$ over-connected only four miRNAs. In our previous human epidemiological study (ACHS), PCB-associated liver necrosis was associated with circulating miRNAs. It showed the necrotic liver disease category (n=359) was associated with four up-regulated miRNAs (miR-99a-5p, miR-122-5p, miR-192-5p, and miR-320a) and five down-regulated miRNAs (let-7d-5p, miR-17-5p, miR-24-3p, miR197-3p, and miR-221-3p). Compared our animal data with human data, they shared 3 common miRNAs, which were miR-122-5p, miR-221-3p, and miR-192-3p, although having different PCB exposures and different species. These primary results provided some insights into the potential mode of action of PCBs, although the exact mechanism of miRNA-induced toxicity needs further study.

There are some limitations for the present study. AhR null mice had severe lipidosis in histology, significantly higher ALT and AST in biomarkers, increased proapoptotic or proinflammatory proteins, like Annexin A5, Protein S100-A11,

Growth arrest-specific protein 2 (Supplemental table 2), all of which suggested the existence of inflammation or apoptosis. On the flip side, inflammation-associated factors including plasma IL-6 and PAI-1 determination were not elevated in AhR null mice. Inflammation and cell death mechanisms can be more rigorously evaluated in the future. In conclusion, the present study showed global AhR gene deletion caused significantly lipid accumulation; AhR activation plays a pivotal role in lipid metabolism; the mechanism of AhR knockout-induced lipidosis was probably through the enhancement of production of fatty acid and decrease of lipid breakdown. At the same time, AhR ablation affected the steroid hormone metabolism, influenced the enzymes in the steroidogenesis and downregulated the synthesis of glucocorticoid leading to the activation of GCR. Besides, AhR ablation demonstrated a beneficiary effect on glucose metabolism, generally lowering the glucose level through increased transport, utilization of glucose in peripheral tissue and promoted conversion of glucose into fat. Lastly, PCB126 did not have significant effect in AhR null mice, suggesting AhR regulates the hepatic proteome and lipid metabolism independent of PCB exposure.

CHAPTER 4

THE ACUTE EXPOSURE EFFECTS AND POTENTIAL MECHANISMS OF
DIFFERENT DOSES OF DL+NDL PCBS ON
THE PANCREATIC PROTEOME

INTRODUCTION

Diabetes has been a major health concern in the US population and across the world. According to the data from Disease Control and Prevention (CDC), 10.5% of the US population has diabetes (30). Diabetes patients aged 50 years or older die 4.6 years earlier, develop disability 6 to 7 years earlier, and spend about 1 to 2 more years in a disabled state than adults without diabetes (100). From 2012 until 2017, excess medical costs per person associated with diabetes increased from $8,417 to $9,601 (30).

Diabetes is characterized by elevated blood sugar levels due to either the result of inadequate amounts of insulin production, inadequate utilization of insulin or a combination of both. Diabetes is categorized as type 1, type 2, gestational diabetes mellitus (GDM), specific types of diabetes due to other causes, e.g., monogenic diabetes syndromes (such as maturity-onset diabetes of the young [MODY]), diseases of the exocrine pancreas (such as cystic fibrosis), and drug- or chemical-induced diabetes.

Multiple epidemiological studies and animal experiments have revealed associations between PCB exposure and DM (101, 102). In a 24-year follow-up study of the Yucheng cohort (PCB poisoning), increased rates of DM in females were observed (4). In 736 PCB-exposed human subjects in the Anniston Community Health Survey (ACHS), a high prevalence of diabetes (27%) was observed, which was almost 3-times higher than the US prevalence rate (6). Also, some papers in animal models reported the correlation between PCBs exposure and DM. Zhang S et.al reported that the treatment with Aroclor 1254 (5, 50, and 500 µg/kg) resulted in a significant increase in blood glucose concentrations in male mice (103). Aroclor1254 is high in both DL PCB (PCB105, PCB118, and PCB156) and non-dioxin-like PCB (PCB 99, PCB 138, and PCB153). PCB77 and PCB126 were found to increase the blood glucose in male C57BL/6 mice (104). The mechanisms by which PCBs cause DM are still controversial with some literature reporting decreased insulin production and others reporting increased IR (105, 106). ACHS-II study showed with the increase of PCBs concentration, the level of insulin decreased (6). In our acute PCB exposure study, the Aroclor1260/PCB126 mixture caused histological changes in pancreas and Ins1 gene expression was decreased, hinting at the effect of PCB mixture on pancreas (29). Banrida Wahlang's sex difference acute PCB exposure study showed Aroclor1260/PCB126 mixture decreased Ins1 gene expression, while increased pancreas weight/body weight ratio, suggesting PCB mixture potentially had affected the pancreas function (36). To further explore the acute effects and potential mechanism of DL/NDL PCB

mixture on pancreas, untargeted proteomics was performed in a female mouse

model.

MATERIALS AND METHODS

Animal studies

The related animal protocol was ratified by the University of Louisville Institutional Animal Care and Use Committee. Adult female C57BL/6 mice (8 weeks old) were purchased from Jackson Laboratory and distributed into three equal groups (n = 10). All mice were fed a control synthetic diet (20.0 %, 69.8 %, and 10.2 % of total calories come from protein, carbohydrate, and fat, TekLad TD 06416) throughout the study period. At 10 weeks of age, ten mice in each group were given either corn oil, low dose of Aroclor1260/PCB126 mixture (20 mg/kg/20 µg/kg) (LD), or high dose of Aroclor1260/PCB126 mixture (100 mg/kg/100 µg/kg) (HD) via a one-time gavage and followed for 2 weeks (Fig. 4.1). At week 2 post gavage, a glucose tolerance test (GTT) was performed as described previously (36). Whole blood for plasma, and pancreas tissue samples were harvested after euthanasia.

Proteomics analysis

Proteins were extracted from liver tissue in RIPA buffer supplemented with protease and phosphatase inhibitors using a bead homogenizer and protein amounts were quantitated by BCA assay. Protein lysates (200 µg) were trypsinized using the modified filter-aided sample preparation method (57) and enriched for phosphopeptides by the TiO_2–SIMAC–HILIC method (58). Briefly, protein samples were reduced with dithiothreitol, denatured with 8M urea, and alkylated with iodoacetamide followed by centrifugation through a high molecular

weight cutoff centrifugal filter (Millipore, 10k MWCO). After overnight digestion with sequencing grade trypsin (Promega), the digested proteins were collected and cleaned with a C18 Proto™ 300 Å Ultra MicroSpin column. Protein digested samples (50 µg) were labeled with tandem mass tag (TMT) TMT10plex™ Isobaric Label Reagent Set (Thermo Fisher, Waltham, MA); samples were then concentrated and desalted with Oasis HLB Extraction cartridges (Waters Corporation, Milford, MA) using a modified protocol for extraction of the digested peptides (59). Samples were then subjected to high pH reversed phase separation with fraction concatenation on a Beckman System Gold LC system supplemented with 126 solvent module and 166 detector in tandem with a Bio-Rad Model 2110 Fraction Collector (60). Liquid chromatography/mass spectrometry was used to measure TMT-labeled peptides. Briefly, every high pH reversed phase fraction was dissolved in 50µL solution of the combination of 2% v/v acetonitrile/0.1% v/v formic acid and 1 µL of each fraction was analyzed on EASYnLC 1000 UHPLC system (Thermo Fisher) and an Orbitrap Elite—ETD mass spectrometer (Thermo Fisher Scientific, Waltham, MA, USA). Proteome Discoverer v2.2.0.388 was used to analyze the raw data collected from the mass spectrometer. Hepatic proteins that had significance abundance were imported into MetaCore software (Clarivate Analytics, Philadelphia, PA) for the following analyses: gene ontology (GO) processes analysis and transcription factor analysis (TFA).

Statistical analysis

Statistical significance was determined by two-way analysis of variance using

GraphPad Prism version 7.02 for Windows (GraphPad Software Inc., La Jolla,

CA, USA). p <0.05 was considered statistically significant. Statistical analysis for

the proteome data was analyzed using the R package as described previously

(61, 62). Given the exploratory nature of the study, significantly altered proteins

were further filtered using an FDR threshold of 0.2.

**Control Diet
& Oral Gavage**

Week 0

2

**Female C57BL/6 Mice
Age: 10 weeks**

**Euthanize Mice and
sample collection**

Group 1. Control: corn oil
Group 2. Low dose of Aroclor1260/PCB126: (20 mg/kg/20 µg/kg) (LD)
Group 3. High dose of Aroclor1260/PCB126: (100 mg/kg/100 µg/kg)
(HD)
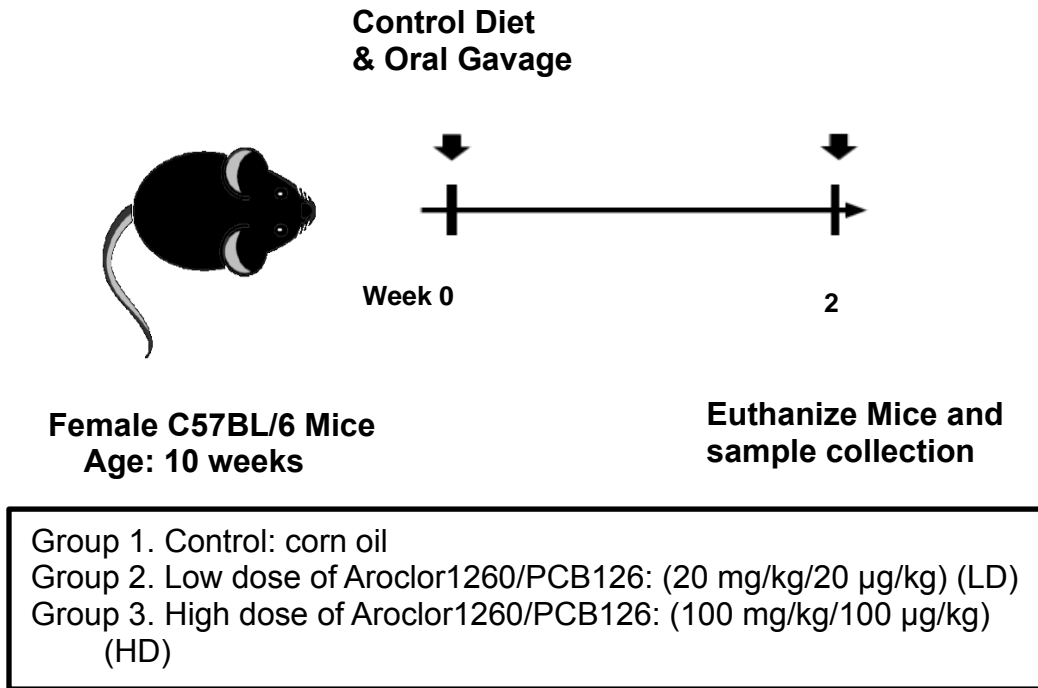
Figure 4.1. Experiment Design of female mice acute PCB mixture study.

Mice were divided into 3 study groups based on the type of exposure. All

animals were fed a chow diet and received a one-time gavage of their

respective dose at the beginning of the study.

RESULTS

Effects of different doses of PCB mixture exposures on body composition and glucose tolerance.

Body weight was measured weekly throughout the 2-week study. There was a gradual increase in body weight in all three groups from week 0 to week 2 (Fig. 4.2A). However, there were no significant differences in body weight and percent change in body weight between these three groups (Fig. 4.2B, 2D). As for the pancreas weight to body weight ratio, no significant differences were found between the groups (Fig. 4.2C). A GTT was performed to examine the effects of different doses of PCB mixture on glucose tolerance (Fig. 4.2E); there were no differences between groups for alteration in glucose uptake (Fig. 4.2F).

Effects of different doses of PCB mixture exposures on the pancreatic proteome

A total of 7671 unique proteins and their isoforms were detected. The alterations of pancreatic abundance proteins content were regulated as follows: Low Dose Aroclor1260/PCB126 group (LD) vs Control (38 increased and 82 decreased) and High Dose Aroclor1260/PCB126 group (HD) vs Control group (256 increased and 288 decreased) (Table 5).

Enrichment by GO processes (Fig. 4.3) showed that both doses of PCB mixture enriched the process of "peptide biosynthetic process". With regard to processes related to inflammation and immunity, low dose Aroclor1260/PCB126 enriched the processed such as "antigen processing and presentation of endogenous Antigen", "regulation of leukocyte mediated cytotoxicity" and
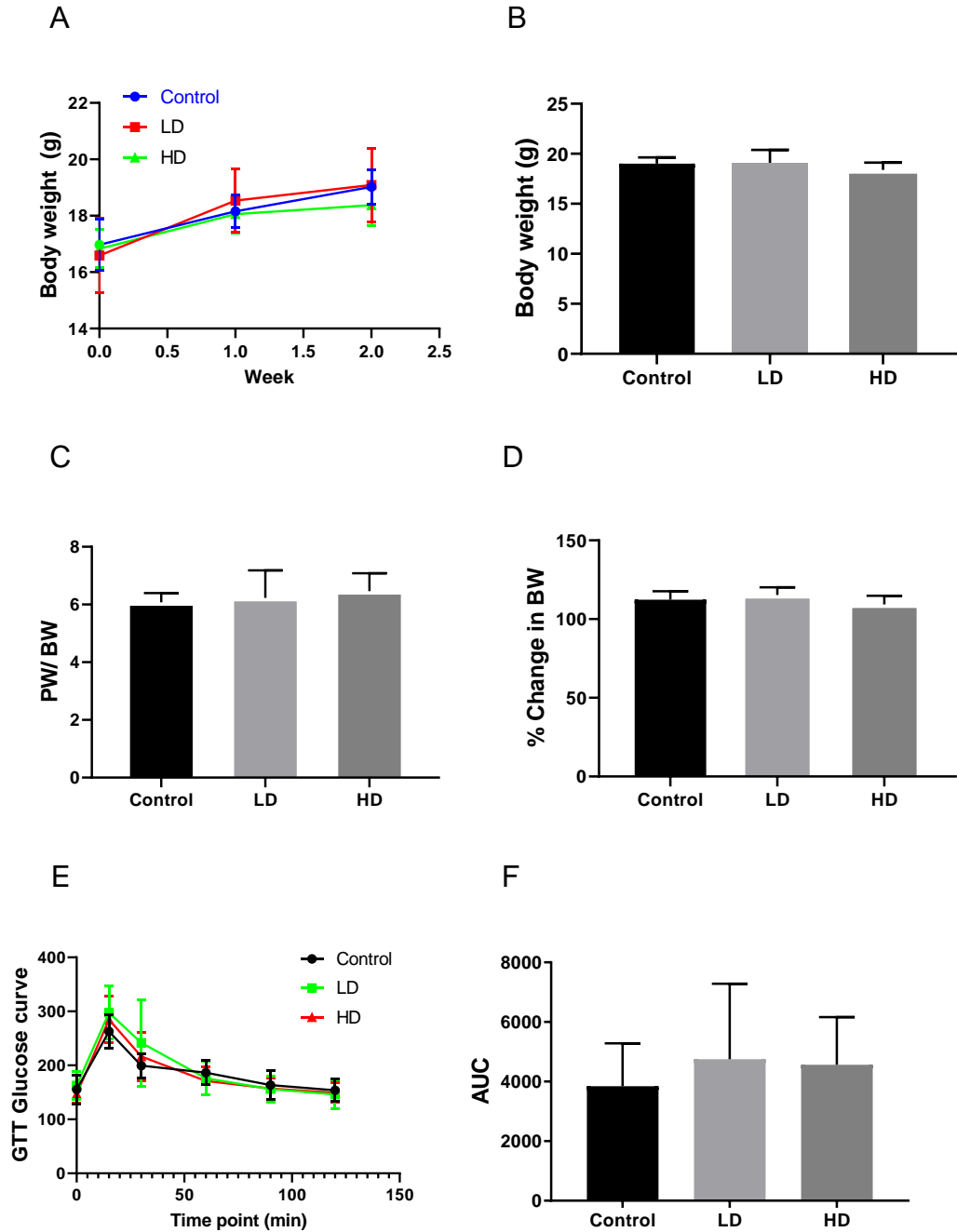
Figure 4.2 Effects of different doses of PCB mixture exposures on body composition and glucose tolerance.

(A, B) Body weight was measured weekly throughout the 2-week study. No signifcant differences were found between the three groups. (D) % change in body weight relative to the initial body weight taken at the beginning of the study

was calculated. Three groups had no significant differences in % change in BW. (C) The pancreas was weighed and their respective weights relative to body weight were calculated. Three groups had no differences in PW/BW. A glucose tolerance test was performed after the second PCB gavage and blood glucose levels were measured; (E) GTT curve was made and (F) AUC (Area Under the Curve) of three groups was calculated. Values are mean ± SD. n=10, Values for $p < 0.05$ are in bold, by one-way ANOVA with Turkey's post hoc comparison..

"antigen processing and presentation of peptide antigen", while the other dose enriched four processes, including " Inflammation_IL-6 signaling", "Immune response_Antigen presentation", "Apoptosis_Apoptotic nucleus" and "Inflammation_NK cell cytotoxicity". In addition, processes associated with insulin signal pathway were enriched by low dose or high dose Aroclor 1260/PCB126 exposure. These processes were "insulin-like growth factor receptor signaling pathway", "receptor tyrosine kinase signaling pathway", "Signal transduction_Insulin signaling" and "Signal transduction_WNT signaling".

Enrichment by transcription factor analysis (TFA) (Fig. 4.4A) showed that low dose and high dose group shared similar overconnected transcription factors. Transcription factors associated with inflammation were overconnected by both doses of Aroclor1260/PCB126, including NF-kB1 (p105), NF-kB2 (p52), and NF-kB1 (p50). Notably, 5 transcription factors related to pancreas function and glucose metabolism by over-connected with low dose or high dose PCB mixture. These were as follows: NEUROD5, HNF1-beta, HNF4-alpha, E2F1, FOXP3, HNF1-alpha.

Table 5. Alterations of diffentially abundant pancreatic proteins

The number of proteins and their isoforms that were altered for the two comparisons between different groups (The data were adjusted by FDR=0.2).

Differentially abundant pancreatic proteins	LD vs Control	HD vs Control
Altered	120	544
Increased	38	256
Decreased	82	288
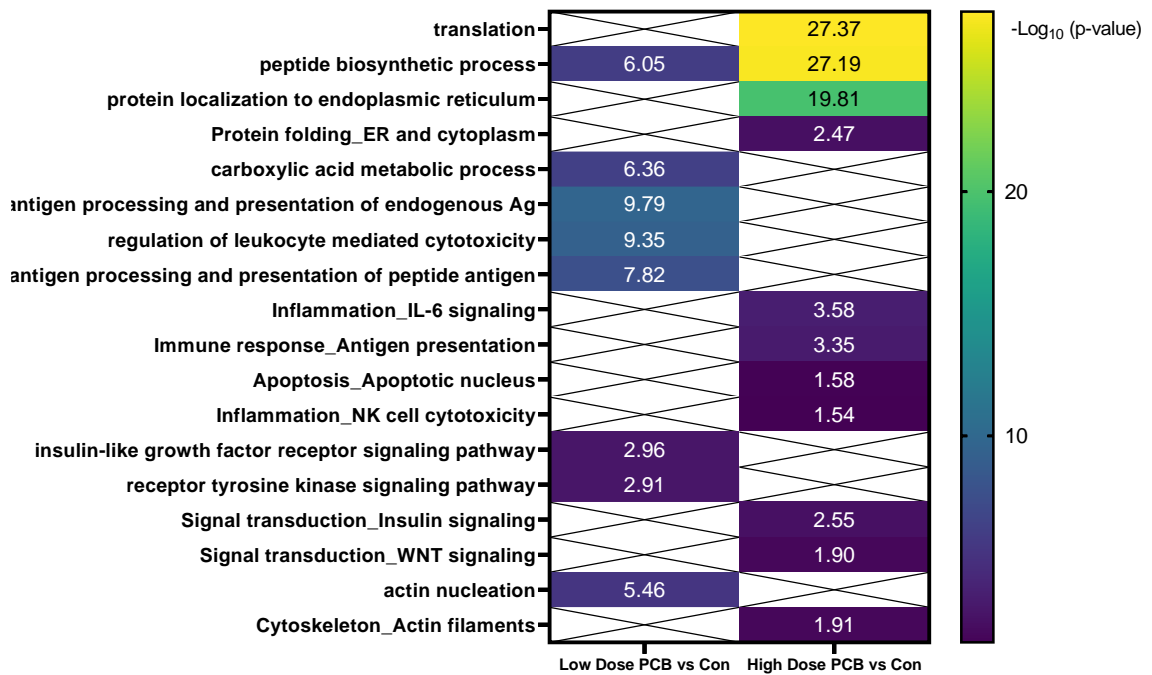
Figure 4.3 Effects of different doses of Aroclor1260/PCB126 exposure on gene ontology (GO) processes.

Heatmap showing different processes that were altered by different doses of Aroclor1260/PCB126 exposure according to the -log(p-value). The processes were obtained by GO processes analysis using MetaCore.
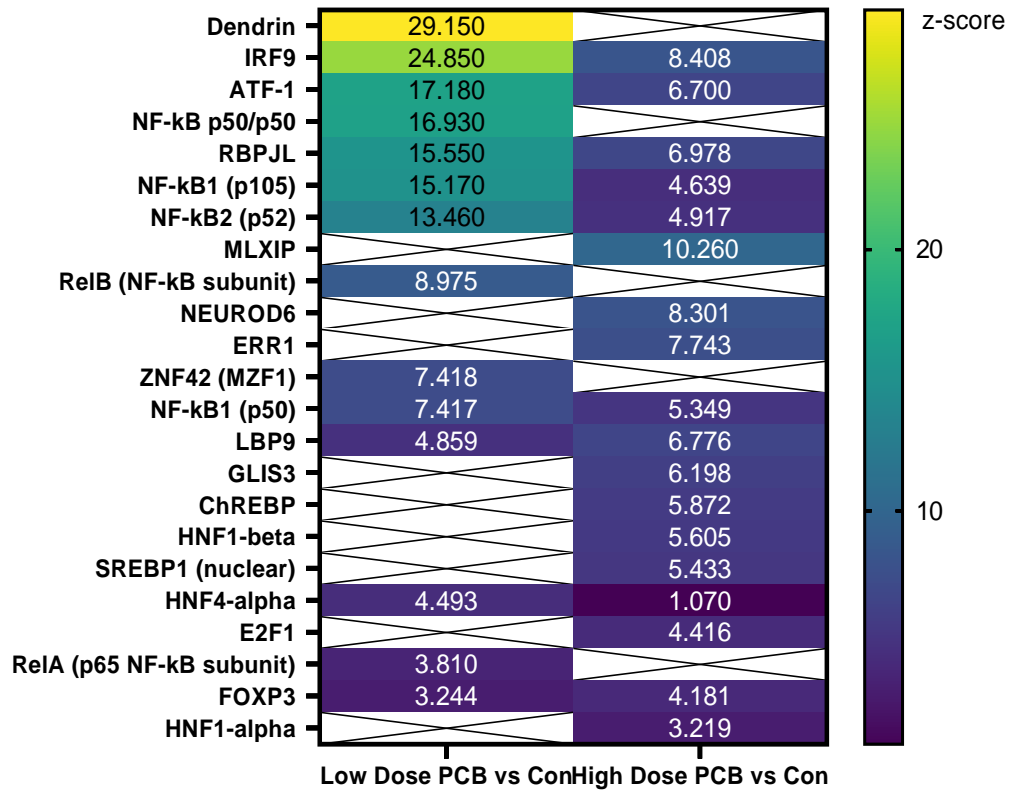
Figure 4.4 Effects of different doses of Aroclor1260/PCB126 exposure on Enrichment by transcription factor analysis (TFA)

Heatmap showing different transcription factors, for the different groups, obtained from the Enrichment by transcription factor analysis (TFA) using MetaCore and their corresponding *z* scores.

DISCUSSION

Considered as a group of multifactorial disease, diabetes is caused by some combination of genetic and environmental factors including environmental pollutants. In recent years, the association between PCB and diabetes has gained concern.

Multiple epidemiological studies and animal studies demonstrated the association of PCB and diabetes. In the follow-up study of Yucheng cohort, females with high PCB exposure had higher prevalence of diabetes (4). In the ACHS study, insulin level was associated with increased PCB concentration. The mechanisms of PCB-induced diabetes remain unclear. Our previous acute PCB exposure study (29) showed Aroclor1260/PCB126 mixture exposure caused "PCB pancreatopathy", presenting with acinar cell atrophy, mild steatosis, and fibrosis absent of ductal changes or immune cell infiltration. PCB mixture decreased Ins1 gene expression, downregulated the expression of Nkx6-1, NR4a1, NR4a3 gene, associated with beta-cell islet identity, suggesting DL/NDL PCB mixture had more effects on pancreas than PCB congeners. Consistent with previous study (107), the potential mechanism of PCB-induced diabetes was associated with impaired islet identity. Our previous sex difference study also showed Aroclor1260/PCB126 mixture decreased Ins1 gene expression in female mice, while increased the pancreas weight to body weight ratio (36).

In the present study, TFA showed that 5 transcription factors associated with pancreatic function and glucose homeostasis were overconnected with either

low dose Aroclor1260/PCB126 or high dose Aroclor1260/PCB126, including

NEUROD5, HNF1-beta, HNF4-alpha, E2F1, FOXP3, and HNF1-alpha. All

these factors were involved in pancreas development, and three of them,

namely, HNF1-beta, HNF4-alpha, and HNF1-alpha, were associated with

MODY in human.

Maturity onset diabetes of the young (MODY) is referred to as monogenic

diabetes, caused by mutations in an autosomal dominant gene disrupting

insulin production. There have been 11 different types of MODY caused by

changes in eleven different genes. MODY 1 is caused due to a loss-of-function

mutation in the HNF4α gene; MODY 3 is due to mutations of the HNF1α gene

(a homeobox gene); MODY 5 is a less common forms of MODY due to defect

in HNF-1 beta gene, has some distinctive clinical features, such as atrophy of

the pancreas and renal disease.

Here, over-connected HNF1-beta were associated with MODY 5, HNF4-

alpha with MODY 1 and HNF1-alpha with MODY 3. This finding from

proteomics may provide us new insight towards the pathogenesis of PCB-

induced diabetes. Will this potential mechanism of PCB-induced diabetes have

some similarity with MODY? In PCB-induced diabetes, some patients have

insulin resistance while others present as pancreatic failure, like type 1

diabetes. And different MODY have diverse presentations, some present

similar to type 1 diabetes, and some just like type 2 diabetes. And the

mechanisms of MODYs are not fully clear. What caused the mutations of

specific genes of different MODY? These questions need to be elucidated.

GO processes analysis showed either low dose or high dose
Aroclor1260/PCB126 exposure enriched the processes related to insulin signal
pathway, including "insulin-like growth factor receptor signaling pathway",
"receptor tyrosine kinase signaling pathway", "Signal transduction_Insulin
signaling" and "Signal transduction_WNT signaling". The results were
consistent with the results from TFA.

Although AUC did not show differences between groups, we got some
meaningful data from proteomics. There are a couple of reasons for this
inconsistency, first, although GTT is relatively easy to perform and minimally
invasive, the interpretation of these tests can be strongly influenced by variable
experimental conditions (like the accurate time point of measurement, the
emotion changes of mice, and the accuracy of glucometer) and data analysis.
Second, the results from GTT may not be able to reflect the early changes in
pancreatic function.

In ongoing research, the results from proteomics will be validated by other
methods, like Western blots, phenotype, plasma insulin, adipokines, HOMA-IR,
HOMA-B, etc.

In conclusion, transcription factor analysis showed transcription factors
related to pancreas function were over-connected with low dose and high dose
Aroclor 1260/PCB 126, like HNF1-alpha, HNF1-beta and HNF4-alpha, which
were associated with MODY 3, MODY 5 and MODY 1 in human. Processes
associated with insulin signal pathway were enriched by either low dose or high
dose of Aroclor 1260/PCB126, including "insulin-like growth factor receptor

signaling pathway", "receptor tyrosine kinase signaling pathway", "Signal

transduction_Insulin signaling". The study is an ongoing research, and more

data are required.

CHAPTER 5

OVERALL SUMMARY

Overall goal and specific aims

As persistent organic pollutants PCBs are associated with non-alcoholic fatty liver disease (NAFLD) and metabolic disruption. Previous studies focus mostly on the effect of NDL PCBs and single PCB congeners. But in real life, people are exposed to DL-PCB and NDL-PCB mixtures. We have built a relevant model, Aroclor1260/PCB126, which increases the amount of DL-PCB (PCB126) (20µg /kg) to activate the AhR. The chronic effects of DL/NDL- PCB mixture need to be investigated. The mechanism of PCB-induced NAFLD still remains unclear. PCBs are predicted to interact with many receptors previously implicated in xenobiotic/energy metabolism and NAFLD, including AhR, Pxr, Car etc. And DL- PCBs are potent AhR ligand, and cause steatosis. The overactivation of AhR can be found in NAFLD. The exact role of AhR in hepatic proteome and lipid metabolism needs to be elucidated. The overall goal of this dissertation was to evaluate the chronic effects of different PCBs exposure by phenotype and untargeted proteomics. To fulfill the goal, we performed the following specific aims:

Aim 1: Investigate the chronic exposure effects and potential mechanisms of DL-PCBs and NDL-PCBs, or co-exposures to both in a diet-induced obesity mouse model.

Aim 2: Evaluate the role of AhR plays in the regulating hepatic proteome and whether this process is independent of PCB exposure or not in an AhR knockout mouse model.

Aim 3: Investigate the acute exposure effects and potential mechanisms of different doses of DL+NDL PCBs on pancreatic proteome in a female mouse model.

Major findings of this dissertation

Chronic PCB exposure study adopted proteomics to observe the effects of different PCB exposures in protein production differences, which provided us new insights towards the mechanism of PCB toxicity. In this study, we found PCB126 rather than Aroclor 1260 decreased hepatic inflammation and fibrosis at the molecular level, while it altered cytoskeletal remodeling, metal homeostasis, and damaged intermediary and xenobiotic metabolism.

In acute AhR knockout study, we used global AhR null mice to observe without AhR, how PCB126 altered hepatic proteome and lipid metabolism whether the process was AhR independent or not. Global AhR gene deletion caused significant lipid accumulation. The effects of PCB126 were not all AhR-dependent, and its effect on hepatic proteome were AhR dependent. This

finding is the first research to confirm the role AhR plays in the regulation of hepatic proteome and lipid metabolism.

In female mice acute PCB mixture exposure study, we found transcription factors (such as HNF1-alpha, HNF1-beta and HNF4-alpha) related to pancreas function were over-connected with both doses of Aroclor 1260/PCB 126 exposure, and observed that processes associated with insulin signal pathway were enriched by low dose or high dose Aroclor 1260/PCB126, including "insulin-like growth factor receptor signaling pathway", "receptor tyrosine kinase signaling pathway", "Signal transduction_Insulin signaling" and "Signal transduction_WNT signaling".

Strengths of this dissertation

There is much strength in this dissertation. First and foremost, for the first time, we discovered the role of AhR in regulating the hepatic proteome and lipid metabolism which was independent of PCB exposure. And we confirmed AhR plays a pivotal physiological role in maintaining lipid homeostasis and hormone production. And we clarify the misunderstanding towards AhR, which is deletion of AhR may bring about a protective effect against lipidosis, on the contrary, whole deletion of AhR gene will cause severe NAFLD.

Secondly, we used hepatic proteomics to explore the underlying mechanisms of PCB exposure effect, which provided us new insights toward their action modes, like PCB126 altered cytoskeletal remodeling and metal homeostasis, xenobiotic metabolism, which were not reported previously.

Another finding is that in acute AhR knockout study, several miRNAs were found to be associated with PCB126 and AhR ablation in mouse model; several miRNAs can also be observed in human samples; some of the miRNAs have strong association with some NASH biomarkers. All these will provide us new direction to our future research.

Lastly, in female mice acute PCB mixture study, for the first time, we observed the association between PCB exposure and some responsible genes involved in MODY in humans, it provides us new insights to explore the association between MODY and PCB exposure, the potential mechanisms of both.

Limitations of this dissertation

There are several weaknesses of this dissertation. Although we described the phenotypic effects of different types of PCB exposure on liver and pancreatic disease, the precise molecular mechanisms, underpinning these observations were not determined. They need further investigation in the future. Potential species differences due to differential AhR ligand binding affinity were not examined. Moreover, potential sex differences need to be pointed out for in PCB exposed populations, men tend to have a slightly higher prevalence of liver disease, while women tended to have a higher prevalence of type 2 diabetes. While proteins regulating metal homeostasis and epigenetics were implicated, direct measurement of hepatic metals and epigenetic signatures was not performed. Another weakness is female mice

acute PCB mixture study, although we got some valuable data from proteomics, all of these remain to be validated by other methods.

Future directions

1. Evaluate the potential effects of species and sex differences on the endocrine disruption and TASH induced by PCB exposures.

2. Use proteomics technique and TMT labelling to analyze different chronic PCB-exposed pancreas samples, to explore the potential mechanism of PCB-induced diabetes.

3. Since PCB-exposure mostly is a chronic process, studies with a longer period may be needed (e.g., 6 months).

Conclusion

Taken together, this dissertation evaluated the acute and chronic effects of PCB exposure on liver and pancreas, also explored the role of AhR in regulating hepatic proteome and lipid metabolism. The chronic exposure study demonstrated PCBs, NDL PCBs, and a more environmentally relevant mixture of both types of PCBs differentially modulated the hepatic proteome and the severity of diet- induced NAFLD. PCB 126 decreased hepatic inflammation at the molecular level, while Aroclor1260 increased hepatic inflammation and promote phosphoprotein signaling disruption consistent with prior research. PCB126 altered cytoskeletal remodeling, and disrupted metal homeostasis, and the intermediary and xenobiotic metabolism; all of them implicated in PCB126's mode of action. Aroclor1260 + PCB126 exposure enriched multiple

epigenetic processes, and these could potentially explain the observed nonadditive effects of the exposures on the hepatic proteome. Acute AhR knockout study showed 12 differentially abundant hepatic proteins related to lipid metabolism were altered by AhR deletion; Gene ontology analysis showed metabolic processes including 'oxidation-reduction process' and 'lipid metabolic process' were enriched in Ahr$^{-/-}$ mice; transcription factors involved in lipid metabolism including Zfp125, LXRα, SREBP1 (nuclear), c-Fos were over-connected with Ahr$^{-/-}$. Global AhR gene deletion caused significantly lipid accumulation rather than had protective effect against NAFLD. The mechanism of AhR knockout-induced lipidosis was probably through the upregulation of lipogenic genes (CD36, Perilipin-2) and downregulation of lipolytic gene (Pnpla3). Most importantly, the study discovered how Ahr regulated hepatic proteome and lipid metabolism independent of PCB exposure. In the female mice acute PCB mixture study, pancreatic proteomics showed transcription factors related to pancreas function were over-connected with low dose and high dose Aroclor 1260/PCB 126, like HNF1-alpha, HNF1-beta and HNF4-alpha, responsible genes of MODY in human; processes related to insulin signal pathway were enriched by low dose or high dose Aroclor 1260/PCB126, including 'insulin-like growth factor receptor signaling pathway', 'receptor tyrosine kinase signaling pathway', 'Signal transduction_Insulin signaling" and "Signal transduction_WNT signaling".

REFERENCES

1. Safe S. Toxicology, structure-function relationship, and human and environmental health impacts of polychlorinated biphenyls: progress and problems. Environmental health perspectives. 1993;100:259-68. PubMed PMID: 8354174; PMCID: PMC1519588.

2. Wahlang B, Song M, Beier JI, Cameron Falkner K, Al-Eryani L, Clair HB, Prough RA, Osborne TS, Malarkey DE, Christopher States J, Cave MC. Evaluation of Aroclor 1260 exposure in a mouse model of diet-induced obesity and non-alcoholic fatty liver disease. Toxicology and applied pharmacology. 2014;279(3):380-90. Epub 2014/07/08. doi: 10.1016/j.taap.2014.06.019. PubMed PMID: 24998970; PMCID: PMC4225625.

3. Yu ML, Guo YL, Hsu CC, Rogan WJ. Increased mortality from chronic liver disease and cirrhosis 13 years after the Taiwan "yucheng" ("oil disease") incident. Am J Ind Med. 1997 Feb;31(2):172-5. doi: 10.1002/(sici)1097-0274(199702)31:2<172::aid-ajim6>3.0.co;2-1. PMID: 9028433.

4. Wang S-L, Tsai P-C, Yang C-Y, Leon Guo Y. Increased Risk of Diabetes and Polychlorinated Biphenyls and Dioxins. A 24-year follow-up study of the Yucheng cohort. 2008;31(8):1574-9. doi: 10.2337/dc07-2449.

5. Silverstone AE, Rosenbaum PF, Weinstock RS, Bartell SM, Foushee HR, Shelton C, Pavuk M. Polychlorinated biphenyl (PCB) exposure and diabetes: results from the Anniston Community Health Survey. Environmental health perspectives. 2012;120(5):727-32. Epub 2012/02/16. doi: 10.1289/ehp.1104247. PubMed PMID: 22334129; PMCID: PMC3346783.

6. Clair HB, Pinkston CM, Rai SN, Pavuk M, Dutton ND, Brock GN, Prough RA, Falkner KC, McClain CJ, Cave MC. Liver Disease in a Residential Cohort With Elevated Polychlorinated Biphenyl Exposures. Toxicological sciences : an official journal of the Society of Toxicology. 2018;164(1):39-49. Epub 2018/04/24. doi: 10.1093/toxsci/kfy076. PubMed PMID: 29684222; PMCID: PMC6016643.

7. Porta M, Zumeta E. Implementing the Stockholm Treaty on Persistent Organic Pollutants. Occupational and Environmental Medicine. 2002;59(10):651-2. doi: 10.1136/oem.59.10.651.

8. Breivik K, Sweetman A, Pacyna JM, Jones KC. Towards a global historical emission inventory for selected PCB congeners — a mass balance approach: 2. Emissions. Science of The Total Environment. 2002;290(1):199-224. doi: https://doi.org/10.1016/S0048-9697(01)01076-2.

9. Mangelsdorf DJ, Thummel C, Beato M, Herrlich P, Schutz G, Umesono K, Blumberg B, Kastner P, Mark M, Chambon P, Evans RM. The nuclear receptor superfamily: the second decade. Cell. 1995;83(6):835-9. Epub 1995/12/15. PubMed PMID: 8521507; PMCID: PMC6159888.

10. Novac N, Heinzel T. Nuclear receptors: overview and classification. Current drug targets Inflammation and allergy. 2004;3(4):335-46. Epub 2004/12/09. PubMed PMID: 15584884.

11. Baes M, Gulick T, Choi HS, Martinoli MG, Simha D, Moore DD. A new orphan member of the nuclear hormone receptor superfamily that interacts with a subset of retinoic acid response elements. Mol Cell Biol. 1994;14(3):1544-52. Epub 1994/03/01. PubMed PMID: 8114692; PMCID: PMC358513.

12. Bertilsson G, Heidrich J, Svensson K, Åsman M, Jendeberg L, Sydow-Bäckman M, Ohlsson R, Postlind H, Blomquist P, Berkenstam A. Identification of a human nuclear receptor defines a new signaling pathway for CYP3A induction. Proceedings of the National Academy of Sciences. 1998;95(21):12208-13. doi: 10.1073/pnas.95.21.12208.

13. Lehmann JM, McKee DD, Watson MA, Willson TM, Moore JT, Kliewer SA. The human orphan nuclear receptor PXR is activated by compounds that regulate CYP3A4 gene expression and cause drug interactions. Journal of Clinical Investigation. 1998;102(5):1016-23. PubMed PMID: PMC508967.

14. Kliewer SA, Goodwin B, Willson TM. The Nuclear Pregnane X Receptor: A Key Regulator of Xenobiotic Metabolism. Endocrine Reviews. 2002;23(5):687-702. doi: 10.1210/er.2001-0038.

15. Van den Berg M, Birnbaum L, Bosveld AT, Brunström B, Cook P, Feeley M, Giesy JP, Hanberg A, Hasegawa R, Kennedy SW, Kubiak T, Larsen JC, van Leeuwen FX, Liem AK, Nolt C, Peterson RE, Poellinger L, Safe S, Schrenk D, Tillitt D, Tysklind M, Younes M, Waern F, Zacharewski T. Toxic equivalency factors (TEFs) for PCBs, PCDDs, PCDFs for humans and

wildlife. Environmental health perspectives. 1998;106(12):775-92. PubMed PMID: PMC1533232.

16. Tsai P-C, Ko Y-C, Huang W, Liu H-S, Guo YL. Increased liver and lupus mortalities in 24-year follow-up of the Taiwanese people highly exposed to polychlorinated biphenyls and dibenzofurans. Science of The Total Environment. 2007;374(2):216-22. doi: https://doi.org/10.1016/j.scitotenv.2006.12.024.

17. Michelotti GA, Machado MV, Diehl AM. NAFLD, NASH and liver cancer. Nature Reviews Gastroenterology &Amp; Hepatology. 2013;10:656. doi: 10.1038/nrgastro.2013.183.

18. Younossi ZM, Koenig AB, Abdelatif D, Fazel Y, Henry L, Wymer M. Global epidemiology of nonalcoholic fatty liver disease—Meta-analytic assessment of prevalence, incidence, and outcomes. Hepatology. 2016;64(1):73-84. doi: doi:10.1002/hep.28431.

19. Buzzetti E, Pinzani M, Tsochatzis EA. The multiple-hit pathogenesis of non-alcoholic fatty liver disease (NAFLD). Metabolism. 2016;65(8):1038-48. doi: https://doi.org/10.1016/j.metabol.2015.12.012.

20. Younossi ZM, Blissett D, Blissett R, Henry L, Stepanova M, Younossi Y, Racila A, Hunt S, Beckerman R. The economic and clinical burden of nonalcoholic fatty liver disease in the United States and Europe. Hepatology. 2016;64(5):1577-86. doi: doi:10.1002/hep.28785.

21. Abumrad N, Coburn C, Ibrahimi A. Membrane proteins implicated in long-chain fatty acid uptake by mammalian cells: CD36, FATP and FABPm. Biochimica et Biophysica Acta (BBA) - Molecular and Cell Biology of Lipids. 1999;1441(1):4-13. doi: https://doi.org/10.1016/S1388-1981(99)00137-7.

22. Bradbury MW. Lipid Metabolism and Liver Inflammation. I. Hepatic fatty acid uptake: possible role in steatosis. American Journal of Physiology-Gastrointestinal and Liver Physiology. 2006;290(2):G194-G8. doi: 10.1152/ajpgi.00413.2005. PubMed PMID: 16407588.

23. Pohl J, Ring A, Herrmann T, Stremmel W. New concepts of cellular fatty acid uptake: role of fatty acid transport proteins and of caveolae. Proceedings of the Nutrition Society. 2007;63(2):259-62. Epub 03/05. doi: 10.1079/PNS2004341.

24. Solinas G, Borén J, Dulloo AG. De novo lipogenesis in metabolic homeostasis: More friend than foe? Molecular Metabolism. 2015;4(5):367-77. doi: https://doi.org/10.1016/j.molmet.2015.03.004.

25. Strable MS, Ntambi JM. Genetic control of de novo lipogenesis: role in diet-induced obesity. Critical Reviews in Biochemistry and Molecular Biology. 2010;45(3):199-214. doi: 10.3109/10409231003667500.

26. Meex RCR, Watt MJ. Hepatokines: linking nonalcoholic fatty liver disease and insulin resistance. Nature Reviews Endocrinology. 2017;13:509. doi: 10.1038/nrendo.2017.56.

27. J D McGarry a, Foster DW. Regulation of Hepatic Fatty Acid Oxidation and Ketone Body Production. Annual Review of Biochemistry. 1980;49(1):395-420. doi: 10.1146/annurev.bi.49.070180.002143. PubMed PMID: 6157353.

28. Cave M, Falkner KC, Ray M, Joshi-Barve S, Brock G, Khan R, Bon Homme M, McClain CJ. Toxicant-associated steatohepatitis in vinyl chloride workers. Hepatology. 2010;51(2):474-81. doi: doi:10.1002/hep.23321.

29. Shi H, Jin J, Hardesty JE, Falkner KC, Prough RA, Balamurugan AN, Mokshagundam SP, Chari ST, Cave MC. Polychlorinated biphenyl exposures differentially regulate hepatic metabolism and pancreatic function: Implications for nonalcoholic steatohepatitis and diabetes. Toxicology and applied pharmacology. 2019;363:22-33. Epub 2018/10/13. doi: 10.1016/j.taap.2018.10.011. PubMed PMID: 30312631.

30. National Diabetes Statistics Report https://www.cdc.gov/diabetes/pdfs/data/statistics/national-diabetes-statistics-report.pdf

31. Song Y, Chou EL, Baecker A, You NC, Song Y, Sun Q, Liu S. Endocrine-disrupting chemicals, risk of type 2 diabetes, and diabetes-related metabolic traits: A systematic review and meta-analysis. Journal of diabetes. 2016;8(4):516-32. Epub 2015/06/30. doi: 10.1111/1753-0407.12325. PubMed PMID: 26119400.

32. Vorkamp K. An overlooked environmental issue? A review of the inadvertent formation of PCB-11 and other PCB congeners and their occurrence in consumer products and in the environment. Science of The Total Environment. 2016;541:1463-76. doi: https://doi.org/10.1016/j.scitotenv.2015.10.019.

33. Kawano Y, Nishiumi S, Tanaka S, Nobutani K, Miki A, Yano Y, Seo Y, Kutsumi H, Ashida H, Azuma T, Yoshida M. Activation of the aryl hydrocarbon receptor induces hepatic steatosis via the upregulation of fatty acid transport. Archives of biochemistry and biophysics. 2010;504(2):221-7. Epub 2010/09/14. doi: 10.1016/j.abb.2010.09.001. PubMed PMID: 20831858.

34. Xu CX, Wang C, Zhang ZM, Jaeger CD, Krager SL, Bottum KM, Liu J, Liao DF, Tischkau SA. Aryl hydrocarbon receptor deficiency protects mice from diet-induced adiposity and metabolic disorders through increased energy expenditure. Int J Obes (Lond). 2015 Aug;39(8):1300-1309. doi: 10.1038/ijo.2015.63. Epub 2015 Apr 24. PMID: 25907315; PMCID: PMC4526411.

35. Schmidt JV, Su GH, Reddy JK, Simon MC, Bradfield CA. Characterization of a murine Ahr null allele: involvement of the Ah receptor in hepatic growth and development. Proc Natl Acad Sci U S A. 1996 Jun 25;93(13):6731-6. doi: 10.1073/pnas.93.13.6731. PMID: 8692887; PMCID: PMC39095.

36. Wahlang B, Jin J, Hardesty JE, Head KZ, Shi H, Falkner KC, Prough RA, Klinge CM, Cave MC. Identifying sex differences arising from polychlorinated biphenyl exposures in toxicant-associated liver disease. Food and chemical toxicology : an international journal published for the British Industrial Biological Research Association. 2019;129:64-76. Epub 2019/04/27. doi: 10.1016/j.fct.2019.04.007. PubMed PMID: 31026535.

37. Heindel JJ, Blumberg B, Cave M, Machtinger R, Mantovani A, Mendez MA, Nadal A, Palanza P, Panzica G, Sargis R, Vandenberg LN, Vom Saal F. Metabolism disrupting chemicals and metabolic disorders. Reproductive toxicology (Elmsford, NY). 2017;68:3-33. Epub 2016/10/21. doi: 10.1016/j.reprotox.2016.10.001. PubMed PMID: 27760374; PMCID: PMC5365353.

38. Cave M, Appana S, Patel M, Falkner KC, McClain CJ, Brock G. Polychlorinated biphenyls, lead, and mercury are associated with liver disease in American adults: NHANES 2003-2004. Environmental health perspectives. 2010;118(12):1735-42. Epub 2010/12/04. doi: 10.1289/ehp.1002720. PubMed PMID: 21126940; PMCID: PMC3002193.

39. Raffetti E, Donato F, Speziani F, Scarcella C, Gaia A, Magoni M. Polychlorinated biphenyls (PCBs) exposure and cardiovascular, endocrine and metabolic diseases: A population-based cohort study in a North Italian highly polluted area. Environment international. 2018;120:215-22. Epub 2018/08/14. doi: 10.1016/j.envint.2018.08.022. PubMed PMID: 30103120.

40. Everett CJ, Frithsen I, Player M. Relationship of polychlorinated biphenyls with type 2 diabetes and hypertension. Journal of environmental monitoring : JEM. 2011;13(2):241-51. Epub 2010/12/04. doi: 10.1039/c0em00400f. PubMed PMID: 21127808.

41. Rosenbaum PF, Weinstock RS, Silverstone AE, Sjodin A, Pavuk M. Metabolic syndrome is associated with exposure to organochlorine pesticides in Anniston, AL, United States. Environment international. 2017;108:11-21. Epub 2017/08/06. doi: 10.1016/j.envint.2017.07.017. PubMed PMID: 28779625; PMCID: PMC5627356.

42. Goncharov A, Haase RF, Santiago-Rivera A, Morse G, McCaffrey RJ, Rej R, Carpenter DO. High serum PCBs are associated with elevation of serum lipids and cardiovascular disease in a Native American population. Environmental research. 2008;106(2):226-39. Epub 2007/12/07. doi: 10.1016/j.envres.2007.10.006. PubMed PMID: 18054906; PMCID: PMC2258089.

43. Addison RF. PCB replacements in dielectric fluid. Environmental science & technology. 1983;17(10):486a-94a. Epub 1983/10/01. doi: 10.1021/es00116a715. PubMed PMID: 22656288.

44. Safe S, Bandiera S, Sawyer T, Robertson L, Safe L, Parkinson A, Thomas PE, Ryan DE, Reik LM, Levin W. PCBs: structure-function relationships and mechanism of action. Environmental health perspectives. 1985;60:47-56. doi: 10.1289/ehp.856047. PubMed PMID: 2992927.

45. Wahlang B, Falkner KC, Clair HB, Al-Eryani L, Prough RA, States JC, Coslo DM, Omiecinski CJ, Cave MC. Human receptor activation by aroclor 1260, a polychlorinated biphenyl mixture. Toxicological sciences : an official journal of the Society of Toxicology. 2014;140(2):283-97. Epub 2014/05/09. doi: 10.1093/toxsci/kfu083. PubMed PMID: 24812009; PMCID: PMC4176050.

46. Wahlang B, Prough RA, Falkner KC, Hardesty JE, Song M, Clair HB, Clark BJ, States JC, Arteel GE, Cave MC. Polychlorinated Biphenyl-Xenobiotic Nuclear Receptor Interactions Regulate Energy Metabolism, Behavior, and Inflammation in Non-alcoholic-Steatohepatitis. Toxicological sciences : an official journal of the Society of Toxicology. 2016;149(2):396-410. Epub 2015/11/28. doi: 10.1093/toxsci/kfv250. PubMed PMID: 26612838; PMCID: PMC4751229.

47. Wahlang B, Beier JI, Clair HB, Bellis-Jones HJ, Falkner KC, McClain CJ, Cave MC. Toxicant-associated steatohepatitis. Toxicologic pathology. 2013;41(2):343-60. Epub 2012/12/25. doi: 10.1177/0192623312468517. PubMed PMID: 23262638; PMCID: PMC5114851.

48. Wahlang B, Jin J, Beier J, Hardesty J, Daly E, Schnegelberger R, Falkner K, Prough R, Kirpich I, Cave M. Mechanisms of Environmental Contributions to Fatty Liver Disease. Current Environmental Health Reports. 2019;6. doi: 10.1007/s40572-019-00232-w.

49. Wahlang B, Hardesty J, Jin J, Falkner K, Cave M. Polychlorinated Biphenyls and Nonalcoholic Fatty Liver Disease. Current Opinion in Toxicology. 2019;14. doi: 10.1016/j.cotox.2019.06.001.

50. Angrish MM, Mets BD, Jones AD, Zacharewski TR. Dietary fat is a lipid source in 2,3,7,8-tetrachlorodibenzo-ρ-dioxin (TCDD)-elicited hepatic steatosis in C57BL/6 mice. Toxicological sciences : an official journal of the Society of Toxicology. 2012;128(2):377-86. Epub 2012/04/28. doi: 10.1093/toxsci/kfs155. PubMed PMID: 22539624; PMCID: PMC3493189.

51. Hardesty JE, Wahlang B, Falkner KC, Shi H, Jin J, Zhou Y, Wilkey DW, Merchant ML, Watson CT, Feng W, Morris AJ, Hennig B, Prough RA, Cave MC. Proteomic Analysis Reveals Novel Mechanisms by Which Polychlorinated Biphenyls Compromise the Liver Promoting Diet-Induced Steatohepatitis. Journal of proteome research. 2019;18(4):1582-94. Epub 2019/02/27. doi: 10.1021/acs.jproteome.8b00886. PubMed PMID: 30807179.

52. Hardesty JE, Wahlang B, Falkner KC, Clair HB, Clark BJ, Ceresa BP, Prough RA, Cave MC. Polychlorinated biphenyls disrupt hepatic epidermal growth factor receptor signaling. Xenobiotica; the fate of foreign compounds in biological systems. 2017;47(9):807-20. Epub 2016/07/28. doi: 10.1080/00498254.2016.1217572. PubMed PMID: 27458090; PMCID: PMC5512701.

53. Hardesty JE, Wahlang B, Falkner KC, Shi H, Jin J, Wilkey D, Merchant M, Watson C, Prough RA, Cave MC. Hepatic signalling disruption by pollutant Polychlorinated biphenyls in steatohepatitis. Cellular signalling. 2019;53:132-9. Epub 2018/10/10. doi: 10.1016/j.cellsig.2018.10.004. PubMed PMID: 30300668; PMCID: PMC6289731.

54. Serdar B, LeBlanc WG, Norris JM, Dickinson LM. Potential effects of polychlorinated biphenyls (PCBs) and selected organochlorine pesticides (OCPs) on immune cells and blood biochemistry measures: a cross-sectional assessment of the NHANES 2003-2004 data. Environmental health : a global access science source. 2014;13:114. Epub 2014/12/18. doi: 10.1186/1476-069x-13-114. PubMed PMID: 25515064; PMCID: PMC4290093.

55. Livak KJ, Schmittgen TD. Analysis of relative gene expression data using real-time quantitative PCR and the 2(-Delta Delta C(T)) Method. Methods 2001;25:402-408.

56. Bligh EG, Dyer WJ. A rapid method of total lipid extraction and purification. Can J Biochem Physiol. 1959;37(8):911-7. Epub 1959/08/01. doi: 10.1139/o59-099. PubMed PMID: 13671378.

57. Wisniewski JR, Zougman A, Nagaraj N, Mann M. Universal sample preparation method for proteome analysis. Nature methods. 2009;6(5):359-62. Epub 2009/04/21. doi: 10.1038/nmeth.1322. PubMed PMID: 19377485.

58. Engholm-Keller K, Larsen MR. Improving the Phosphoproteome Coverage for Limited Sample Amounts Using TiO2-SIMAC-HILIC (TiSH) Phosphopeptide Enrichment and Fractionation. Methods in molecular biology (Clifton, NJ). 2016;1355:161-77. Epub 2015/11/21. doi: 10.1007/978-1-4939-3049-4_11. PubMed PMID: 26584925.

59. Keshishian H, Burgess MW, Gillette MA, Mertins P, Clauser KR, Mani DR, Kuhn EW, Farrell LA, Gerszten RE, Carr SA. Multiplexed, Quantitative Workflow for Sensitive Biomarker Discovery in Plasma Yields Novel Candidates for Early Myocardial Injury. Molecular & cellular proteomics : MCP. 2015;14(9):2375-93. Epub 2015/03/01. doi: 10.1074/mcp.M114.046813. PubMed PMID: 25724909; PMCID: PMC4563722.

60. McDowell GS, Gaun A, Steen H. iFASP: combining isobaric mass tagging with filter-aided sample preparation. Journal of proteome research. 2013;12(8):3809-12. Epub 2013/05/23. doi: 10.1021/pr400032m. PubMed PMID: 23692318; PMCID: PMC4416645.

61. Srivastava S, Merchant M, Rai A, Rai SN. Interactive Web Tool for Standardizing Proteomics Workflow for Liquid Chromatography-Mass Spectrometry Data. Journal of proteomics & bioinformatics. 2019;12(4):85-8. Epub 2019/01/01. PubMed PMID: 32148360; PMCID: PMC7059686.

62. Srivastava S, Merchant M, Rai A, Rai SN. Standardizing Proteomics Workflow for Liquid Chromatography-Mass Spectrometry: Technical and Statistical Considerations. Journal of proteomics & bioinformatics. 2019;12(3):48-55. Epub 2019/01/01. doi: 10.35248/0974-276x.19.12.496. PubMed PMID: 32148359; PMCID: PMC7059694.

63. Zhao J, O'Neil M, Vittal A, Weinman SA, Tikhanovich I. PRMT1-Dependent Macrophage IL-6 Production Is Required for Alcohol-Induced HCC Progression. Gene expression. 2019;19(2):137-50. Epub 2018/09/22. doi: 10.3727/105221618x15372014086197. PubMed PMID: 30236171; PMCID: PMC6466176.

64. Koh MY, Gagea M, Sargis T, Lemos R Jr, Grandjean G, Charbono A, Bekiaris V, Sedy J, Kiriakova G, Liu X, Roberts LR, Ware C, Powis G. A new HIF-1α/RANTES-driven pathway to hepatocellular carcinoma mediated by germline haploinsufficiency of SART1/HAF in mice.

Hepatology. 2016 May;63(5):1576-91. doi: 10.1002/hep.28468. Epub 2016 Mar 7. PMID: 26799785; PMCID: PMC4840057.

65. Wahlang B, Barney J, Thompson B, Wang C, Hamad OM, Hoffman JB, Petriello MC, Morris AJ, Hennig B. Editor's Highlight: PCB126 Exposure Increases Risk for Peripheral Vascular Diseases in a Liver Injury Mouse Model. Toxicol Sci. 2017 Dec 1;160(2):256-267. doi: 10.1093/toxsci/kfx180. PMID: 28973532; PMCID: PMC5837513.

66. Wahlang B, Perkins JT, Petriello MC, Hoffman JB, Stromberg AJ, Hennig B. A compromised liver alters polychlorinated biphenyl-mediated toxicity. Toxicology. 2017 Apr 1;380:11-22. doi: 10.1016/j.tox.2017.02.001. Epub 2017 Feb 2. PMID: 28163111; PMCID: PMC5374277.

67. Hardesty JE, Al-Eryani L, Wahlang B, Falkner KC, Shi H, Jin J, Vivace BJ, Ceresa BP, Prough RA, Cave MC. Epidermal Growth Factor Receptor Signaling Disruption by Endocrine and Metabolic Disrupting Chemicals. Toxicological sciences : an official journal of the Society of Toxicology. 2018;162(2):622-34. Epub 2018/01/13. doi: 10.1093/toxsci/kfy004. PubMed PMID: 29329451; PMCID: PMC5888991.

68. Patandin S, Koopman-Esseboom C, de Ridder MA, Weisglas-Kuperus N, Sauer PJ. Effects of environmental exposure to polychlorinated biphenyls and dioxins on birth size and growth in Dutch children. Pediatr Res. 1998 Oct;44(4):538-45. doi: 10.1203/00006450-199810000-00012. PMID: 9773843.

69. ten Tusscher GW, Steerenberg PA, van Loveren H, Vos JG, von dem Borne AE, Westra M, van der Slikke JW, Olie K, Pluim HJ, Koppe JG. Persistent hematologic and immunologic disturbances in 8-year-old Dutch children associated with perinatal dioxin exposure. Environ Health Perspect. 2003 Sep;111(12):1519-23. doi: 10.1289/ehp.5715. PMID: 12948893; PMCID: PMC1241656.

70. Jan YH, Lai TC, Yang CJ, Huang MS, Hsiao M. A co-expressed gene status of adenylate kinase 1/4 reveals prognostic gene signature associated with prognosis and sensitivity to EGFR targeted therapy in lung adenocarcinoma. Sci Rep. 2019 Aug 23;9(1):12329. doi: 10.1038/s41598-019-48243-9. PMID: 31444368; PMCID: PMC6707279.

71. Abera MB, Kazanietz MG. Protein kinase Cα mediates erlotinib resistance in lung cancer cells. Mol Pharmacol. 2015 May;87(5):832-41. doi: 10.1124/mol.115.097725. Epub 2015 Feb 27. PMID: 25724832; PMCID: PMC4407729.

72. Lei CT, Wei YH, Tang H, Wen Q, Ye C, Zhang C, Su H. PKC-α Triggers EGFR Ubiquitination, Endocytosis and ERK Activation in Podocytes

Stimulated with High Glucose. Cell Physiol Biochem. 2017;42(1):281-294. doi: 10.1159/000477329. Epub 2017 May 25. PMID: 28535513.

73. Yin N, Lepp A, Ji Y, Mortensen M, Hou S, Qi XM, Myers CR, Chen G. The K-Ras effector p38γ MAPK confers intrinsic resistance to tyrosine kinase inhibitors by stimulating EGFR transcription and EGFR dephosphorylation. J Biol Chem. 2017 Sep 8;292(36):15070-15079. doi: 10.1074/jbc.M117.779488. Epub 2017 Jul 24. PMID: 28739874; PMCID: PMC5592682.

74. González-Terán B, Matesanz N, Nikolic I, Verdugo MA, Sreeramkumar V, Hernández-Cosido L, Mora A, Crainiciuc G, Sáiz ML, Bernardo E, Leiva-Vega L, Rodríguez E, Bondía V, Torres JL, Perez-Sieira S, Ortega L, Cuenda A, Sanchez-Madrid F, Nogueiras R, Hidalgo A, Marcos M, Sabio G. p38γ and p38δ reprogram liver metabolism by modulating neutrophil infiltration. EMBO J. 2016 Mar 1;35(5):536-52. doi: 10.15252/embj.201591857. Epub 2016 Feb 3. PMID: 26843485; PMCID: PMC4772851.

75. Zhou L, Tang J, Yang X, Dong H, Xiong X, Huang J, Zhang L, Qin H, Yan S. Five Constituents in Psoralea corylifolia L. Attenuate Palmitic Acid-Induced Hepatocyte Injury via Inhibiting the Protein Kinase C-α/Nicotinamide-Adenine Dinucleotide Phosphate Oxidase Pathway. Front Pharmacol. 2020 Jan 28;10:1589. doi: 10.3389/fphar.2019.01589. PMID: 32116659; PMCID: PMC7025552.

76. Klaren WD, Gadupudi GS, Wels B, Simmons DL, Olivier AK, Robertson LW. Progression of micronutrient alteration and hepatotoxicity following acute PCB126 exposure. Toxicology. 2015;338:1-7. Epub 2015/09/28. doi: 10.1016/j.tox.2015.09.004. PubMed PMID: 26410179; PMCID: PMC4658301.

77. Klaren WD, Vine D, Vogt S, Robertson LW. Spatial distribution of metals within the liver acinus and their perturbation by PCB126. Environ Sci Pollut Res Int. 2018 Jun;25(17):16427-16433. doi: 10.1007/s11356-017-0202-0. Epub 2017 Sep 23. PMID: 28940161; PMCID: PMC5866157.

78. Bagu ET, Layoun A, Calvé A, Santos MM. Friend of GATA and GATA-6 modulate the transcriptional up-regulation of hepcidin in hepatocytes during inflammation. Biometals. 2013 Dec;26(6):1051-65. doi: 10.1007/s10534-013-9683-6. Epub 2013 Nov 1. PMID: 24179092.

79. Shepard BD, Tuma PL. Alcohol-induced alterations of the hepatocyte cytoskeleton. World J Gastroenterol. 2010 Mar 21;16(11):1358-65. doi: 10.3748/wjg.v16.i11.1358. PMID: 20238403; PMCID: PMC2842528.

80. Sizemore GM, Pitarresi JR, Balakrishnan S, Ostrowski MC. The ETS

family of oncogenic transcription factors in solid tumours. Nat Rev Cancer. 2017 Jun;17(6):337-351. doi: 10.1038/nrc.2017.20. Epub 2017 Apr 28. PMID: 28450705.

81. Marcher AB, Bendixen SM, Terkelsen MK, Hohmann SS, Hansen MH, Larsen BD, Mandrup S, Dimke H, Detlefsen S, Ravnskjaer K. Transcriptional regulation of Hepatic Stellate Cell activation in NASH. Sci Rep. 2019 Feb 20;9(1):2324. doi: 10.1038/s41598-019-39112-6. PMID: 30787418; PMCID: PMC6382845.

82. Rommelaere S, Millet V, Vu Manh TP, Gensollen T, Andreoletti P, Cherkaoui-Malki M, Bourges C, Escalière B, Du X, Xia Y, Imbert J, Beutler B, Kanai Y, Malissen B, Malissen M, Tailleux A, Staels B, Galland F, Naquet P. Sox17 regulates liver lipid metabolism and adaptation to fasting. PLoS One. 2014 Aug 20;9(8):e104925. doi: 10.1371/journal.pone.0104925. PMID: 25141153; PMCID: PMC4139292.

83. Merino-Azpitarte M, Lozano E, Perugorria MJ, Esparza-Baquer A, Erice O, Santos-Laso Á, O'Rourke CJ, Andersen JB, Jiménez-Agüero R, Lacasta A, D'Amato M, Briz Ó, Jalan-Sakrikar N, Huebert RC, Thelen KM, Gradilone SA, Aransay AM, Lavín JL, Fernández-Barrena MG, Matheu A, Marzioni M, Gores GJ, Bujanda L, Marin JJG, Banales JM. SOX17 regulates cholangiocyte differentiation and acts as a tumor suppressor in cholangiocarcinoma. J Hepatol. 2017 Jul;67(1):72-83. doi: 10.1016/j.jhep.2017.02.017. Epub 2017 Feb 22. PMID: 28237397; PMCID: PMC5502751.

84. Niopek K, Üstünel BE, Seitz S, Sakurai M, Zota A, Mattijssen F, Wang X, Sijmonsma T, Feuchter Y, Gail AM, Leuchs B, Niopek D, Staufer O, Brune M, Sticht C, Gretz N, Müller-Decker K, Hammes HP, Nawroth P, Fleming T, Conkright MD, Blüher M, Zeigerer A, Herzig S, Berriel Diaz M. A Hepatic GAbp-AMPK Axis Links Inflammatory Signaling to Systemic Vascular Damage. Cell Rep. 2017 Aug 8;20(6):1422-1434. doi: 10.1016/j.celrep.2017.07.023. PMID: 28793265.

85. Bakiri L, Hamacher R, Graña O, Guío-Carrión A, Campos-Olivas R, Martinez L, Dienes HP, Thomsen MK, Hasenfuss SC, Wagner EF. Liver carcinogenesis by FOS-dependent inflammation and cholesterol dysregulation. J Exp Med. 2017 May 1;214(5):1387-1409. doi: 10.1084/jem.20160935. Epub 2017 Mar 29. PMID: 28356389; PMCID: PMC5413325.

86. Ding W, Tan H, Li X, Zhang Y, Fang F, Tian Y, Li J, Pan X. MicroRNA-493 suppresses cell proliferation and invasion by targeting ZFX in human hepatocellular carcinoma. Cancer Biomark. 2018;22(3):427-434. doi: 10.3233/CBM-171036. PMID: 29758928.

87. Qin XY, Suzuki H, Honda M, Okada H, Kaneko S, Inoue I, Ebisui E, Hashimoto K, Carninci P, Kanki K, Tatsukawa H, Ishibashi N, Masaki T, Matsuura T, Kagechika H, Toriguchi K, Hatano E, Shirakami Y, Shiota G, Shimizu M, Moriwaki H, Kojima S. Prevention of hepatocellular carcinoma by targeting MYCN-positive liver cancer stem cells with acyclic retinoid. Proc Natl Acad Sci U S A. 2018 May 8;115(19):4969-4974. doi: 10.1073/pnas.1802279115. Epub 2018 Apr 23. PMID: 29686061; PMCID: PMC5949003.

88. Murray IA, Patterson AD, Perdew GH. Aryl hydrocarbon receptor ligands in cancer: friend and foe. Nature reviews Cancer. 2014;14(12):801-14. Epub 2015/01/09. doi: 10.1038/nrc3846. PubMed PMID: 25568920;

89. Esser C, Rannug A. The aryl hydrocarbon receptor in barrier organ physiology, immunology, and toxicology. Pharmacol Rev. 2015;67(2):259-79. doi: 10.1124/pr.114.009001. PMID: 25657351.

90. Lee JH, Wada T, Febbraio M, He J, Matsubara T, Lee MJ, Gonzalez FJ, Xie W. A novel role for the dioxin receptor in fatty acid metabolism and hepatic steatosis. Gastroenterology. 2010;139(2):653-63. Epub 2010/03/23. doi: 10.1053/j.gastro.2010.03.033. PubMed PMID: 20303349; PMCID: PMC2910786.

91. Angrish MM, Jones AD, Harkema JR, Zacharewski TR. Aryl hydrocarbon receptor-mediated induction of Stearoyl-CoA desaturase 1 alters hepatic fatty acid composition in TCDD-elicited steatosis. Toxicol Sci. 2011 Dec;124(2):299-310. doi: 10.1093/toxsci/kfr226. Epub 2011 Sep 2. PMID: 21890736; PMCID: PMC3216411.

92. Gadupudi GS, Klaren WD, Olivier AK, Klingelhutz AJ, Robertson LW. PCB126-Induced Disruption in Gluconeogenesis and Fatty Acid Oxidation Precedes Fatty Liver in Male Rats. Toxicol Sci. 2016 Jan;149(1):98-110. doi: 10.1093/toxsci/kfv215. Epub 2015 Sep 22. PMID: 26396156; PMCID: PMC4731404.

93. Wang C, Xu CX, Krager SL, Bottum KM, Liao DF, Tischkau SA. Aryl hydrocarbon receptor deficiency enhances insulin sensitivity and reduces PPAR-α pathway activity in mice. Environ Health Perspect. 2011 Dec;119(12):1739-44. doi: 10.1289/ehp.1103593. Epub 2011 Aug 17. PMID: 21849270; PMCID: PMC3261983.

94. Wada T, Sunaga H, Miyata K, Shirasaki H, Uchiyama Y, Shimba S. Aryl Hydrocarbon Receptor Plays Protective Roles against High Fat Diet (HFD)-induced Hepatic Steatosis and the Subsequent Lipotoxicity via Direct Transcriptional Regulation of Socs3 Gene Expression. J Biol Chem.

2016 Mar 25;291(13):7004-16. doi: 10.1074/jbc.M115.693655. Epub 2016 Feb 10. PMID: 26865635; PMCID: PMC4807284.

95. Chi Y, Lin Y, Lu Y, Huang Q, Ye G, Dong S. Gut microbiota dysbiosis correlates with a low-dose PCB126-induced dyslipidemia and non-alcoholic fatty liver disease. Sci Total Environ. 2019 Feb 25;653:274-282. doi: 10.1016/j.scitotenv.2018.10.387. Epub 2018 Oct 30. PMID: 30412872.

96. Su H, Liu J, Wu G, Long Z, Fan J, Xu Z, Liu J, Yu Z, Cao M, Liao N, Peng J, Yu W, Li W, Wu H, Wang X. Homeostasis of gut microbiota protects against polychlorinated biphenyl 126-induced metabolic dysfunction in liver of mice. Sci Total Environ. 2020 Jun 10;720:137597. doi: 10.1016/j.scitotenv.2020.137597. Epub 2020 Feb 26. PMID: 32143051.

97. Gadupudi GS, Elser BA, Sandgruber FA, Li X, Gibson-Corley KN, Robertson LW. PCB126 Inhibits the Activation of AMPK-CREB Signal Transduction Required for Energy Sensing in Liver. Toxicol Sci. 2018 Jun 1;163(2):440-453. doi: 10.1093/toxsci/kfy041. PMID: 29474705; PMCID: PMC5974782.

98. Abbott BD, Perdew GH, Buckalew AR, Birnbaum LS. Interactive regulation of Ah and glucocorticoid receptors in the synergistic induction of cleft palate by 2,3,7,8-tetrachlorodibenzo-p-dioxin and hydrocortisone. Toxicol Appl Pharmacol. 1994 Sep;128(1):138-50. doi: 10.1006/taap.1994.1191. PMID: 8079347.

99. Cohen S, Janicki-Deverts D, Doyle WJ, Miller GE, Frank E, Rabin BS, Turner RB. Chronic stress, glucocorticoid receptor resistance, inflammation, and disease risk. Proc Natl Acad Sci U S A. 2012 Apr 17;109(16):5995-9. doi: 10.1073/pnas.1118355109. Epub 2012 Apr 2. PMID: 22474371; PMCID: PMC3341031.

100. Bardenheier BH, Lin J, Zhuo X, et al. Disability-free life -years lost among adults aged ≥50 years with and without diabetes. Diabetes Care. 2016;39(7):1222–1229.

101. Thayer KA, Heindel JJ, Bucher JR, Gallo MA. Role of environmental chemicals in diabetes and obesity: a National Toxicology Program workshop review. Environmental health perspectives. 2012;120(6):779-89.

102. Perkins JT, Petriello MC, Newsome BJ, Hennig B. Polychlorinated biphenyls and links to cardiovascular disease. Environmental Science and Pollution Research. 2016;23(3):2160-72.

103. Zhang S, Wu T, Chen M, Guo Z, Yang Z, Zuo Z, Wang C. Chronic Exposure to Aroclor 1254 Disrupts Glucose Homeostasis in Male Mice via

Inhibition of the Insulin Receptor Signal Pathway. Environmental science & technology. 2015;49(16):10084-92. Epub 2015/07/21. doi: 10.1021/acs.est.5b01597. PubMed PMID: 26190026.

104. Baker NA, Karounos M, English V, Fang J, Wei Y, Stromberg A, Sunkara M, Morris AJ, Swanson HI, Cassis LA. Coplanar polychlorinated biphenyls impair glucose homeostasis in lean C57BL/6 mice and mitigate beneficial effects of weight loss on glucose homeostasis in obese mice. Environmental health perspectives. 2013;121(1):105-10.

105. Gray SL, Shaw AC, Gagne AX, Chan HM. Chronic exposure to PCBs (Aroclor 1254) exacerbates obesity-induced insulin resistance and hyperinsulinemia in mice. Journal of toxicology and environmental health Part A. 2013;76(12):701-15.

106. Takuma M, Ushijima K, Kumazaki M, Ando H, Fujimura A. Influence of dioxin on the daily variation of insulin sensitivity in mice. Environmental Toxicology and Pharmacology. 2015;40(2):349-51.

107. Rutter GA. Diabetes: Controlling the identity of the adult pancreatic β cell. Nature reviews Endocrinology. 2017;13(3):129-30. Epub 2017/01/21. doi: 10.1038/nrendo.2017.1. PubMed PMID: 28106150.

Supplemental Table 1: Differentially Hepatic Abundant Proteins

Altered by Different PCBs in Chronic Study

List of hepatic proteins (fold change, *p*-value) altered by PCB exposure.

Fold change >1 , protein upregulation; fold change <1, protein downregulation.

Accession Number (Protein Name)	PCB Exposure		
	Ar1260	PCB126	Ar1260+PCB126
Q62293 (T-cell-specific guanine nucleotide triphosphate-binding protein 1)	2.57, 1.62E-04		
P31996-2 (Isoform Short of Macrosialin)	2.26, 1.83E-04		
P31996 (Macrosialin)	2.26, 1.85E-04		
O08800 (Serpin B8)	2.18, 6.19E-04	1.81, 5.72E-03	
Q922Z0 (D-aspartate oxidase)	2.17, 2.31E-04		1.63, 9.89E-03
Q9D1X0 (Nucleolar protein 3)	1.91, 2.19E-03	1.56, 2.58E-02	
Q9D0M0 (Exosome complex exonuclease RRP42)	1.87, 3.30E-03		
Q8R4U6 (DNA topoisomerase I)	1.76, 2.30E-03		1.56, 1.31E-02
Q9EPA7 (Nicotinamide/nicotinic acid mononucleotide adenylyltransferase 1)	1.76, 1.61E-03		
Q8BW41 (Protein O-linked-mannose beta-1,4-N-acetylglucosaminyltransferase 2)	1.67, 1.09E-03	1.55, 3.83E-03	2.21, 1.14E-05
Q8BW41-2 (Isoform 2 of Protein O-linked-mannose beta-1,4-N-acetylglucosaminyltransferase 2)	1.67, 1.09E-03	1.55, 3.83E-03	2.21, 1.14E-05
Q8BX09 (Retinoblastoma-binding protein 5)	1.66, 2.67E-03		
Q68ED3 (Non-canonical poly(A) RNA polymerase PAPD5)	1.65, 4.27E-04		
P56400 (Platelet glycoprotein Ib beta chain)	1.65, 9.86E-04		
O35730-2 (Isoform 2 of E3 ubiquitin-protein ligase RING1)	1.57, 5.01E-05		1.51, 1.27E-04
O35730 (E3 ubiquitin-protein ligase RING1)	1.57, 5.04E-05		1.51, 1.27E-04
Q8C8R3-3 (Isoform 3 of Ankyrin-2)	1.55, 8.77E-04		1.61, 4.43E-04
Q8C8R3 (Ankyrin-2)	1.55, 8.89E-04		1.61, 4.49E-04
Q8C8R3-5 (Isoform 5 of Ankyrin-2)	1.55, 9.31E-04		1.60, 4.68E-04
Q8C8R3-4 (Isoform 4 of Ankyrin-2)	1.54, 9.51E-04		1.60, 4.77E-04
Q8C8R3-2 (Isoform 2 of Ankyrin-2)	1.54, 9.55E-04		1.60, 4.79E-04
P13808 (Anion exchange protein 2)	1.54, 1.99E-03		1.44, 6.67E-03
Q60932 (Voltage-dependent anion-selective channel protein 1)	1.54, 1.42E-03		1.68, 2.60E-04

Protein			
Q60932-2 (Isoform Mt-VDAC1 of Voltage-dependent anion-selective channel protein 1)	1.54, 1.42E-03		1.68, 2.60E-04
P13808-3 (Isoform B2 of Anion exchange protein 2)	1.53, 2.06E-03		1.44, 6.92E-03
P13808-2 (Isoform B1 of Anion exchange protein 2)	1.53, 2.19E-03		1.43, 7.31E-03
O08992 (Syntenin-1)	1.53, 2.04E-04		
Q60931 (Voltage-dependent anion-selective channel protein 3)	1.51, 2.67E-03		
Q99PM3 (Transcription initiation factor IIA subunit 1)	1.48, 5.09E-06		
Q61179 (Interferon regulatory factor 9)	1.48, 2.45E-04		
Q8R2W9 (Pantothenate kinase 3)	1.45, 1.36E-04		
P0DJF2 (Protein PET117 homolog)	1.44, 8.30E-07		1.44, 9.30E-07
Q8BYK4 (Retinol dehydrogenase 12)	1.44, 4.30E-05		
O35153 (BET1-like protein)	1.42, 5.15E-05	1.57, 2.52E-06	1.56, 3.25E-06
Q8VDP2 (UPF0428 protein CXorf56 homolog)	1.42, 4.19E-05		
Q8VBX6-4 (Isoform 4 of Multiple PDZ domain protein)	0.71, 2.09E-04		
Q99N57-2 (Isoform 2 of RAF proto-oncogene serine/threonine-protein kinase)	0.71, 5.52E-04		
Q9D0I8 (mRNA turnover protein 4 homolog)	0.71, 9.17E-06		
Q9D0B5 (Thiosulfate sulfurtransferase/rhodanese-like domain-containing protein 3)	0.71, 1.54E-04		
Q91WP0 (Mannan-binding lectin serine protease 2)	0.70, 1.10E-03		
Q99N57 (RAF proto-oncogene serine/threonine-protein kinase)	0.70, 5.47E-04		
P23204 (Peroxisome proliferator-activated receptor alpha)	0.70, 1.97E-03		
Q9DAG5 (Protein STPG4)	0.70, 1.94E-03		
Q69ZZ9 (Uncharacterized protein KIAA0754)	0.70, 9.30E-04		
Q9DCV3 (Diacylglycerol O-acyltransferase 2)	0.70, 1.14E-04		
Q6QI06-2 (Isoform 2 of Rapamycin-insensitive companion of mTOR)	0.70, 1.09E-04		
O70458-2 (Isoform 2 of Oncostatin-M-specific receptor subunit beta)	0.70, 7.66E-04	0.68, 4.96E-04	
B1AY10 (Transcriptional repressor NF-X1)	0.70, 1.12E-05		
O70458 (Oncostatin-M-specific receptor subunit beta)	0.70, 7.58E-04	0.68, 4.96E-04	
Q6QI06 (Rapamycin-insensitive companion of mTOR)	0.69, 1.01E-04		
B1AY10-2 (Isoform 2 of Transcriptional repressor NF-X1)	0.69, 1.11E-05		
B1AY10-3 (Isoform 3 of Transcriptional repressor NF-X1)	0.69, 1.12E-05		
Q9CR02-2 (Isoform 2 of Translation machinery-associated protein 16)	0.69, 3.01E-04		

Protein	Col 1	Col 2	Col 3
Q3UCQ1 (Forkhead box protein K2)	0.69, 2.35E-03		
Q9CR02 (Translation machinery-associated protein 16)	0.69, 2.91E-04		
Q8CCB4 (Vacuolar protein sorting-associated protein 53 homolog)	0.69, 3.62E-03		0.67, 2.11E-03
Q3UCQ1-2 (Isoform 2 of Forkhead box protein K2)	0.69, 2.35E-03		
Q8R2R1 (Protein O-mannosyl-transferase 1)	0.69, 9.98E-04		
A2AQ25-2 (Isoform 2 of Sickle tail protein)	0.69, 2.04E-03		
A2AQ25 (Sickle tail protein)	0.68, 1.93E-03		
Q8QZZ8 (Ras-related protein Rab-38)	0.68, 1.47E-03		
Q9CQ02 (COMM domain-containing protein 4)	0.68, 3.69E-04		
Q8BGS1-3 (Isoform 3 of Band 4.1-like protein 5)	0.68, 2.25E-03		
Q8BGS1 (Band 4.1-like protein 5)	0.67, 2.08E-03		
P35922-5 (Isoform 5 of Synaptic functional regulator FMR1)	0.67, 1.07E-03		0.66, 8.56E-04
Q6P9R4-2 (Isoform 2 of Rho guanine nucleotide exchange factor 18)	0.67, 2.85E-03		0.62, 6.89E-04
Q6P9R4 (Rho guanine nucleotide exchange factor 18)	0.67, 2.85E-03		0.62, 6.90E-04
P35922-4 (Isoform 4 of Synaptic functional regulator FMR1)	0.67, 1.07E-03		0.66, 8.68E-04
P35922-11 (Isoform 11 of Synaptic functional regulator FMR1)	0.67, 1.06E-03		0.66, 8.92E-04
P35922-10 (Isoform 10 of Synaptic functional regulator FMR1)	0.67, 1.06E-03		0.66, 9.10E-04
P35922-6 (Isoform 6 of Synaptic functional regulator FMR1)	0.67, 1.05E-03		0.66, 9.36E-04
P35922-12 (Isoform 12 of Synaptic functional regulator FMR1)	0.67, 1.05E-03		0.66, 9.38E-04
Q8VDH1-2 (Isoform 2 of F-box only protein 21)	0.66, 1.97E-03		
P01592 (Immunoglobulin J chain)	0.66, 1.17E-03		
Q8VDH1 (F-box only protein 21)	0.66, 1.78E-03		
P05201 (Aspartate aminotransferase)	0.64, 2.18E-03	0.68, 5.82E-03	
Q69ZR9 (Protein TASOR)	0.64, 3.76E-07		
Q69ZR9-2 (Isoform 2 of Protein TASOR)	0.64, 3.86E-07		
Q8BH97 (Reticulocalbin-3)	0.61, 1.95E-03		
P01659 (Ig kappa chain V-III region TEPC 124)	0.49, 1.39E-03	0.50, 1.81E-03	
P01660 (Ig kappa chain V-III region PC 3741/TEPC 111)	0.49, 1.39E-03	0.50, 1.81E-03	
P01658 (Ig kappa chain V-III region MOPC 321)	0.49, 1.40E-03	0.49, 1.39E-03	
Q922U2 (Keratin)	0.28, 2.12E-03		
P20801 (Troponin C)		120.33, 1.30E-03	
P68134 (Actin)		55.47, 7.38E-03	
P09542 (Myosin light chain 3)		33.67, 1.27E-02	

Q9JKS4-3 (Isoform 3 of LIM domain-binding protein 3)	15.36, 7.74E-03	
Q9JKS4-4 (Isoform 4 of LIM domain-binding protein 3)	15.34, 7.76E-03	
Q9JKS4-5 (Isoform 5 of LIM domain-binding protein 3)	15.28, 7.82E-03	
Q9JKS4-6 (Isoform 6 of LIM domain-binding protein 3)	15.28, 7.83E-03	
Q9JKS4-2 (Isoform 2 of LIM domain-binding protein 3)	15.27, 7.85E-03	
Q9JKS4 (LIM domain-binding protein 3)	15.24, 7.88E-03	
P00184 (Cytochrome P450 1A1)	9.09, 7.10E-06	
Q9QZ47-10 (Isoform B3e17 of Troponin T)	8.60, 3.35E-02	
Q9QZ47-3 (Isoform A3e17 of Troponin T)	8.59, 3.37E-02	
Q9QZ47-12 (Isoform B4e17 of Troponin T)	8.59, 3.37E-02	
Q9QZ47-5 (Isoform A5e17 of Troponin T)	8.57, 3.38E-02	
Q9QZ47-2 (Isoform A2e17 of Troponin T)	8.57, 3.39E-02	
Q9QZ47-4 (Isoform A4e17 of Troponin T)	8.56, 3.40E-02	
Q9QZ47-6 (Isoform A6e17 of Troponin T)	8.55, 3.39E-02	
Q9QZ47-8 (Isoform B2e17 of Troponin T)	8.55, 3.40E-02	
Q9QZ47 (Troponin T)	8.54, 3.40E-02	
P00186 (Cytochrome P450 1A2)	5.85, 3.10E-08	2.39, 2.68E-04
Q8CHY6 (Transcriptional repressor p66 alpha	3.95, 4.49E-04	
Q9JIY8 (Probable N-acetyltransferase CML3)	3.37, 1.39E-02	
O35127 (Protein C10)	3.21, 1.45E-05	2.59, 1.43E-04
Q8JZU0 (Nucleoside diphosphate-linked moiety X motif 13)	2.89, 9.89E-05	3.44, 1.70E-05
Q9D6N5 (Dr1-associated corepressor)	2.79, 4.53E-04	2.41, 1.77E-03
Q8C7V3 (U3 small nucleolar RNA-associated protein 15 homolog)	2.78, 3.37E-02	
Q9D0B1 (Zinc finger protein 524)	2.30, 2.47E-03	
B5X0G2 (Major urinary protein 17)	2.30, 3.35E-02	
Q9D816 (Cytochrome P450 2C55)	2.28, 1.01E-03	1.66, 2.66E-02
Q8CGR7 (Uridine phosphorylase 2)	2.27, 2.65E-04	2.99, 9.95E-06
P86049 (Probable RNA-binding protein 46)	2.21, 1.59E-02	
P11589 (Major urinary protein 2)	2.16, 2.38E-02	2.34, 1.37E-02
O88573 (AF4/FMR2 family member 1)	2.16, 5.14E-05	
Q6ZWQ0 (Nesprin-2)	2.15, 1.21E-03	2.24, 7.56E-04
Q8VC19 (5-aminolevulinate synthase)	2.13, 4.05E-03	2.49, 8.81E-04
Q62452 (UDP-glucuronosyltransferase 1-9)	2.11, 1.49E-02	

Q9CY34 (NEDD8-conjugating enzyme UBE2F)	2.11, 9.57E-03	
Q91XQ0 (Dynein heavy chain 8)	2.06, 8.14E-03	
Q91XQ0-2 (Isoform 2 of Dynein heavy chain 8)	2.05, 8.19E-03	
Q8K0V2 (DCN1-like protein 3)	2.03, 2.32E-04	1.55, 1.10E-02
Q3TZ89 (Protein transport protein Sec31B)	2.02, 6.51E-03	1.72, 2.89E-02
Q3TZ89-2 (Isoform 2 of Protein transport protein Sec31B)	2.02, 6.51E-03	1.72, 2.89E-02
Q9D3A8 (Carboxyl-terminal PDZ ligand of neuronal nitric oxide synthase protein)	1.99, 1.08E-03	1.90, 1.93E-03
Q9D3A8-2 (Isoform 2 of Carboxyl-terminal PDZ ligand of neuronal nitric oxide synthase protein)	1.98, 1.11E-03	1.89, 1.98E-03
Q8BKI2-2 (Isoform 2 of Trinucleotide repeat-containing gene 6B protein)	1.96, 3.61E-05	
Q80V94 (AP-4 complex subunit epsilon-1)	1.87, 3.98E-02	
Q8VHP7 (Leukocyte elastase inhibitor B)	1.86, 7.05E-05	
Q5SV42 (Leukocyte elastase inhibitor C)	1.85, 8.47E-05	
Q68FL4-2 (Isoform 2 of Putative adenosylhomocysteinase 3)	1.85, 1.71E-05	1.52, 9.17E-04
Q8VHI3 (GDP-fucose protein O-fucosyltransferase 2)	1.84, 1.02E-02	
Q91WG0 (Acylcarnitine hydrolase)	1.84, 6.97E-04	1.46, 2.17E-02
P56654 (Cytochrome P450 2C37)	1.84, 2.11E-03	
P20852 (Cytochrome P450 2A5)	1.83, 3.91E-04	
Q8VBV3 (Exosome complex component RRP4)	1.83,1.51E-03	1.78, 2.13E-03
Q8VCE1 (DnaJ homolog subfamily C member 28)	1.83,1.51E-03	2.54, 3.71E-06
Q9D0R4 (Probable ATP-dependent RNA helicase DDX56)	1.78,1.32E-02	2.39, 5.91E-04
Q8CHT6 (Protein FAM169B)	1.77,5.57E-06	1.53, 1.52E-04
B2RSH2 (Guanine nucleotide-binding protein G(i) subunit alpha-1)	1.77,3.02E-03	
Q8K0C9 (GDP-mannose 4,6 dehydratase)	1.76,3.71E-03	
P46425 (Glutathione S-transferase P 2)	1.76,1.76E-02	
Q91ZJ9-2 (Isoform 2 of Hyaluronidase-1)	1.75,2.91E-08	1.71, 5.24E-08
Q8C0L9-2 (Isoform 2 of Glycerophosphocholine phosphodiesterase GPCPD1)	1.75,2.67E-04	1.83, 1.25E-04
Q91ZJ9 (Hyaluronidase-1)	1.74, 3.25E-08	1.70, 5.88E-08
Q9CQB7 (LYR motif-containing protein 1)	1.70, 3.20E-04	
P10628 (Homeobox protein Hox-D4)	1.66, 6.61E-05	1.54, 3.50E-04
Q8C0L9 (Glycerophosphocholine phosphodiesterase GPCPD1)	1.66, 7.71E-04	1.76, 2.76E-04
P21570 (Angiogenin)	1.66, 2.03E-03	
Q9D7B1 (tRNA-dihydrouridine(20) synthase [NAD(P)+]-like)	1.66, 4.12E-02	

O88502 (High affinity cAMP-specific and IBMX-insensitive 3',5'-cyclic phosphodiesterase 8A)	1.65, 1.55E-02	
Q9Z0H8 (CAP-Gly domain-containing linker protein 2)	1.65, 1.55E-02	
Q9Z0H8-2 (Isoform 2 of CAP-Gly domain-containing linker protein 2)	1.65, 1.55E-02	
Q8K012 (Formin-binding protein 1-like)	1.63, 1.19E-02	
Q8K012-2 (Isoform 2 of Formin-binding protein 1-like)	1.63, 1.19E-02	
P09926 (Surfeit locus protein 2)	1.62, 1.73E-02	
Q8K419 (Galectin-4)	1.62, 3.40E-03	1.72, 1.28E-03
Q8BG60-2 (Isoform 2 of Thioredoxin-interacting protein)	1.62, 2.51E-08	1.80, 1.14E-09
Q8BR90 (UPF0600 protein C5orf51 homolog)	1.62, 1.49E-03	1.51, 5.06E-03
Q8BR90-2 (Isoform 2 of UPF0600 protein C5orf51 homolog)	1.62, 1.49E-03	
P11590 (Major urinary protein 4)	1.61, 4.01E-02	1.66, 3.13E-02
O54891 (Galectin-6)	1.61, 3.48E-03	
Q641P0-2 (Isoform 2 of Actin-related protein 3B)	1.61, 4.00E-02	
Q8BG60 (Thioredoxin-interacting protein)	1.61, 2.43E-08	1.78, 1.06E-09
Q3U6N9-3 (Isoform 3 of UPF0488 protein C8orf33 homolog)	1.59, 2.87E-03	
Q8QZZ7 (EKC/KEOPS complex subunit Tprkb)	1.58, 1.17E-06	1.68, 1.91E-07
Q9D845 (Testis-expressed protein 9)	1.58, 6.66E-05	1.70, 1.11E-05
Q3U6N9 (UPF0488 protein C8orf33 homolog)	1.57, 3.28E-03	
Q9DBN9 (Probable ATP-dependent RNA helicase DDX59)	1.57, 6.93E-05	1.69, 1.14E-05
Q3U6N9-2 (Isoform 2 of UPF0488 protein C8orf33 homolog)	1.57, 3.47E-03	
D3Z423 (RING finger protein 212B)	1.57, 6.94E-05	
Q8C4Y3 (Negative elongation factor B)	1.56, 6.97E-06	
Q9WTK7-2 (Isoform 2 of Serine/threonine-protein kinase STK11)	1.56, 4.30E-05	
Q8K0R6 (Glycolipid transfer protein domain-containing protein 2)	1.56, 1.35E-04	1.58, 1.00E-04
Q9WTK7 (Serine/threonine-protein kinase STK11)	1.56, 4.54E-05	
Q9CYI4 (Putative RNA-binding protein Luc7-like 1)	1.56, 2.83E-02	
Q3TKT4 (Transcription activator BRG1)	1.55, 6.91E-06	1.52, 1.20E-05
Q3TKT4-2 (Isoform 2 of Transcription activator BRG1)	1.54, 7.41E-06	1.51, 1.29E-05
B1AVY7 (Kinesin-like protein KIF16B)	1.54, 2.61E-04	1.67, 4.03E-05
Q80TF6 (StAR-related lipid transfer protein 9)	1.54, 2.61E-04	1.67, 4.03E-05
Q80TJ1-4 (Isoform 4 of Calcium-dependent secretion activator 1)	1.54, 5.79E-03	

Protein	Value 1	Value 2
Q80TJ1-2 (Isoform 2 of Calcium-dependent secretion activator 1)	1.54, 5.83E-03	
Q8BXL7 (ADP-ribosylation factor-related protein 1)	1.54, 6.64E-04	1.47, 1.68E-03
Q80TJ1 (Calcium-dependent secretion activator 1)	1.53, 5.94E-03	
Q9CZP0 (Ufm1-specific protease 1)	1.53, 5.42E-04	
Q8C0L9-3 (Isoform 3 of Glycerophosphocholine phosphodiesterase GPCPD1)	1.52, 2.05E-03	1.63, 5.70E-04
Q641P0 (Actin-related protein 3B)	1.52, 4.02E-02	
Q80XC2 (tRNA (adenine(58)-N(1))-methyltransferase catalytic subunit TRMT61A)	1.52, 6.09E-03	
P56656 (Cytochrome P450 2C39)	1.52, 2.96E-02	
Q99388 (Component of Sp100-rs)	1.51, 3.73E-04	1.43, 1.40E-03
Q99L43 (Phosphatidate cytidylyltransferase 2)	1.51, 6.36E-05	2.10, 2.47E-08
Q9Z0E8 (Solute carrier family 22 member 5)	1.50, 1.23E-05	1.48, 1.85E-05
Q80V62 (Fanconi anemia group D2 protein homolog)	1.50, 8.40E-04	1.94, 4.09E-06
P49813 (Tropomodulin-1)	1.49, 1.62E-04	
Q9JKK7 (Tropomodulin-2)	1.49, 1.62E-04	
Q9JKK7-3 (Isoform 3 of Tropomodulin-2)	1.49, 1.62E-04	
Q9D902 (General transcription factor IIE subunit 2)	1.49, 3.23E-04	
Q8C1A9-3 (Isoform 3 of Protein ABHD18)	1.48, 8.72E-05	
Q8C1A9-2 (Isoform 2 of Protein ABHD18)	1.48, 7.64E-05	
Q6PDD0 (UDP-glucuronosyltransferase 2A2)	1.47, 4.69E-04	1.55, 1.32E-04
Q80X89 (UDP-glucuronosyltransferase 2A1)	1.47, 4.69E-04	1.55, 1.32E-04
Q9JJ59 (ATP-binding cassette sub-family B member 9)	1.47, 1.64E-03	1.73, 4.60E-05
Q9JJ59-2 (Isoform 2 of ATP-binding cassette sub-family B member 9)	1.47, 1.64E-03	1.73, 4.60E-05
Q9Z0Y9 (Oxysterols receptor LXR-alpha)	1.47, 1.81E-02	
Q91X77-2 (Isoform 2 of Cytochrome P450 2C50)	1.47, 1.98E-02	
Q91X77 (Cytochrome P450 2C50)	1.46, 1.92E-02	
Q64458 (Cytochrome P450 2C29)	1.46, 2.30E-02	
Q61056 (Short transient receptor potential channel 1)	1.46, 1.35E-03	
Q61056-2 (Isoform Beta of Short transient receptor potential channel 1)	1.46, 1.35E-03	
Q8BGT6-2 (Isoform 2 of MICAL-like protein 1)	1.46, 7.28E-05	
P21126 (Ubiquitin-like protein 4A)	1.46, 2.75E-03	

Q8CHK3 (Lysophospholipid acyltransferase 7)	1.46, 2.38E-03	
Q8BGT6 (MICAL-like protein 1)	1.45, 6.17E-05	
Q5U4E2 (Replication initiator 1)	1.45, 6.08E-03	
Q8CEC0 (Nuclear pore complex protein Nup88)	1.45, 8.97E-06	
Q8CEC0-2 (Isoform 2 of Nuclear pore complex protein Nup88)	1.45, 9.64E-06	
Q8CEC0-3 (Isoform 3 of Nuclear pore complex protein Nup88)	1.44, 9.73E-06	
Q9DBB5 (Eukaryotic translation initiation factor 4E type 3)	1.44, 2.62E-04	
Q9R1C8 (5-hydroxytryptamine receptor 6)	1.44, 5.39E-04	1.61, 3.30E-05
Q9CPQ8 (ATP synthase subunit g, mitochondrial)	1.43, 4.41E-03	
Q3UYK3 (TBC1 domain family member 9)	1.43, 9.52E-05	1.45, 7.03E-05
Q3UYK3-2 (Isoform 2 of TBC1 domain family member 9)	1.43, 9.52E-05	1.45, 7.03E-05
Q8BZR9 (Nuclear cap-binding protein subunit 3)	1.43, 7.61E-04	1.84, 1.78E-06
Q5ND34-3 (Isoform 3 of WD repeat-containing protein 81)	1.43, 5.05E-04	
Q9JHI2 (tRNA-specific adenosine deaminase 1)	1.42, 1.72E-02	
Q9JHI2-2 (Isoform 2 of tRNA-specific adenosine deaminase 1)	1.42, 1.72E-02	
Q9JHI2-3 (Isoform 3 of tRNA-specific adenosine deaminase 1)	1.42, 1.72E-02	
Q8R0T6 (Adhesion G protein-coupled receptor G3)	1.42, 2.14E-02	
Q5ND34-2 (Isoform 2 of WD repeat-containing protein 81)	1.42, 5.29E-04	
Q5ND34 (WD repeat-containing protein 81)	1.42, 5.34E-04	
Q9JHW9 (Aldehyde dehydrogenase family 1 member A3)	1.42, 2.91E-02	1.43, 2.67E-02
Q3V0M2 (Leucine-rich repeat-containing protein 36)	1.42, 1.93E-02	
Q9DA03 (Complex III assembly factor LYRM7)	1.42, 2.03E-05	
Q91Z69 (SLIT-ROBO Rho GTPase-activating protein 1)	1.42, 3.41E-03	
Q9JLJ5 (Elongation of very long chain fatty acids protein 1)	1.41, 4.03E-02	
Q80W54 (CAAX prenyl protease 1 homolog)	0.71, 2.75E-03	
Q9QYF1 (Retinol dehydrogenase 11)	0.71, 1.51E-02	
P61226 (Ras-related protein Rap-2b)	0.71, 1.39E-02	
D3Z5L6 (MFS-type transporter SLC18B1)	0.71, 1.12E-02	
Q8BXB6 (Solute carrier organic anion transporter family member 2B1)	0.70, 2.02E-03	
P14069 (Protein S100-A6)	0.70, 9.25E-03	

Protein	Value 1	Value 2
P62254 (Ubiquitin-conjugating enzyme E2 G1)	0.70, 1.66E-02	0.59, 9.59E-04
Q91V01 (Lysophospholipid acyltransferase 5)	0.70, 2.92E-04	
P01631 (Ig kappa chain V-II region 26-10)	0.70, 3.30E-02	
Q91VA3 (Calpain-8)	0.70, 4.01E-03	
Q99MX0 (Transketolase-like protein 1)	0.70, 5.96E-03	
Q9D735 (Telomerase RNA component interacting RNase)	0.70, 1.46E-03	
Q5M8N4 (Epimerase family protein SDR39U)	0.70, 4.19E-04	
Q5M8N4-2 (Isoform 2 of Epimerase family protein SDR39U1)	0.70, 4.19E-04	
O70456 (14-3-3 protein sigma)	0.70, 2.75E-02	0.57, 1.26E-03
Q69ZP3 (Probable hydrolase PNKD)	0.70, 4.50E-03	0.69, 3.97E-03
Q69ZP3-3 (Isoform 3 of Probable hydrolase PNKD)	0.70, 4.50E-03	0.69, 3.97E-03
Q69ZP3-4 (Isoform 4 of Probable hydrolase PNKD)	0.70, 4.50E-03	0.69, 3.97E-03
Q6P6M5-2 (Isoform 2 of Peroxisomal membrane protein 11C)	0.70, 9.89E-05	
Q8C0E2-2 (Isoform 2 of Vacuolar protein sorting-associated protein 26B)	0.70, 1.78E-03	
P55772 (Ectonucleoside triphosphate diphosphohydrolase 1)	0.70, 2.88E-02	0.70, 2.86E-02
P48453 (Serine/threonine-protein phosphatase 2B catalytic subunit beta isoform)	0.70, 8.27E-03	
P48453-2 (Isoform 1 of Serine/threonine-protein phosphatase 2B catalytic subunit beta isoform)	0.70, 8.27E-03	
Q3UDW8 (Heparan-alpha-glucosaminide N-acetyltransferase)	0.69, 7.67E-07	
Q3UDW8-2 (Isoform 2 of Heparan-alpha-glucosaminide N-acetyltransferase)	0.69, 7.67E-07	
Q8BG18 (N-terminal EF-hand calcium-binding protein 1)	0.69, 1.46E-02	
Q62167 (ATP-dependent RNA helicase DDX3X)	0.69, 7.83E-03	0.64, 1.89E-03
P21300 (Aldose reductase-related protein 1)	0.69, 3.84E-02	
P54227 (Stathmin)	0.69, 1.79E-02	
Q5PR73 (GTP-binding protein Di-Ras2)	0.69, 3.33E-03	0.57, 6.52E-05
Q91Z61 (GTP-binding protein Di-Ras1)	0.69, 3.33E-03	0.57, 6.52E-05
Q91Y47 (Coagulation factor XI)	0.69, 2.40E-03	
P43136 (Nuclear receptor subfamily 2 group F member 6)	0.69, 1.14E-02	0.63, 2.69E-03
P55821 (Stathmin-2)	0.69, 1.88E-02	
O70311 (Glycylpeptide N-tetradecanoyltransferase 2)	0.69, 4.75E-04	
P97287 (Induced myeloid leukemia cell differentiation protein Mcl-1 homolog)	0.69, 1.49E-02	
Q9JHK5 (Pleckstrin)	0.69, 1.39E-03	

P36916-2 (Isoform 2 of Guanine nucleotide-binding protein-like 1)	0.69, 3.04E-02	
P35922-3 (Isoform 3 of Synaptic functional regulator FMR1)	0.69, 3.42E-03	0.66, 1.81E-03
P35922-9 (Isoform 9 of Synaptic functional regulator FMR1)	0.69, 3.42E-03	0.66, 1.81E-03
Q920L1 (Fatty acid desaturase 1)	0.68, 9.32E-03	0.70, 1.35E-02
O89086 (RNA-binding protein 3)	0.68, 2.64E-03	0.69, 2.78E-03
Q99MR1 (GRB10-interacting GYF protein 1)	0.68, 3.67E-02	
Q61464 (Zinc finger protein 638)	0.68, 4.06E-04	
Q61464-2 (Isoform 2 of Zinc finger protein 638)	0.68, 4.06E-04	
Q61464-3 (Isoform 3 of Zinc finger protein 638)	0.68, 4.06E-04	
Q61464-4 (Isoform 4 of Zinc finger protein 638)	0.68, 4.06E-04	
Q61464-5 (Isoform 5 of Zinc finger protein 638)	0.68, 4.06E-04	
Q61464-7 (Isoform 7 of Zinc finger protein 638)	0.68, 4.06E-04	
Q99J83 (Autophagy protein 5)	0.68, 1.90E-03	
Q9WV91 (Prostaglandin F2 receptor negative regulator)	0.68, 2.93E-03	
Q61474 (RNA-binding protein Musashi homolog 1)	0.68, 1.72E-05	
Q61474-2 (Isoform 2 of RNA-binding protein Musashi homolog 1)	0.68, 1.72E-05	
P12399 (Protein CTLA-2-alpha)	0.68, 3.84E-03	
Q9CYL5 (Golgi-associated plant pathogenesis-related protein 1)	0.68, 4.36E-03	
Q91WG2-2 (Isoform 3 of Rab GTPase-binding effector protein 2)	0.68, 3.40E-03	
Q8K4G1 (Latent-transforming growth factor beta-binding protein 4)	0.68, 4.03E-02	
Q8K4G1-2 (Isoform 2 of Latent-transforming growth factor beta-binding protein 4)	0.68, 4.03E-02	
Q8K4G1-3 (Isoform 3 of Latent-transforming growth factor beta-binding protein 4)	0.68, 4.03E-02	
P02463 (Collagen alpha-1(IV) chain)	0.68, 2.26E-02	
Q8C052 (Microtubule-associated protein 1S)	0.68, 5.94E-04	
Q3SXB8 (Collectin-11)	0.68, 3.63E-03	
Q3SXB8-2 (Isoform 2 of Collectin-11)	0.68, 3.63E-03	
O35988 (Syndecan-4)	0.68, 1.08E-03	0.63, 1.97E-04
Q9CQB5 (CDGSH iron-sulfur domain-containing protein 2)	0.68, 1.56E-03	
Q8BZN6-4 (Isoform 4 of Dedicator of cytokinesis protein 10)	0.68, 2.76E-02	
Q99J47 (Dehydrogenase/reductase SDR family member 7B)	0.67, 1.38E-02	

Q99J47-2 (Isoform 2 of Dehydrogenase/reductase SDR family member 7B)	0.67, 1.38E-02	
Q9CWU6 (Ubiquinol-cytochrome-c reductase complex assembly factor 1)	0.67, 9.88E-04	
Q9JHH6 (Carboxypeptidase B2)	0.67, 9.18E-03	0.65, 5.26E-03
Q9CZR2 (N-acetylated-alpha-linked acidic dipeptidase 2)	0.67, 2.28E-04	
Q810U5-2 (Isoform 2 of Coiled-coil domain-containing protein 50)	0.67, 4.20E-02	
Q64337 (Sequestosome-1)	0.67, 1.55E-03	0.67, 1.78E-03
Q6ZWY8 (Thymosin beta-10)	0.67, 1.11E-02	
P28666 (Murinoglobulin-2)	0.67, 3.30E-02	
Q64337-2 (Isoform 2 of Sequestosome-1)	0.66, 4.60E-04	0.70, 1.43E-03
Q571B6 (WASP homolog-associated protein with actin)	0.66, 1.83E-03	0.59, 1.74E-04
P28740-2 (Isoform 2 of Kinesin-like protein KIF2A)	0.66, 5.69E-03	0.69, 1.22E-02
P56542 (Deoxyribonuclease-2-alpha)	0.66, 7.41E-03	
Q6ZPR6 (Inhibitor of Bruton tyrosine kinase)	0.66, 6.62E-05	
Q6ZPR6-2 (Isoform 2 of Inhibitor of Bruton tyrosine kinase)	0.66, 6.62E-05	
Q8R121 (Protein Z-dependent protease inhibitor)	0.66, 5.20E-03	
Q8R121-2 (Isoform 2 of Protein Z-dependent protease inhibitor)	0.66, 5.20E-03	
Q9QXD8 (LIM domain-containing protein 1)	0.66, 6.66E-03	0.63, 2.93E-03
Q91YT2 (E3 ubiquitin-protein ligase RNF185)	0.66, 2.66E-02	0.56, 3.62E-03
Q91YT2-2 (Isoform 2 of E3 ubiquitin-protein ligase RNF185)	0.66, 2.66E-02	0.56, 3.62E-03
Q9DBQ7-2 (Isoform 2 of Protein-associating with the carboxyl-terminal domain of ezrin)	0.66, 2.04E-02	
Q8BIL5 (Protein Hook homolog 1)	0.66, 1.27E-02	0.62, 5.51E-03
Q8BIL5-2 (Isoform 2 of Protein Hook homolog 1)	0.66, 1.27E-02	0.62, 5.51E-03
P11835 (Integrin beta-2)	0.66, 3.07E-02	0.62, 1.39E-02
Q8CGA4 (Maturin)	0.66, 1.91E-02	
Q501J2 (Protein FAM173A)	0.66, 5.97E-03	
Q8JZV9 (3-hydroxybutyrate dehydrogenase type 2)	0.66, 7.11E-04	
Q6P6M5 (Peroxisomal membrane protein 11C)	0.66, 1.22E-04	0.69, 4.16E-04
Q61029 (Lamina-associated polypeptide 2, isoforms beta/delta/epsilon/gamma)	0.66, 1.68E-03	0.61, 3.77E-04
Q3TJ91 (Lethal(2) giant larvae protein homolog 2)	0.66, 2.61E-04	
Q60715 (Prolyl 4-hydroxylase subunit alpha-1)	0.66, 1.42E-03	
Q60715-2 (Isoform 2 of Prolyl 4-hydroxylase subunit alpha-1)	0.66, 1.42E-03	

Q9DBQ7-3 (Isoform 3 of Protein-associating with the carboxyl-terminal domain of ezrin)	0.66, 1.89E-02	
Q9DBQ7 (Protein-associating with the carboxyl-terminal domain of ezrin)	0.65, 1.90E-02	
P18654 (Ribosomal protein S6 kinase alpha-3)	0.65, 1.28E-04	
Q61029-3 (Isoform Epsilon of Lamina-associated polypeptide 2)	0.65, 1.54E-03	
O88822 (Lathosterol oxidase)	0.65, 8.23E-03	0.71, 2.59E-02
P35922 (Synaptic functional regulator FMR1)	0.65, 4.71E-03	0.63, 2.31E-03
P35922-2 (Isoform 2 of Synaptic functional regulator FMR1)	0.65, 4.71E-03	0.63, 2.31E-03
P35922-7 (Isoform 7 of Synaptic functional regulator FMR1)	0.65, 4.71E-03	0.63, 2.31E-03
P35922-8 (Isoform 8 of Synaptic functional regulator FMR1)	0.65, 4.71E-03	0.63, 2.31E-03
Q99J45 (Nuclear receptor-binding protein)	0.65, 2.17E-02	
Q9Z247 (Peptidyl-prolyl cis-trans isomerase FKBP9)	0.65, 4.60E-04	
Q9DBE0 (Cysteine sulfinic acid decarboxylase)	0.65, 2.54E-02	
Q91UZ5 (Inositol monophosphatase 2)	0.65, 1.26E-02	
Q640M1 (U3 small nucleolar RNA-associated protein 14 homolog A)	0.65, 7.63E-03	0.62, 4.48E-03
P59222 (Scavenger receptor class F member 2)	0.65, 6.67E-03	
Q0VFX2 (Cilia- and flagella-associated protein 157)	0.65, 3.03E-02	0.53, 3.35E-03
O89001 (Carboxypeptidase D)	0.64, 4.00E-03	
Q922X9 (Protein arginine N-methyltransferase 7)	0.64, 9.69E-04	0.70, 4.74E-03
Q61205 (Platelet-activating factor acetylhydrolase IB subunit gamma)	0.64, 6.05E-04	
P01837 (Ig kappa chain C region)	0.64, 3.42E-02	
Q9Z2Z9 (Glutamine--fructose-6-phosphate aminotransferase [isomerizing] 2)	0.64, 1.50E-03	
P49945 (Ferritin light chain 2)	0.64, 1.44E-02	
Q8K2F8 (Protein LSM14 homolog A)	0.64, 3.54E-04	0.56, 2.90E-05
Q9D1G2-3 (Isoform 3 of Phosphomevalonate kinase)	0.63, 4.19E-04	0.69, 2.85E-03
P29391 (Ferritin light chain 1)	0.63, 1.24E-02	
Q91X84 (CREB-regulated transcription coactivator 3)	0.63, 1.40E-02	
P70236 (Dual specificity mitogen-activated protein kinase 6)	0.63, 8.90E-03	0.59, 3.58E-03
Q8VDM6-3 (Isoform 3 of Heterogeneous nuclear ribonucleoprotein U-like protein 1)	0.63, 6.43E-03	0.52, 4.44E-04
Q8K4I3 (Rho guanine nucleotide exchange factor 6)	0.62, 5.53E-03	0.65, 9.82E-03

O54998 (Peptidyl-prolyl cis-trans isomerase FKBP7)	0.62, 1.51E-03	0.66, 4.27E-03
Q9CZS1 (Aldehyde dehydrogenase X)	0.62, 7.33E-03	
Q8CF02 (Protein FAM25C)	0.62, 3.19E-03	0.56, 6.17E-04
Q9WUA3 (ATP-dependent 6-phosphofructokinase, platelet type)	0.61, 6.53E-03	
Q9WUA3-2 (Isoform 2 of ATP-dependent 6-phosphofructokinase, platelet type)	0.61, 6.53E-03	
Q3TFQ1 (SPRY domain-containing protein 7)	0.61, 5.54E-03	0.53, 6.46E-04
Q6ZWR4-2 (Isoform 2 of Serine/threonine-protein phosphatase 2A 55 kDa regulatory subunit B beta isoform)	0.61, 2.75E-03	0.65, 7.78E-03
Q6ZWR4-3 (Isoform 3 of Serine/threonine-protein phosphatase 2A 55 kDa regulatory subunit B beta isoform)	0.61, 2.75E-03	0.65, 7.76E-03
Q6ZWR4 (Serine/threonine-protein phosphatase 2A 55 kDa regulatory subunit B beta isoform)	0.61, 2.78E-03	0.65, 7.83E-03
P48455 (Serine/threonine-protein phosphatase 2B catalytic subunit gamma isoform)	0.61, 5.93E-03	
Q8K4Q8 (Collectin-12)	0.60, 2.16E-02	0.65, 4.20E-02
Q6P9J9 (Anoctamin-6)	0.60, 2.62E-03	
Q6P9J9-2 (Isoform 2 of Anoctamin-6)	0.60, 2.62E-03	
Q08481 (Platelet endothelial cell adhesion molecule)	0.60, 3.16E-02	0.55, 1.38E-02
Q08481-2 (Isoform 2 of Platelet endothelial cell adhesion molecule)	0.60, 3.16E-02	0.55, 1.38E-02
Q08481-3 (Isoform 3 of Platelet endothelial cell adhesion molecule)	0.60, 3.16E-02	0.55, 1.38E-02
Q08481-4 (Isoform 4 of Platelet endothelial cell adhesion molecule)	0.60, 3.16E-02	0.55, 1.38E-02
Q62507 (Cochlin)	0.60, 2.11E-02	
Q80YR6 (DNA endonuclease RBBP8)	0.60, 3.49E-02	
P09528 (Ferritin heavy chain)	0.60, 6.11E-03	
O35930 (Platelet glycoprotein Ib alpha chain)	0.60, 3.13E-03	
P27545 (Ceramide synthase 1)	0.59, 2.07E-02	
Q62036 (Centrosomal protein of 131 kDa)	0.59, 2.07E-02	
Q9D454 (Uncharacterized protein CXorf49 homolog)	0.59, 2.07E-02	
Q8R5L3-2 (Isoform 2 of Vam6/Vps39-like protein)	0.59, 1.79E-04	
Q8R5L3 (Vam6/Vps39-like protein)	0.59, 1.73E-04	
Q60738 (Zinc transporter 1)	0.59, 3.16E-03	0.54, 1.11E-03
Q3U269 (Thiosulfate sulfurtransferase/rhodanese-like domain-containing protein 2)	0.58, 2.27E-04	
Q9Z0G0 (PDZ domain-containing protein GIPC1)	0.58, 1.25E-02	0.48, 1.52E-03

Q08761 (Vitamin K-dependent protein S)	0.58, 6.12E-03	
Q7TSE6 (Serine/threonine-protein kinase 38-like)	0.57, 4.26E-02	0.44, 5.16E-03
Q7TSE6-2 (Isoform 2 of Serine/threonine-protein kinase 38-like)	0.57, 4.26E-02	0.44, 5.16E-03
Q8BPB5 (EGF-containing fibulin-like extracellular matrix protein 1)	0.57, 9.35E-04	
Q8CAQ8-3 (Isoform 3 of MICOS complex subunit Mic60)	0.56, 1.15E-02	
Q9JJI6 (GPI ethanolamine phosphate transferase 3)	0.55, 6.05E-03	
Q9CQ45 (Neudesin)	0.55, 3.46E-03	
Q78IQ7 (Zinc transporter ZIP4)	0.55, 3.09E-02	
Q78IQ7-2 (Isoform 2 of Zinc transporter ZIP4)	0.55, 3.09E-02	
Q9CQ19 (Myosin regulatory light polypeptide 9)	0.55, 2.93E-02	
A2ARA8 (Integrin alpha-8)	0.55, 8.86E-03	
Q8BP99 (UPF0500 protein C1orf216 homolog)	0.55, 7.38E-03	0.55, 8.11E-03
P01633 (Ig kappa chain V19-17)	0.54, 3.57E-02	
Q61285 (ATP-binding cassette sub-family D member 2)	0.54, 2.45E-02	
Q80UG1 (Fatty acid desaturase 6)	0.53, 2.82E-02	0.46, 8.86E-03
Q80UG1-2 (Isoform 2 of Fatty acid desaturase 6)	0.53, 2.82E-02	0.46, 8.86E-03
Q80YV4 (Pantothenate kinase 4)	0.53, 3.59E-03	
Q80YV4-2 (Isoform 2 of Pantothenate kinase 4)	0.53, 3.59E-03	
Q9CR41-2 (Isoform 2 of Huntingtin-interacting protein K)	0.53, 3.17E-04	
P08905 (Lysozyme C-2)	0.53, 5.81E-04	
P17897 (Lysozyme C-1)	0.53, 5.81E-04	
Q9WVH9 (Fibulin-5)	0.53, 2.82E-02	0.55, 3.81E-02
Q3TRM8 (Hexokinase-3)	0.52, 2.53E-03	
P04942 (Ig kappa chain V-VI region NQ5-61.1.2)	0.52, 1.30E-02	
P84750 (Ig kappa chain V region Mem5 (Fragment))	0.52, 1.68E-02	
P35576 (Glucose-6-phosphatase)	0.51, 1.33E-02	
P04940 (Ig kappa chain V-VI region NQ2-17.4.1)	0.51, 8.52E-03	
P04941 (Ig kappa chain V-VI region NQ2-48.2.2)	0.51, 8.52E-03	
P04943 (Ig kappa chain V-VI region NQ6-8.3.1)	0.51, 8.52E-03	
P04944 (Ig kappa chain V-VI region NQ5-78.2.6)	0.51, 8.52E-03	
P11247 (Myeloperoxidase)	0.51, 1.79E-03	
Q62393 (Tumor protein D52)	0.51, 1.58E-02	
Q62393-2 (Isoform 2 of Tumor protein D52)	0.51, 1.58E-02	
Q62393-3 (Isoform 3 of Tumor protein D52)	0.51, 1.58E-02	

Q68FF7 (SLAIN motif-containing protein 1)	0.51, 1.92E-02	
Q68FF7-2 (Isoform 2 of SLAIN motif-containing protein 1)	0.51, 1.92E-02	
Q6DID3 (Protein SCAF8)	0.50, 2.22E-02	
P03987 (Ig gamma-3 chain C region)	0.50, 1.52E-03	
P03987-2 (Isoform 2 of Ig gamma-3 chain C region)	0.50, 1.52E-03	
Q9CQA1 (Trafficking protein particle complex subunit 5)	0.50, 4.16E-02	
P01872 (Ig mu chain C region)	0.49, 8.90E-03	
P01872-2 (Isoform 2 of Ig mu chain C region)	0.49, 8.90E-03	
Q3U0J8 (TBC1 domain family member 2B)	0.49, 6.57E-04	
Q80T19 (Hepcidin-2)	0.49, 3.71E-05	
Q9EQ21 (Hepcidin)	0.49, 3.71E-05	
P08071 (Lactotransferrin)	0.48, 1.42E-03	
Q45VN2 (Alpha-defensin 20)	0.48, 2.90E-02	0.40, 7.95E-03
P01680 (Ig kappa chain V-IV region S107B)	0.48, 5.70E-03	
Q9R0E1 (Procollagen-lysine,2-oxoglutarate 5-dioxygenase 3)	0.47, 2.28E-02	
O70333 (Cysteine-rich PDZ-binding protein)	0.47, 1.67E-04	
Q3U487-2 (Isoform 2 of E3 ubiquitin-protein ligase HECTD3)	0.47, 1.18E-03	
Q9CZW4 (Long-chain-fatty-acid--CoA ligase 3)	0.47, 2.13E-04	0.44, 9.27E-05
P01635 (Ig kappa chain V-V region K2 (Fragment))	0.46, 6.36E-03	0.47, 7.31E-03
Q8CI12 (Smoothelin-like protein 2)	0.44, 2.78E-03	
Q9R0I7 (YLP motif-containing protein 1)	0.44, 3.05E-02	0.43, 2.44E-02
A2BE28 (Ribosomal biogenesis protein LAS1L)	0.44, 5.76E-03	0.44, 5.85E-03
A2BE28-2 (Isoform 2 of Ribosomal biogenesis protein LAS1L)	0.44, 5.76E-03	0.44, 5.85E-03
P00688 (Pancreatic alpha-amylase)	0.44, 2.96E-02	
Q64362 (AKT-interacting protein)	0.44, 2.05E-03	
P10648 (Glutathione S-transferase A2)	0.43, 2.69E-03	0.52, 1.55E-02
Q9WU56 (tRNA pseudouridine synthase A)	0.42, 8.39E-03	
Q9WU56-2 (Isoform 2 of tRNA pseudouridine synthase A)	0.42, 8.39E-03	
Q9WU56-3 (Isoform 3 of tRNA pseudouridine synthase A)	0.42, 8.39E-03	
Q9WU56-4 (Isoform 4 of tRNA pseudouridine synthase A)	0.42, 8.39E-03	
Q61093 (Cytochrome b-245 heavy chain)	0.42, 3.96E-02	
G5E8P0 (Gamma-tubulin complex component 6)	0.41, 2.30E-02	
P01634 (Ig kappa chain V-V region MOPC 21)	0.41, 1.03E-02	
Q3V384 (AFG1-like ATPase)	0.40, 2.63E-02	

Q5NBX1 (Protein cordon-bleu)	0.38, 4.57E-03	
Q5NBX1-2 (Isoform 2 of Protein cordon-bleu)	0.38, 4.57E-03	
Q5NBX1-3 (Isoform 3 of Protein cordon-bleu)	0.38, 4.56E-03	
P11404 (Fatty acid-binding protein, heart)	0.36, 2.85E-02	
Q6ZPS6 (Ankyrin repeat and IBR domain-containing protein 1)	0.36, 1.73E-04	
Q6P8U6 (Pancreatic triacylglycerol lipase)	0.32, 1.15E-02	
P27005 (Protein S100-A8)	0.32, 8.05E-03	
P17892 (Pancreatic lipase-related protein 2)	0.23, 2.54E-03	
P11588 (Major urinary protein 1)		3.54, 1.58E-02
O88843 (Death domain-containing protein CRADD)		3.54,1.58E-02
Q9CRA5-2 (Isoform 2 of Golgi phosphoprotein 3)		2.33, 2.08E-04
Q8R088-3 (Isoform 3 of Golgi phosphoprotein 3-like)		2.33, 2.14E-04
Q8R088 (Golgi phosphoprotein 3-like)		2.32, 2.26E-04
Q3TZM9 (GDP-Man:Man(3)GlcNAc(2)-PP-Dol alpha-1,2-mannosyltransferase		2.17, 9.12E-03
Q3TZM9-2 (Isoform 2 of GDP-Man:Man(3)GlcNAc(2)-PP-Dol alpha-1,2-mannosyltransferase)		2.17, 9.12E-03
Q3TZM9-3 (Isoform 3 of GDP-Man:Man(3)GlcNAc(2)-PP-Dol alpha-1,2-mannosyltransferase)		2.17, 9.12E-03
Q3U2I3-2 (Isoform 2 of FTS and Hook-interacting protein)		2.09, 3.75E-02
Q3U2I3-3 (Isoform 3 of FTS and Hook-interacting protein)		2.09, 3.75E-02
Q3U2I3 (FTS and Hook-interacting protein)		2.08, 3.77E-02
Q99MZ3-5 (Isoform 5 of Carbohydrate-responsive element-binding protein)		2.05, 3.82E-03
Q8BZF8 (Phosphoglucomutase-like protein 5)		2.02, 3.57E-02
O09043 (Napsin-A)		1.90, 1.55E-04
P50446 (Keratin, type II cytoskeletal 6A)		1.89, 1.34E-02
Q9Z331 (Keratin, type II cytoskeletal 6B)		1.89, 1.34E-02
Q1HKZ5 (Mitogen-activated protein kinase 13)		1.88, 3.13E-04
O08532 (Voltage-dependent calcium channel subunit alpha-2/delta-1)		1.81, 6.26E-03
O08532-2 (Isoform 2B of Voltage-dependent calcium channel subunit alpha-2/delta-1)		1.81, 6.26E-03
O08532-3 (Isoform 2C of Voltage-dependent calcium channel subunit alpha-2/delta-1)		1.81, 6.26E-03

O08532-4 (Isoform 2D of Voltage-dependent calcium channel subunit alpha-2/delta-1)	1.81, 6.26E-03
O08532-5 (Isoform 2E of Voltage-dependent calcium channel subunit alpha-2/delta-1)	1.81, 6.26E-03
Q8BZM1 (Glomulin)	1.79, 2.31E-02
A2AFR3 (FERM and PDZ domain-containing protein 4)	1.78, 4.11E-02
Q9JMD1 (Scm-like with four MBT domains protein 1)	1.78, 8.40E-04
Q02013 (Aquaporin-1)	1.76, 2.68E-03
P26011 (Integrin beta-7)	1.75, 4.37E-03
Q6P5G6 (UBX domain-containing protein 7)	1.72, 2.18E-04
Q9R0H0-2 (Isoform 2 of Peroxisomal acyl-coenzyme A oxidase 1)	1.70, 4.60E-03
Q8QZZ7 (EKC/KEOPS complex subunit Tprkb)	1.68, 1.91E-07
Q9QUM0 (Integrin alpha-IIb)	1.67, 1.97E-02
P12787 (Cytochrome c oxidase subunit 5A, mitochondrial)	1.67, 1.14E-03
P02798 (Metallothionein-2)	1.66, 3.79E-02
Q61982 (Neurogenic locus notch homolog protein 3)	1.65, 1.11E-03
Q8C1D8 (Protein IWS1 homolog)	1.64, 8.84E-04
Q8C1D8-2 (Isoform 2 of Protein IWS1 homolog)	1.64, 8.84E-04
Q61206 (Platelet-activating factor acetylhydrolase IB subunit beta)	1.58, 9.17E-06
Q791V5 (Mitochondrial carrier homolog 2)	1.57, 6.46E-04
Q8CI61 (BAG family molecular chaperone regulator 4)	1.57, 1.70E-02
Q8BRH0 (Transmembrane and TPR repeat-containing protein 3)	1.56, 6.50E-03
P19783 (Cytochrome c oxidase subunit 4 isoform 1, mitochondrial)	1.54, 1.75E-03
Q99JY8 (Phospholipid phosphatase 3)	1.54, 1.12E-02
Q78XF5 (Oligosaccharyltransferase complex subunit OSTC)	1.53, 1.67E-05
P58466 (Carboxy-terminal domain RNA polymerase II polypeptide A small phosphatase 1)	1.52, 9.20E-04
Q3TBW2 (39S ribosomal protein L10, mitochondrial)	1.52, 6.86E-04
P62305 (Small nuclear ribonucleoprotein E)	1.52, 2.26E-05
P34928 (Apolipoprotein C-I)	1.50, 2.01E-04
Q80VR3 (Sulfotransferase 1C1)	1.49, 3.55E-02
Q09M05 (Cytosolic carboxypeptidase 4)	1.49, 2.24E-02
Q09M05-2 (Isoform 2 of Cytosolic carboxypeptidase 4)	1.49, 2.24E-02

Q09M05-3 (Isoform 3 of Cytosolic carboxypeptidase 4)	1.49, 2.24E-02
Q09M05-4 (Isoform 4 of Cytosolic carboxypeptidase 4)	1.49, 2.24E-02
Q8K561 (Otoancorin)	1.49, 2.24E-02
Q9CQ58 (Prolactin-8A9)	1.49, 2.24E-02
G5E870 (E3 ubiquitin-protein ligase TRIP12)	1.48, 2.85E-03
Q9D0J4 (ADP-ribosylation factor-like protein 2)	1.47, 2.18E-02
Q00560 (Interleukin-6 receptor subunit beta)	1.47, 1.63E-04
Q9CQ37 (Ubiquitin-conjugating enzyme E2 T)	1.46, 3.13E-04
Q9D074-4 (Isoform 4 of E3 ubiquitin-protein ligase MGRN1)	1.46, 1.69E-05
Q9JI13 (Something about silencing protein 10)	1.46, 1.11E-02
Q9JI13-2 (Isoform 2 of Something about silencing protein 10)	1.45, 1.12E-02
Q9D074-2 (Isoform 2 of E3 ubiquitin-protein ligase MGRN1)	1.45, 1.54E-05
Q9D074 (E3 ubiquitin-protein ligase MGRN1)	1.45, 1.54E-05
Q9D074-5 (Isoform 5 of E3 ubiquitin-protein ligase MGRN1)	1.45, 1.53E-05
Q9D074-3 (Isoform 3 of E3 ubiquitin-protein ligase MGRN1)	1.45, 1.51E-05
Q8CI32 (BAG family molecular chaperone regulator 5)	1.45, 1.42E-04
Q8VEK0 (Cell cycle control protein 50A)	1.44, 1.66E-03
P28843 (Dipeptidyl peptidase 4)	1.43, 9.36E-03
Q9DCC8 (Mitochondrial import receptor subunit TOM20 homolog)	1.43, 4.36E-04
Q61735 (Leukocyte surface antigen CD47)	1.42, 3.16E-03
Q61735-2 (Isoform 2 of Leukocyte surface antigen CD47)	1.42, 3.16E-03
Q8BG94 (COMM domain-containing protein 7)	0.71, 1.52E-03
Q91ZH7 (Phospholipase ABHD3)	0.71, 7.81E-03
Q91ZH7-2 (Isoform 2 of Phospholipase ABHD3)	0.71, 7.81E-03
O08807 (Peroxiredoxin-4)	0.71, 2.15E-04
Q9Z0S9 (Prenylated Rab acceptor protein 1)	0.71, 9.50E-03
O88735 (Ensconsin)	0.70, 1.30E-02
O88735-2 (Isoform 2 of Ensconsin)	0.70, 1.30E-02
Q9Z2H1 (Regulator of G-protein signaling 11)	0.70, 2.42E-02
Q9Z2H1-2 (Isoform 2 of Regulator of G-protein signaling 11)	0.70, 2.42E-02
Q8R5M8-6 (Isoform 6 of Cell adhesion molecule 1)	0.70, 2.26E-03

Q8R5M8-7 (Isoform 7 of Cell adhesion molecule 1)	0.70, 2.26E-03
Q8BYZ7 (Engulfment and cell motility protein 3)	0.70, 1.02E-02
Q60865 (Caprin-1)	0.70, 1.14E-04
P62911 (60S ribosomal protein L32)	0.70, 2.84E-03
P53995 (Anaphase-promoting complex subunit 1)	0.70, 5.89E-03
A2AWA9-2 (Isoform 2 of Rab GTPase-activating protein 1)	0.70, 9.23E-03
Q61029-2 (Isoform Delta of Lamina-associated polypeptide 2)	0.70, 1.42E-03
Q61029-4 (Isoform Gamma of Lamina-associated polypeptide 2)	0.70, 1.42E-03
Q91WE1 (Sorting nexin-15)	0.70, 3.24E-03
Q9D7N6 (39S ribosomal protein L30)	0.70, 1.65E-03
Q9CRG1 (Transmembrane 7 superfamily member 3)	0.70, 4.04E-02
Q99M73 (Keratin, type II cuticular Hb4)	0.70, 2.42E-02
Q148V7-2 (Isoform 2 of LisH domain and HEAT repeat-containing protein KIAA1468)	0.70, 1.56E-02
Q9JL99 (C-type lectin domain family 1 member B)	0.69, 1.63E-02
Q9JL99-2 (Isoform 2 of C-type lectin domain family 1 member B)	0.69, 1.63E-02
P41105 (60S ribosomal protein L28)	0.69, 6.83E-03
Q8CBG9-2 (Isoform 2 of E3 ubiquitin-protein ligase RNF170)	0.69, 2.25E-03
Q8CBG9 (E3 ubiquitin-protein ligase RNF170)	0.69, 2.25E-03
Q9WUK2 (Eukaryotic translation initiation factor 4H)	0.69, 1.89E-03
Q8BTV2-3 (Isoform 3 of Cleavage and polyadenylation specificity factor subunit 7)	0.69, 3.55E-04
Q923D5(WW domain-binding protein 11)	0.69, 3.47E-03
Q91V81 (RNA-binding protein 42)	0.69, 8.01E-03
Q91V81-2 (Isoform 2 of RNA-binding protein 42)	0.69, 8.01E-03
Q8CH72 (E3 ubiquitin-protein ligase TRIM32)	0.69, 2.24E-02
Q8BJM3 (Coiled-coil domain-containing protein R3HCC1L)	0.68, 2.17E-03
Q8BH79-3 (Isoform 3 of Anoctamin-10)	0.68, 9.48E-03
Q99JW1 (Protein ABHD17A)	0.68, 1.89E-03
Q99JW1-2 (Isoform 2 of Protein ABHD17A)	0.68, 1.89E-03
Q9QXA1 (Cysteine and histidine-rich protein 1)	0.68, 3.97E-02
Q9QXA1-2 (Isoform 2 of Cysteine and histidine-rich protein 1)	0.68, 3.97E-02

Q9QXA1-3 (Isoform 3 of Cysteine and histidine-rich protein 1)	0.68, 3.97E-02
Q6ZQM8 (UDP-glucuronosyltransferase 1-7C)	0.68, 1.58E-02
P83882 (60S ribosomal protein L36a)	0.68, 1.79E-02
P70288 (Histone deacetylase 2)	0.68, 1.13E-02
P56389 (Cytidine deaminase)	0.68, 2.60E-03
P61514 (60S ribosomal protein L37a)	0.67, 7.30E-03
Q3UFF7 (Lysophospholipase-like protein 1)	0.67, 4.11E-02
P0DOV1-2 (Isoform 2 of Interferon-activable protein 205-B)	0.67, 2.45E-03
Q8BHN1 (Gamma-taxilin)	0.67, 5.96E-03
Q8BHN1-3 (Isoform 3 of Gamma-taxilin)	0.67, 5.96E-03
Q9D0K1 (Peroxisomal membrane protein PEX13)	0.67, 1.39E-03
Q07133 (Histone H1t)	0.67, 1.40E-02
O08716 (Fatty acid-binding protein 9)	0.67, 2.87E-02
P24526 (Myelin P2 protein)	0.67, 2.87E-02
Q8K1A5 (Transmembrane protein 41B)	0.67, 4.12E-02
Q8K1A5-2 (Isoform 2 of Transmembrane protein 41B)	0.67, 4.12E-02
Q8K1A5-3 (Isoform 3 of Transmembrane protein 41B)	0.67, 4.12E-02
Q9Z2A5 (Arginyl-tRNA--protein transferase 1)	0.67, 1.69E-02
Q80YR4 (E3 ubiquitin-protein ligase ZNF598)	0.67, 2.00E-02
Q80YR4-2 (Isoform 2 of E3 ubiquitin-protein ligase ZNF598)	0.67, 2.00E-02
Q80YR4-3 (Isoform 3 of E3 ubiquitin-protein ligase ZNF598)	0.67, 2.00E-02
P43276 (Histone H1.5)	0.67, 2.45E-02
Q6IQX8 (Zinc finger protein 219)	0.67, 2.55E-02
O70443 (Guanine nucleotide-binding protein G(z) subunit alpha)	0.66, 5.29E-03
P43274 (Histone H1.4)	0.66, 8.87E-03
Q924C1 (Exportin-5)	0.66, 2.07E-02
Q8K1L5 (E3 ubiquitin-protein ligase PPP1R11)	0.66, 8.06E-04
Q61704 (Inter-alpha-trypsin inhibitor heavy chain H3)	0.66, 2.00E-02
Q8BRT1-5 (Isoform 2 of CLIP-associating protein 2)	0.66, 5.40E-03
Q8K2H1 (Periphilin-1)	0.66, 4.13E-02
Q8K2H1-2 (Isoform 2 of Periphilin-1)	0.66, 4.13E-02
Q8CGE8 (Interferon-activable protein 205-A)	0.66, 2.10E-03
O35409 (Glutamate carboxypeptidase 2)	0.65, 3.90E-03
Q8K2D3 (Enhancer of mRNA-decapping protein 3)	0.65, 9.16E-03

Q80SZ7 (Guanine nucleotide-binding protein G(I)/G(S)/G(O) subunit gamma-5)	0.64, 6.42E-03
Q3TXX3 (Protrudin)	0.64, 1.90E-03
Q3TXX3-2 (Isoform 2 of Protrudin)	0.64, 1.90E-03
Q6NXY9 (DNA-directed RNA polymerase III subunit RPC7)	0.63, 1.82E-02
P15864 (Histone H1.2)	0.63, 5.98E-04
Q9QZU9 (Ubiquitin/ISG15-conjugating enzyme E2 L6)	0.63, 9.46E-03
Q9Z2G6 (Protein sel-1 homolog 1)	0.63, 1.33E-02
Q9Z2G6-2 (Isoform 2 of Protein sel-1 homolog 1)	0.63, 1.33E-02
P07744 (Keratin, type II cytoskeletal 4)	0.62, 4.19E-02
Q9CPV3 (39S ribosomal protein L42)	0.62, 1.16E-02
P31725 (Protein S100-A9)	0.62, 4.35E-02
A2AI08 (Taperin)	0.61 2.59E-02
Q8BFS6-5 (Isoform 5 of Serine/threonine-protein phosphatase CPPED1)	0.61 1.12E-02
Q9DAS9 (Guanine nucleotide-binding protein G(I)/G(S)/G(O) subunit gamma-12)	0.61 1.16E-03
Q8C570 (mRNA export factor)	0.61 1.32E-03
Q8BRT1-6 (Isoform 3 of CLIP-associating protein 2)	0.61 4.32E-03
Q04519 (Sphingomyelin phosphodiesterase)	0.61, 2.39E-02
Q09014 (Neutrophil cytosol factor 1)	0.61, 3.80E-02
Q8BRT1 (CLIP-associating protein 2)	0.61, 1.48E-03
Q61029-3 (Isoform Epsilon of Lamina-associated polypeptide 2)	0.61, 3.42E-04
Q9ERN0 (Secretory carrier-associated membrane protein 2)	0.61, 3.13E-03
Q62018 (RNA polymerase-associated protein CTR9 homolog)	0.60, 7.64E-04
Q62018-2 (Isoform 2 of RNA polymerase-associated protein CTR9 homolog)	0.60, 7.64E-04
Q62018-3 (Isoform 3 of RNA polymerase-associated protein CTR9 homolog)	0.60, 7.64E-04
Q8R003 (Muscleblind-like protein 3)	0.60, 2.41E-02
Q00651 (Integrin alpha-4)	0.60, 3.63E-05
O88845 (A-kinase anchor protein 10)	0.59, 1.28E-03
O88845-2 (Isoform 2 of A-kinase anchor protein 10)	0.59, 1.28E-03
O88845-3 (Isoform 3 of A-kinase anchor protein 10)	0.59, 1.28E-03
Q99LW6 (YY1-associated factor 2)	0.59, 4.13E-02
Q9EST4 (Proteasome assembly chaperone 2)	0.59, 9.02E-03
Q9EST4-3 (Isoform 3 of Proteasome assembly chaperone 2)	0.59, 9.02E-03

Q9JM52 (Misshapen-like kinase 1)	0.59, 3.29E-02
Q9JM52-2 (Isoform 1 of Misshapen-like kinase 1)	0.59, 3.29E-02
Q9JM52-3 (Isoform 3 of Misshapen-like kinase 1)	0.59, 3.29E-02
Q8CD26 (Solute carrier family 35 member E1)	0.59, 2.91E-02
Q9D159 (Melanocortin-2 receptor accessory protein)	0.59, 8.81E-03
O08692 (Neutrophilic granule protein)	0.58, 1.17E-02
Q3TCJ1 (BRISC complex subunit Abraxas 2)	0.58, 4.59E-03
Q66JT0 (Wee1-like protein kinase 2)	0.57, 5.73E-03
Q8BHN1-2 (Isoform 2 of Gamma-taxilin)	0.57, 5.96E-03
O54828 (Regulator of G-protein signaling 9)	0.57, 3.54E-03
O54828-2 (Isoform 1 of Regulator of G-protein signaling 9)	0.57, 3.54E-03
O70131 (Ninjurin-1)	0.57, 3.31E-03
Q5ISE2 (mRNA decay activator protein ZFP36L3)	0.56, 1.41E-02
Q6NZF1 (Zinc finger CCCH domain-containing protein 11A)	0.56, 1.12E-03
P50543 (Protein S100-A11)	0.56, 2.43E-02
Q9QYI5 (DnaJ homolog subfamily B member 2)	0.55, 7.80E-03
Q9QYI5-1 (Isoform 2 of DnaJ homolog subfamily B member 2)	0.55, 7.80E-03
Q6P5E6 (ADP-ribosylation factor-binding protein GGA2)	0.55, 2.90E-03
O70451 (Monocarboxylate transporter 2)	0.55, 1.12E-02
Q9CYT6 (Adenylyl cyclase-associated protein 2)	0.55, 1.35E-03
Q61462 (Cytochrome b-245 light chain)	0.55, 5.27E-03
Q61462-2 (Isoform 2 of Cytochrome b-245 light chain)	0.55, 5.27E-03
P17932 (Putative 60S ribosomal protein L32')	0.54, 6.29E-04
Q80Y55 (BSD domain-containing protein 1)	0.53, 2.37E-02
Q9QXP4 (Protein downstream neighbor of Son)	0.53, 1.69E-02
Q80YA7 (Dipeptidyl peptidase 8)	0.53, 1.27E-02
Q8K2X3 (CST complex subunit STN1)	0.53, 1.13E-02
P11680 (Properdin)	0.52, 1.59E-03
Q9CQT2 (RNA-binding protein 7)	0.52, 2.57E-03
Q8VBT1 (Beta-taxilin)	0.51, 2.34E-02
Q99J23 (GH3 domain-containing protein)	0.51, 1.03E-03
P97427 (Dihydropyrimidinase-related protein 1)	0.51, 1.79E-02
Q922H9 (Zinc finger protein 330)	0.50, 1.70E-03
Q922H9-2 (Isoform 2 of Zinc finger protein 330)	0.50, 1.70E-03

O70469 (Docking protein 2)	0.49, 3.43E-03
Q0VGY8 (Protein TANC1)	0.49, 3.03E-03
Q0VGY8-2 (Isoform 2 of Protein TANC1)	0.49, 3.03E-03
Q5SSM3 (Rho GTPase-activating protein 44)	0.48, 7.94E-03
Q5SSM3-2 (Isoform 2 of Rho GTPase-activating protein 44)	0.48, 7.94E-03
Q5SSM3-3 (Isoform 3 of Rho GTPase-activating protein 44)	0.48, 7.94E-03
Q8VIM9 (Immunity-related GTPase family Q protein)	0.48, 1.02E-03
Q9D3S3 (Sorting nexin-29)	0.48, 2.37E-02
P02802 (Metallothionein-1)	0.46, 3.87E-02
Q3UQS8 (RNA-binding protein 20)	0.46, 1.77E-02
Q9Z172-2 (Isoform 2 of Small ubiquitin-related modifier 3)	0.46, 7.93E-03
Q8VCW4 (Protein unc-93 homolog B1)	0.46, 4.27E-02
Q3U1T9 (DENN domain-containing protein 1B)	0.44, 7.81E-03
Q3U1T9-2 (Isoform 2 of DENN domain-containing protein 1B)	0.44, 7.81E-03
Q3U1T9-4 (Isoform 4 of DENN domain-containing protein 1B)	0.44, 7.81E-03
P61957 (Small ubiquitin-related modifier 2)	0.44, 1.24E-02
O35445 (E3 ubiquitin-protein ligase RNF5)	0.43, 1.44E-02
Q9Z0F4 (Calcium and integrin-binding protein 1)	0.43, 4.35E-04
Q6ZWS8 (Speckle-type POZ protein)	0.41, 3.01E-02
Q717B4 (TD and POZ domain-containing protein 3)	0.41, 3.01E-02
Q8CFE5 (BTB/POZ domain-containing protein 7)	0.41, 3.01E-02
Q6YCH2 (TD and POZ domain-containing protein 4)	0.41, 3.01E-02
Q9CQ33 (Leucine-zipper-like transcriptional regulator 1)	0.41, 3.00E-02
Q5SWZ9 (Mitochondrial cardiolipin hydrolase)	0.41, 3.00E-02
Q6YCH1 (TD and POZ domain-containing protein 5)	0.41, 3.00E-02
Q8CFE5-3 (Isoform 3 of BTB/POZ domain-containing protein 7)	0.41, 2.99E-02
Q717B2 (TD and POZ domain-containing protein 2)	0.41, 2.99E-02
Q9CQ33-2 (Isoform 2 of Leucine-zipper-like transcriptional regulator 1)	0.41, 2.99E-02
Q8CFE5-2 (Isoform 2 of BTB/POZ domain-containing protein 7)	0.41, 2.99E-02
Q5SWZ9-2 (Isoform 2 of Mitochondrial cardiolipin hydrolase)	0.41, 2.99E-02
P06880 (Somatotropin)	0.39, 1.49E-02

Q91W67 (Ubiquitin-like protein 7)	0.39, 2.66E-03
Q62266 (Cornifin-A)	0.33, 4.45E-02
Q5XKN4 (Protein jagunal homolog 1)	0.33, 1.20E-02
P11672 (Neutrophil gelatinase-associated lipocalin)	0.30, 2.41E-02
P97861 (Keratin, type II cuticular Hb6)	0.30, 3.85E-02
Q6IMF0 (Keratin, type II cuticular 87)	0.30, 3.85E-02
Q9ERE2 (Keratin, type II cuticular Hb1)	0.30, 3.85E-02
Q9Z2T6 (Keratin, type II cuticular Hb5)	0.30, 3.85E-02
Q9DAF3 (Protein DDI1 homolog 1)	0.28, 2.51E-03
Q9ES46 (Beta-parvin)	0.24, 2.06E-02

Supplemental Table 2: Differentially Hepatic Abundant Proteins Altered by PCB126 and Ahr$^{-/-}$

List of hepatic proteins (Log$_2$ FC, *p*-value) altered by PCB126, Ahr$^{-/-}$ or both. Log$_2$ FC≥1 , protein upregulation; Log$_2$ FC≤ -1, protein downregulation.

Accession Number (Protein Name)	WT PCB126 vs WT Vehicle	Ahr$^{-/-}$ Vehicle vs WT Vehicle	Ahr$^{-/-}$ PCB126 vs WT PCB126
P00184 (Cytochrome P450 1A1)	4.82, 3.19E-04		-4.90, 4.66E-06
P00186 (Cytochrome P450 1A2)	4.36, 7.65E-07	1.91,4.33E-04	-6.43, 1.58E-10
O55137(Acyl-coenzyme A thioesterase 1)	2.05, 1.79E-02	2.97, 2.57E-06	
Q91X77-2 (Isoform 2 of Cytochrome P450 2C50)	1.35, 4.06E-02	-2.13, 9.02E-06	-4.07, 2.74E-09
P56395 (Cytochrome b5)	1.10, 4.29E-02		
P61967 (AP-1 complex subunit sigma-1A)	-1.15, 3.55E-02		
Q05816 (Fatty acid-binding protein 5)	-1.16, 2.67E-02	-3.80, 9.88E-11	-2.55, 3.15E-08
O55239 (Nicotinamide N-methyltransferase)	-1.19, 3.55E-02		1.30, 2.84E-04
P13745 (Glutathione S-transferase A1)		4.97,9.68E-08	5.13, 8.00E-08
Q99P91 (Transmembrane glycoprotein NMB)		4.65, 4.96E-07	4.61, 8.08E-07
Q62266 (Cornifin-A)		3.90, 3.03E-05	3.53, 1.15E-04
P19639 (Glutathione S-transferase Mu 3)		3.76, 7.63E-09	3.21, 8.00E-08
Q64459 (Cytochrome P450 3A11)		3.61, 2.33E-07	2.38, 4.83E-05
Q62267 (Cornifin-B)		3.60, 3.70E-05	3.01, 2.05E-04
Q9JHW9 (Aldehyde dehydrogenase family 1 member A3)		3.56, 4.50E-09	3.50, 8.05E-09
Q08857 (Platelet glycoprotein 4)		3.37, 1.53E-04	1.79, 2.54E-02
Q64481 (Cytochrome P450 3A16)		3.36, 3.64E-07	2.11, 1.24E-04
Q9CZS1 (Aldehyde dehydrogenase X, mitochondrial)		3.14, 1.22E-13	3.06, 2.07E-13
P24472 (Glutathione S-transferase A4)		3.06, 1.03E-08	2.17, 1.34E-06
Q9R092 (17-beta-hydroxysteroid dehydrogenase type 6)		3.02, 3.51E-08	2.24, 2.18E-06
Q9D379 (Epoxide hydrolase 1)		3.02, 6.18E-10	1.85, 6.83E-07
Q8VCR2(17-beta-hydroxysteroid dehydrogenase 13)		3.02, 2.68E-09	2.29, 1.71E-07
Q8CI94 (Glycogen phosphorylase, brain form)		3.00, 1.21E-08	2.43, 3.01E-07
P01756 (Ig heavy chain V region MOPC 104E)		2.95, 1.24E-06	2.51, 1.14E-05
P01757 (Ig heavy chain V region J558)		2.95, 1.24E-06	2.51, 1.14E-05
Q8VCR2-2 (Isoform 2 of 17-beta-hydroxysteroid dehydrogenase 13)		2.94, 1.86E-09	2.35, 5.83E-08
P01878 (Ig alpha chain C region)		2.91, 1.32E-09	2.53, 1.57E-08
Q9QYR9 (Acyl-coenzyme A thioesterase 2, mitochondrial)		2.90, 7.77E-12	1.99, 2.74E-09
Q9DBE0 (Cysteine sulfinic acid		2.81, 1.16E-07	1.94, 1.70E-05

decarboxylase)		
P43276 (Histone H1.5)	2.72, 4.49E-08	2.49, 1.82E-07
Q9DBM2 (Peroxisomal bifunctional enzyme)	2.71, 5.45E-08	1.93, 5.26E-06
P47740 (Fatty aldehyde dehydrogenase)	2.63, 1.40E-08	1.06, 8.58E-04
P06330 (Ig heavy chain V region AC38 205.12)	2.62, 6.45E-07	2.40, 2.38E-06
P01867 (Ig gamma-2B chain C region)	2.56, 4.33E-04	1.35, 4.49E-02
P01867-2 (Isoform 2 of Ig gamma-2B chain C region)	2.56, 4.33E-04	1.35, 4.49E-02
O35728 (Cytochrome P450 4A14)	2.51, 1.03E-03	
Q3TW96-2 (Isoform 2 of UDP-N-acetylhexosamine pyrophosphorylase-like protein 1)	2.50, 3.13E-07	2.18, 2.10E-06
P97315 (Cysteine and glycine-rich protein 1)	2.44, 1.89E-05	1.78, 6.16E-04
P01837 (Immunoglobulin kappa constant)	2.42, 5.99E-07	1.84, 2.30E-05
Q9D8W7 (OCIA domain-containing protein 2)	2.40, 3.27E-04	
P16045 (Galectin-1)	2.38, 1.35E-05	2.30, 2.38E-05
P18581 (Cationic amino acid transporter 2)	2.37, 3.74E-06	1.89, 6.33E-05
P18581-2 (Isoform 2 of Cationic amino acid transporter 2)	2.37, 3.74E-06	1.89, 6.33E-05
Q3TW96 (UDP-N-acetylhexosamine pyrophosphorylase-like protein 1)	2.37, 1.14E-06	2.09, 6.28E-06
P48036 (Annexin A5)	1.93, 2.05E-07	2.10, 5.83E-08
Q8VCH0 (3-ketoacyl-CoA thiolase B, peroxisomal)	2.33, 1.03E-09	1.33, 2.52E-06
P43275 (Histone H1.1)	2.33, 2.82E-06	2.51, 1.32E-06
P37804 (Transgelin)	2.30, 2.62E-04	2.00, 1.18E-03
P50543 (Protein S100-A11)	2.29, 3.13E-07	2.45, 1.70E-07
P01868 (Ig gamma-1 chain C region secreted form)	2.29, 2.16E-04	
P01869 (Ig gamma-1 chain C region, membrane-bound form)	2.29, 2.16E-04	
P11862 (Growth arrest-specific protein 2)	2.28, 2.80E-08	1.84, 6.36E-07
Q6P549 (Phosphatidylinositol 3,4,5-trisphosphate 5-phosphatase 2)	2.27, 1.23E-04	1.75, 1.67E-03
Q8R1S9 (Sodium-coupled neutral amino acid transporter 4)	2.27, 1.36E-04	1.55, 4.69E-03
P43883 (Perilipin-2)	2.24, 1.18E-03	1.97, 3.88E-03
P68433 (Histone H3.1)	2.24, 7.34E-06	2.31, 5.82E-06
P10649 (Glutathione S-transferase Mu 1)	2.23, 5.45E-08	1.66, 3.09E-06
Q9DCX8(Iodotyrosine deiodinase 1)	2.22,1.33E-03	
Q80WP8 (Acidic amino acid decarboxylase GADL1)	2.21, 1.53E-04	1.76, 1.56E-03
Q80WP8-2 (Isoform 2 of Acidic amino acid decarboxylase GADL1)	2.21,1.53E-04	1.76, 1.56E-03
O09111 (NADH dehydrogenase [ubiquinone] 1 beta subcomplex subunit 11, mitochondrial)	2.18, 3.72E-03	
P0DN34 (NADH dehydrogenase [ubiquinone] 1 beta subcomplex subunit 1)	2.18, 1.03E-03	
P28654 (Decorin)	2.15, 2.00E-03	2.06, 3.24E-03

P19783 (Cytochrome c oxidase subunit 4 isoform 1, mitochondrial)	2.15, 8.29E-03	
Q8BWN8 (Acyl-coenzyme A thioesterase 4)	2.14, 9.68E-08	1.21, 1.30E-04
P46412 (Glutathione peroxidase 3)	2.14, 2.32E-05	2.30, 1.18E-05
Q80X19 (Collagen alpha-1(XIV) chain)	2.10, 1.03E-09	1.96, 4.74E-09
Q80X19-2 (Isoform 2 of Collagen alpha-1(XIV) chain)	2.10, 1.03E-09	1.96, 4.74E-09
P16110 (Galectin-3)	2.03, 9.83E-07	2.43, 1.24E-07
Q9CR61 (NADH dehydrogenase [ubiquinone] 1 beta subcomplex subunit 7)	2.02, 1.04E-02	
Q9CQZ6 (NADH dehydrogenase [ubiquinone] 1 beta subcomplex subunit 3)	2.01, 8.77E-03	
Q9JK53 (Prolargin)	2.00, 4.77E-06	1.62, 7.05E-05
P01864 (Ig gamma-2A chain C region secreted form)	1.98, 2.84E-03	1.62, 1.31E-02
Q9DCS9 (NADH dehydrogenase [ubiquinone] 1 beta subcomplex subunit 10)	1.94, 2.18E-03	
P47934(Carnitine O-acetyltransferase)	1.92, 8.51E-06	1.61, 7.55E-05
Q8R519 (2-amino-3-carboxymuconate-6-semialdehyde decarboxylase)	1.90, 7.05E-08	2.13, 2.07E-08
Q9CPQ1 (Cytochrome c oxidase subunit 6C)	1.90, 7.16E-03	
Q9JKJ9 (24-hydroxycholesterol 7-alpha-hydroxylase)	1.89, 1.03E-05	1.87, 1.41E-05
P17665 (Cytochrome c oxidase subunit 7C, mitochondrial)	1.89, 6.72E-03	
P13011 (Acyl-CoA desaturase 2)	1.87, 3.41E-02	
Q99PL7 (Acyl-CoA desaturase 3)	1.87, 3.41E-02	
Q9QUJ7 (Long-chain-fatty-acid--CoA ligase 4)	1.87, 3.20E-05	2.12, 9.24E-06
Q9QUJ7-2 (Isoform Short of Long-chain-fatty-acid--CoA ligase 4)	1.87, 3.20E-05	2.12, 9.24E-06
Q9WUZ9 (Ectonucleoside triphosphate diphosphohydrolase 5)	1.86, 3.51E-08	1.35, 2.61E-06
Q8R1L4 (ER lumen protein-retaining receptor 3)	1.82, 1.17E-02	
Q99JH8 (ER lumen protein-retaining receptor 1)	1.82, 1.17E-02	
Q9CQM2 (ER lumen protein-retaining receptor 2)	1.82, 1.17E-02	
Q3UIU2 (NADH dehydrogenase [ubiquinone] 1 beta subcomplex subunit 6)	1.80, 7.16E-03	
Q60854 (Serpin B6)	1.78, 6.78E-07	1.62, 2.65E-06
P07356 (Annexin A2)	1.76, 1.07E-05	1.62, 3.32E-05
Q9EQQ2 (Protein YIPF5)	1.76, 7.18E-04	1.04, 3.40E-02
P97792 (Coxsackievirus and adenovirus receptor homolog)	1.76, 7.94E-04	
P97792-2 (Isoform 2 of Coxsackievirus and adenovirus receptor homolog)	1.76, 7.94E-04	
Q920L1 (Fatty acid desaturase 1)	1.75, 6.73E-05	1.59, 2.10E-04
O35423 (Serine--pyruvate aminotransferase, mitochondrial)	1.74, 6.28E-10	1.50, 5.51E-09
P12787 (Cytochrome c oxidase subunit 5A, mitochondrial)	1.73, 5.39E-04	1.11, 1.77E-02

Protein	Value 1	Value 2
O88958 (Glucosamine-6-phosphate isomerase 1)	1.73, 9.30E-09	
Q32MW3 (Acyl-coenzyme A thioesterase 10, mitochondrial)	1.71, 3.67E-07	1.56, 1.59E-06
Q9R0X4 (Acyl-coenzyme A thioesterase 9, mitochondrial)	1.71, 3.67E-07	1.56, 1.59E-06
O35423-2 (Isoform Peroxisomal of Serine--pyruvate aminotransferase, mitochondrial)	1.71, 6.28E-10	
P51885 (Lumican)	1.71, 4.26E-04	1.67, 6.47E-04
P54071 (Isocitrate dehydrogenase [NADP], mitochondrial)	1.71, 3.02E-08	1.46, 3.32E-07
P30681(High mobility group protein B2)	1.71, 1.37E-07	1.52, 8.77E-07
Q00915 (Retinol-binding protein 1)	1.71, 5.22E-06	2.14, 4.17E-07
Q9CQU3 (Protein RER1)	1.70, 3.51E-04	
Q60932 (Voltage-dependent anion-selective channel protein 1)	1.69, 3.25E-03	
Q60932-2 (Isoform Mt-VDAC1 of Voltage-dependent anion-selective channel protein 1)	1.69, 3.25E-03	
P28653 (Biglycan)	1.68, 6.85E-05	1.56, 1.83E-04
P03888 (NADH-ubiquinone oxidoreductase chain 1)	1.68, 2.94E-03	
Q8BWU8 (Ethanolamine-phosphate phospho-lyase)	1.68, 7.56E-07	1.43, 6.95E-06
P19536 (Cytochrome c oxidase subunit 5B, mitochondrial)	1.66, 3.00E-03	
Q60931 (Voltage-dependent anion-selective channel protein 3)	1.66, 3.51E-04	
Q9Z2G9 (Oxidoreductase HTATIP2)	1.65, 2.01E-05	
Q9DCP2 (Sodium-coupled neutral amino acid transporter 3)	1.64, 4.58E-05	1.56, 1.09E-04
Q8R2Q8 (Bone marrow stromal antigen 2)	1.62, 8.32E-04	1.05, 2.26E-02
P13516 (Acyl-CoA desaturase 1)	1.62, 2.87E-02	
Q3UVK0(Endoplasmic reticulum metallopeptidase 1)	1.61, 2.97E-04	
P00405(Cytochrome c oxidase subunit 2)	1.60, 1.30E-02	
P55096 (ATP-binding cassette sub-family D member 3)	1.60, 1.26E-04	
Q9JJ00 (Phospholipid scramblase 1)	1.59, 2.95E-03	
P97792-3 (Isoform 3 of Coxsackievirus and adenovirus receptor homolog)	1.59, 9.87E-03	
P11930 (Nucleoside diphosphate-linked moiety X motif 19)	1.58, 1.94E-07	1.04, 4.41E-05
Q8BIG7 (Catechol O-methyltransferase domain-containing protein 1)	1.57, 1.43E-04	1.56, 1.86E-04
Q9JLJ4 (Elongation of very long chain fatty acids protein 2)	1.57, 8.38E-04	1.34, 3.58E-03
Q9CWS0(N(G),N(G)-dimethylarginine dimethylaminohydrolase 1)	1.55, 1.35E-05	
Q61070(Etoposide-induced protein 2.4)	1.55, 8.37E-03	
Q80W54 (CAAX prenyl protease 1 homolog)	1.55, 8.63E-05	
P51855 (Glutathione synthetase)	1.55, 8.22E-10	1.42, 4.55E-09
P01863 (Ig gamma-2A chain C region, A allele)	1.54, 1.90E-03	
P01865 (Ig gamma-2A chain C region, membrane-bound form)	1.54, 1.90E-03	
P19324 (Serpin H1)	1.54, 2.21E-06	1.61, 1.44E-06

Q9Z0R9 (Fatty acid desaturase 2)	1.53, 3.52E-07	1.29, 3.58E-06
Q80YX1 (Tenascin)	1.53, 1.80E-04	1.53, 2.03E-04
Q80YX1-2 (Isoform 2 of Tenascin)	1.53, 1.80E-04	1.53, 2.03E-04
Q80YX1-3 (Isoform 3 of Tenascin)	1.53, 1.80E-04	1.53, 2.03E-04
Q80YX1-4 (Isoform 4 of Tenascin)	1.53, 1.80E-04	1.53, 2.03E-04
Q80YX1-5 (Isoform 5 of Tenascin)	1.53, 1.80E-04	1.53, 2.03E-04
Q62426 (Cystatin-B)	1.53, 1.37E-07	1.30, 1.44E-06
Q8VCH6 (Delta(24)-sterol reductase)	1.53, 3.87E-07	1.20, 1.09E-05
P06728 (Apolipoprotein A-IV)	1.51, 3.65E-06	2.22, 3.15E-08
P18608 (Non-histone chromosomal protein HMG-14)	1.50, 3.02E-04	1.26, 1.71E-03
Q8BH24 (Transmembrane 9 superfamily member 4)	1.49, 6.72E-03	
O35639 (Annexin A3)	1.48, 3.39E-04	1.21, 2.39E-03
P48758 (Carbonyl reductase [NADPH] 1)	1.48, 8.26E-08	1.18, 1.70E-06
Q8R5M8 (Cell adhesion molecule 1)	1.47, 1.03E-05	
Q8R5M8-2 (Isoform 2 of Cell adhesion molecule 1)	1.47, 1.03E-05	
Q8R5M8-3 (Isoform 3 of Cell adhesion molecule 1)	1.47, 1.03E-05	
Q8R5M8-4 (Isoform 4 of Cell adhesion molecule 1)	1.47, 1.03E-05	
Q8R5M8-5 (Isoform 5 of Cell adhesion molecule 1)	1.47, 1.03E-05	
Q8R5M8-6 (Isoform 6 of Cell adhesion molecule 1)	1.47, 1.03E-05	
Q8R5M8-7 (Isoform 7 of Cell adhesion molecule 1)	1.47, 1.03E-05	
Q60930 (Voltage-dependent anion-selective channel protein 2)	1.46, 5.62E-05	
Q03311 (Cholinesterase)	1.44, 3.72E-03	1.38, 6.13E-03
Q04447 (Creatine kinase B-type)	1.43, 1.05E-04	1.41, 1.56E-04
P18242 (Cathepsin D)	1.43, 4.08E-07	1.32, 1.44E-06
Q9Z2G9-2 (Isoform 2 of Oxidoreductase HTATIP2)	1.43, 1.04E-04	
Q99K41 (EMILIN-1)	1.42, 3.70E-06	1.22, 2.88E-05
P15626 (Glutathione S-transferase Mu 2)	1.42, 3.02E-08	
Q922Q1 (Mitochondrial amidoxime reducing component 2)	1.41, 8.27E-04	
Q6WVG3 (BTB/POZ domain-containing protein KCTD12)	1.39, 1.71E-05	1.16, 1.47E-04
P01872 (Immunoglobulin heavy constant mu)	1.39, 2.67E-04	1.51, 1.40E-04
P01872-2 (Isoform 2 of Immunoglobulin heavy constant mu)	1.39, 2.67E-04	1.51, 1.40E-04
Q64310 (Surfeit locus protein 4)	1.39, 5.25E-03	
Q9CQX2 (Cytochrome b5 type B)	1.38, 1.15E-02	
Q9CQJ8 (NADH dehydrogenase [ubiquinone] 1 beta subcomplex subunit 9)	1.38, 1.88E-02	
Q791V5 (Mitochondrial carrier homolog 2)	1.37, 2.45E-02	
P62897 (Cytochrome c, somatic)	1.37, 8.90E-05	
Q64176 (Carboxylesterase 1E)	1.37, 1.01E-03	
O35405 (Phospholipase D3)	1.37, 1.26E-04	1.30, 2.43E-04
Q9DC50 (Peroxisomal carnitine O-octanoyltransferase)	1.36, 1.85E-04	1.13, 1.29E-03
Q91WS0 (CDGSH iron-sulfur domain-containing protein 1)	1.36, 7.54E-03	
O70475 (UDP-glucose 6-dehydrogenase)	1.35, 3.49E-07	

Q64505 (Cholesterol 7-alpha-monooxygenase)	1.34, 1.84E-03	
P17095-1(Isoform HMG-Y of High mobility group protein HMG-I/HMG-Y)	1.33, 2.85E-03	1.00, 2.26E-02
Q99M07 (Cytochrome c oxidase assembly factor 5)	1.33, 1.74E-05	1.12, 1.44E-04
Q9QXD1 (Peroxisomal acyl-coenzyme A oxidase 2)	1.33, 9.58E-08	1.09, 1.44E-06
Q99P72-1 (Isoform 3 of Reticulon-4)	1.33, 2.04E-04	1.37, 1.75E-04
P97449 (Aminopeptidase N)	1.33, 2.07E-03	
P07309 (Transthyretin)	1.32, 1.53E-04	
Q80XN0 (D-beta-hydroxybutyrate dehydrogenase, mitochondrial)	1.32, 5.13E-06	
O35143 (ATPase inhibitor, mitochondrial)	1.32, 6.06E-05	
Q6GV12 (3-ketodihydrosphingosine reductase)	1.32, 3.69E-06	
P00416 (Cytochrome c oxidase subunit 3)	1.31, 2.25E-02	
P20152 (Vimentin)	1.31, 1.71E-05	1.53, 3.01E-06
Q9CQH3(NADH dehydrogenase [ubiquinone] 1 beta subcomplex subunit 5, mitochondrial)	1.31, 1.97E-02	
P56393 (Cytochrome c oxidase subunit 7B, mitochondrial)	1.31, 3.60E-02	
P49586 (Choline-phosphate cytidylyltransferase A)	1.29, 1.61E-06	1.09, 1.70E-05
P50427 (Steryl-sulfatase)	1.29, 1.23E-06	
O09117 (Synaptophysin-like protein 1)	1.28, 5.11E-03	
O09117-2(Isoform 2 of Synaptophysin-like protein 1)	1.28, 5.11E-03	
Q9DD20 (Methyltransferase-like protein 7B)	1.28, 1.71E-05	1.15, 7.29E-05
Q99P72 (Reticulon-4)	1.27, 1.29E-05	
Q9D711 (Pirin)	1.27, 9.01E-06	1.10, 5.42E-05
Q99JF8(PC4 and SFRS1-interacting protein)	1.27, 6.28E-05	
Q99JF8-2 (Isoform 2 of PC4 and SFRS1-interacting protein)	1.27, 6.28E-05	
O35945 (Aldehyde dehydrogenase, cytosolic 1)	1.26, 2.77E-06	
Q9WVA4 (Transgelin-2)	1.26, 3.84E-06	1.83, 3.69E-08
Q9WV68 (Peroxisomal 2,4-dienoyl-CoA reductase)	1.25, 2.35E-05	
P20065 (Thymosin beta-4)	1.24, 7.13E-03	1.60, 1.16E-03
P20065-2(Isoform Short of Thymosin beta-4)	1.24, 7.13E-03	1.60, 1.16E-03
Q9D7S7 (60S ribosomal protein L22-like 1)	1.23, 3.81E-04	1.50, 6.33E-05
Q9D7S7-2 (Isoform 2 of 60S ribosomal protein L22-like 1)	1.23, 3.81E-04	1.50, 6.33E-05
A2AKK5-2 (Isoform 2 of Acyl-coenzyme A amino acid N-acyltransferase 1)	1.23, 1.16E-04	1.10, 4.55E-04
P04117 (Fatty acid-binding protein, adipocyte)	1.23, 1.84E-02	1.11, 3.69E-02
Q8BGH2 (Sorting and assembly machinery component 50 homolog)	1.23, 1.04E-03	
B2RX12 (Canalicular multispecific organic anion transporter 2)	1.23, 2.65E-03	
B2RX12-2 (Isoform 2 of Canalicular multispecific organic anion transporter 2)	1.23, 2.65E-03	

Protein	Value 1	Value 2
B2RX12-3 (Isoform 3 of Canalicular multispecific organic anion transporter 2)	1.23, 2.65E-03	
Q8BW75 (Amine oxidase [flavin-containing] B)	1.22, 1.16E-05	
P61022 (Calcineurin B homologous protein 1)	1.22, 2.22E-04	1.08, 8.45E-04
Q8VCC2 (Liver carboxylesterase 1)	1.22, 8.49E-05	
Q9D6M3 (Mitochondrial glutamate carrier 1)	1.22, 1.80E-06	
Q99J47 (Dehydrogenase/reductase SDR family member 7B)	1.21, 1.18E-03	
Q99J47-2 (Isoform 2 of Dehydrogenase/reductase SDR family member 7B)	1.21, 1.18E-03	
Q14DH7-2(Isoform 2 of Acyl-CoA synthetase short-chain family member 3, mitochondrial)	1.21, 6.35E-04	
Q9QYA2(Mitochondrial import receptor subunit TOM40 homolog)	1.20, 3.39E-02	
Q8VCN5 (Cystathionine gamma-lyase)	1.20, 3.64E-07	
Q9CQ00 (Distal membrane-arm assembly complex protein 1)	1.20, 3.76E-02	
P97872 (Dimethylaniline mono-oxygenase [N-oxide-forming] 5)	1.20, 1.48E-05	
Q8VDP6 (CDP-diacylglycerol—inositol 3-phosphatidyltransferase)	1.20, 3.19E-05	1.13, 7.61E-05
Q9Z0J0 (NPC intracellular cholesterol transporter 2)	1.19, 1.24E-06	1.27, 8.08E-07
Q6ZWY8 (Thymosin beta-10)	1.19, 6.78E-04	1.54, 6.43E-05
Q99JI6 (Ras-related protein Rap-1b)	1.18, 2.67E-04	
Q811Q9 (Choline-phosphate cytidylyltransferase B)	1.18, 1.01E-04	
Q811Q9-2 (Isoform 2 of Choline-phosphate cytidylyltransferase B)	1.18, 1.01E-04	
Q8R5J9 (PRA1 family protein 3)	1.17, 3.36E-05	
Q14DH7 (Acyl-CoA synthetase short-chain family member 3, mitochondrial)	1.16, 9.24E-05	
P68510 (14-3-3 protein eta)	1.15, 3.98E-05	1.21, 3.15E-05
P13020 (Gelsolin)	1.15, 1.87E-05	
P13020-2 (Isoform 2 of Gelsolin)	1.15, 1.87E-05	
Q07133 (Histone H1t)	1.15, 5.84E-06	
P21981(Protein-glutamine gamma-glutamyltransferase 2)	1.14, 2.97E-04	1.58, 1.10E-05
Q921H9 (Cytochrome c oxidase assembly factor 7)	1.14, 4.15E-04	1.11, 6.37E-04
Q9D8V0 (Minor histocompatibility antigen H13)	1.14, 5.45E-03	
Q9D8V0-3 (Isoform 3 of Minor histocompatibility antigen H13)	1.14, 5.45E-03	
Q9D8V0-4 (Isoform 4 of Minor histocompatibility antigen H13)	1.14, 5.45E-03	
Q8BFZ9 (Erlin-2)	1.14, 1.62E-02	1.31, 7.93E-03
Q8R238 (Serine dehydratase-like)	1.14, 1.58E-04	1.06, 3.84E-04
A2AKK5 (Acyl-coenzyme A amino acid N-acyltransferase 1)	1.14, 7.34E-05	
P04919 (Band 3 anion transport protein)	1.13, 3.18E-02	
P04919-2 (Isoform 2 of Band 3 anion transport protein)	1.13, 3.18E-02	
P09803 (Cadherin-1)	1.13, 3.98E-05	1.41, 3.45E-06
Q9CQI6 (Coactosin-like protein)	1.13, 3.60E-05	1.11, 5.27E-05

B2RSH2 (Guanine nucleotide-binding protein G(i) subunit alpha-1)	1.12, 4.29E-05	
Q5XKN4 (Protein jagunal homolog 1)	1.12, 1.36E-03	
P11835 (Integrin beta-2)	1.11, 9.66E-04	1.32, 2.17E-04
Q4KML4 (Costars family protein ABRACL)	1.11, 6.07E-05	
Q91XV3 (Brain acid soluble protein 1)	1.11, 5.67E-03	1.74, 1.29E-04
Q61941 (NAD(P) transhydrogenase, mitochondrial)	1.10, 3.15E-06	
Q99P72-3 (Isoform 2 of Reticulon-4)	1.10, 8.24E-05	
Q9Z0V7 (Mitochondrial import inner membrane translocase subunit Tim17-B)	1.09, 5.47E-04	
Q8BZW8 (NHL repeat-containing protein 2)	1.09, 2.56E-03	
Q9DCR2 (AP-3 complex subunit sigma-1)	1.09, 1.97E-02	1.00, 3.49E-02
Q80XL6 (Acyl-CoA dehydrogenase family member 11)	1.09, 2.80E-06	
P48771 (Cytochrome c oxidase subunit 7A2, mitochondrial)	1.09, 2.53E-02	
Q2TPA8 (Hydroxysteroid dehydrogenase-like protein 2)	1.08, 4.78E-08	
Q3UTJ2-6 (Isoform 6 of Sorbin and SH3 domain-containing protein 2)	1.07, 1.01E-04	1.02, 1.91E-04
Q3UTJ2-7(Isoform 7 of Sorbin and SH3 domain-containing protein 2)	1.07, 1.01E-04	1.02, 1.91E-04
P58774-2 (Isoform 2 of Tropo-myosin beta chain)	1.06, 4.51E-02	
P00158 (Cytochrome b)	1.06, 4.39E-03	
P62141(Serine/threonine-protein phosphatase PP1-beta catalytic subunit)	1.06, 1.44E-03	
Q3UTJ2 (Sorbin and SH3 domain-containing protein 2)	1.06, 3.13E-07	
Q3UTJ2-2(Isoform 2 of Sorbin and SH3 domain-containing protein 2)	1.06, 3.13E-07	
Q3UTJ2-5 (Isoform 5 of Sorbin and SH3 domain-containing protein 2)	1.06, 3.13E-07	
O89053 (Coronin-1A)	1.05, 7.45E-03	
Q9JKF1 (Ras GTPase-activating-like protein IQGAP1)	1.05, 3.16E-07	1.28, 3.15E-08
P57746 (V-type proton ATPase subunit D)	1.05, 6.71E-05	
P51660 (Peroxisomal multifunctional enzyme type 2)	1.05, 6.52E-05	
Q9WVD5 (Mitochondrial ornithine transporter 1)	1.04, 2.30E-05	
P37040 (NADPH--cytochrome P450 reductase)	1.04, 1.43E-05	
Q3UTJ2-3 (Isoform 3 of Sorbin and SH3 domain-containing protein 2)	1.04, 4.30E-06	
P27661 (Histone H2AX)	1.04, 2.36E-03	1.59, 5.04E-05
P43277 (Histone H1.3)	1.03, 1.80E-03	1.00, 2.66E-03
O88456 (Calpain small subunit 1)	1.03, 5.03E-04	
Q9D7J7 (Calpain small subunit 2)	1.03, 5.03E-04	
Q9DB41 (Mitochondrial glutamate carrier 2)	1.03, 4.56E-03	
Q9DB41-2 (Isoform 2 of Mitochondrial glutamate carrier 2)	1.03, 4.56E-03	
Q61879 (Myosin-10)	1.03, 3.72E-03	
Q9CQB5 (CDGSH iron-sulfur domain-	1.03, 2.39E-03	

containing protein 2)		
P14733 (Lamin-B1)	1.02, 5.25E-08	
P26645 (Myristoylated alanine-rich C-kinase substrate)	1.01, 1.18E-03	
Q8BGG9-2 (Isoform 2 of Acyl-coenzyme A amino acid N-acyltransferase 2)	1.01, 4.70E-03	1.20, 1.41E-03
Q8BIW1 (Exopolyphosphatase PRUNE1)	1.01, 1.55E-02	
Q3UTJ2-4 (Isoform 4 of Sorbin and SH3 domain-containing protein 2)	1.01, 2.54E-06	
P45952 (Medium-chain specific acyl-CoA dehydrogenase, mitochondrial)	1.00, 3.52E-07	
Q9DCM2 (Glutathione S-transferase kappa 1)	1.00, 1.49E-06	
Q8VCM7 (Fibrinogen gamma chain)	-1.01, 2.40E-03	
P11714 (Cytochrome P450 2D9)	-1.02, 2.50E-04	-1.04, 2.43E-04
Q91WL5 (Cytochrome P450 4A12A)	-1.02, 3.77E-02	-1.83, 8.08E-04
E9PV24 (Fibrinogen alpha chain)	-1.03, 1.07E-03	
E9PV24-2 (Isoform 2 of Fibrinogen alpha chain)	-1.03, 1.07E-03	
P70266 (6-phosphofructo-2-kinase/fructose-2,6-bisphosphatase 1)	-1.05, 1.80E-05	
P70266-2 (Isoform 2 of 6-phosphofructo-2-kinase/fructose-2,6-bisphosphatase 1)	-1.07, 1.83E-05	
P81117 (Nucleobindin-2)	-1.08, 7.57E-03	
Q9ET01 (Glycogen phosphorylase, liver form)	-1.09, 7.20E-04	-1.51, 3.11E-05
Q9D5J6 (Sedoheptulokinase)	-1.10, 7.34E-04	
Q62392 (Pleckstrin homology-like domain family A member 1)	-1.10, 2.48E-04	
Q8R1H0 (Homeodomain-only protein)	-1.13, 3.85E-05	-1.00, 1.77E-04
Q9WVM8(Kynurenine/alpha-aminoadipate aminotransferase, mitochondrial)	-1.13, 3.55E-04	-1.47, 2.92E-05
Q9DBG1 (Sterol 26-hydroxylase, mitochondrial)	-1.17, 4.04E-06	-1.68, 5.24E-08
Q9CYW4 (Haloacid dehalogenase-like hydrolase domain-containing protein 3)	-1.18, 7.22E-04	
P46656 (Adrenodoxin, mitochondrial)	-1.21, 1.25E-04	-1.17, 1.99E-04
Q9D0S9 (Histidine triad nucleotide-binding protein 2, mitochondrial)	-1.22, 1.74E-05	-1.04, 1.23E-04
A6X935 (Inter alpha-trypsin inhibitor, heavy chain 4)	-1.24, 2.44E-02	
A6X935-2 (Isoform 2 of Inter alpha-trypsin inhibitor, heavy chain 4)	-1.25, 2.66E-02	
Q9CYA0 (Cysteine-rich with EGF-like domain protein 2)	-1.26, 8.93E-04	
P09813 (Apolipoprotein A-II)	-1.30, 4.81E-04	-1.19, 1.27E-03
Q7TNG8 (Probable D-lactate dehydrogenase, mitochondrial)	-1.31, 2.61E-06	
P02798 (Metallothionein-2)	-1.32, 4.88E-02	
P97328 (Ketohexokinase)	-1.32, 8.51E-06	-1.15, 5.18E-05
Q64458 (Cytochrome P450 2C29)	-1.38, 3.58E-04	-2.94, 5.37E-08
Q91WP6 (Serine protease inhibitor A3N)	-1.40, 2.35E-02	
P19096 (Fatty acid synthase)	-1.40, 2.93E-05	-1.20, 1.84E-04
Q9D2R0 (Acetoacetyl-CoA synthetase)	-1.42, 2.47E-04	-1.26, 9.54E-04
Q9QXG4 (Acetyl-coenzyme A synthetase, cytoplasmic)	-1.46, 4.11E-05	-1.37, 1.09E-04
P16301 (Phosphatidylcholine-sterol acyltransferase)	-1.49, 4.26E-03	-2.09, 2.73E-04
E9Q4Z2 (Acetyl-CoA carboxylase 2)	-1.52, 2.62E-06	

P19157(Glutathione S-transferase P1)	-1.54, 6.82E-07	-1.49, 1.44E-06
Q8K182 (Complement component C8 alpha chain)	-1.55, 9.71E-05	
P31532 (Serum amyloid A-4 protein)	-1.63, 1.71E-05	-2.04, 1.28E-06
Q8VCU1 (Carboxylesterase 3B)	-1.67, 1.49E-06	-1.53, 5.08E-06
Q5F2F2 (Protein ABHD15)	-1.67, 3.74E-02	
P06801 (NADP-dependent malic enzyme)	-1.68, 3.98E-05	-2.02, 5.46E-06
Q8VCU1-2 (Isoform 2 of Carboxylesterase 3B)	-1.69, 1.80E-06	-1.52, 7.94E-06
Q91X77 (Cytochrome P450 2C50)	-1.71, 1.80E-03	-3.49, 1.10E-06
Q920E5 (Farnesyl pyrophosphate synthase)	-1.77, 3.25E-05	-1.49, 2.49E-04
O88962(7-alpha-hydroxycholest-4-en-3-one 12-alpha-hydroxylase)	-1.78, 1.01E-04	-1.94, 5.04E-05
P04939 (Major urinary protein 3)	-1.86, 2.21E-06	-2.56, 4.05E-08
Q9EP96 (Solute carrier organic anion transporter family member 1A4)	-2.13, 1.81E-02	-3.49, 5.26E-04
Q63836 (Selenium-binding protein2)	-2.13, 2.16E-06	-2.27, 1.23E-06
P53657 (Pyruvate kinase PKLR)	-2.23, 1.94E-07	-2.53, 4.66E-08
Q91YY5(Solute carrier organic anion transporter family member 1A5)	-2.53, 6.29E-03	-3.26, 9.92E-04
Q3UY96 (Cilia- and flagella-associated protein 74)	-2.67, 1.08E-07	-2.19, 1.68E-06
Q3UY96-2 (Isoform 2 of Cilia- and flagella-associated protein 74)	-2.67, 1.08E-07	-2.19, 1.68E-06
P15105 (Glutamine synthetase)	-2.74, 3.04E-10	-2.79, 2.24E-10
Q60590 (Alpha-1-acid glycoprotein 1)	-2.84, 3.86E-03	
Q9QXZ6 (Solute carrier organic anion transporter family member 1A1)	-2.85, 1.38E-04	-4.71, 4.76E-07
Q6XVG2 (Cytochrome P450 2C54)	-2.89, 2.53E-04	-5.03, 5.63E-07
Q60991(25-hydroxycholesterol 7-alpha-hydroxylase)	-3.77, 1.16E-07	-3.44, 5.88E-07
P11589 (Major urinary protein 2)	-3.79, 4.73E-07	-4.29, 1.29E-07
Q61694 (3 beta-hydroxysteroid dehydrogenase type 5)	-4.28, 9.00E-12	-4.59, 3.47E-12
Q62264 (Thyroid hormone-inducible hepatic protein)	-4.45, 3.13E-07	-2.67, 1.68E-04
B5X0G2 (Major urinary protein 17)	-5.00, 9.68E-08	-6.01, 1.03E-08
P11588 (Major urinary protein 1)	-5.58, 1.03E-09	-6.46, 1.71E-10
P48962 (ADP/ATP translocase 1)		2.27, 3.88E-02
P14602 (Heat shock protein beta-1)		2.06, 2.56E-03
P14602-2 (Isoform B of Heat shock protein beta-1)		2.06, 2.56E-03
P14602-3 (Isoform C of Heat shock protein beta-1)		2.06, 2.56E-03
P31001 (Desmin)		1.62, 2.08E-02
P05064 (Fructose-bisphosphate aldolase A)		1.54, 4.68E-02
P14069 (Protein S100-A6)		1.46, 1.35E-02
Q7TPW1 (Nexilin)		2.13, 4.53E-04
Q61029 (Lamina-associated polypeptide 2, isoforms beta/delta/epsilon/gamma)		1.05, 2.35E-03
Q61029-3 (Isoform Epsilon of Lamina-associated polypeptide 2,isoforms beta/delta/epsilon/gamma)		1.05, 2.35E-03
P70429 (Ena/VASP-like protein)		1.76, 2.30E-05
P70429-2 (Isoform 1 of Ena/VASP-like protein)		1.76, 2.30E-05

Q6TEK5 (Vitamin K epoxide reductase complex subunit 1-like protein 1)	1.01, 3.99E-02
P52480-2 (Isoform M1 of Pyruvate kinase PKM)	1.03, 3.62E-02
P10107 (Annexin A1)	1.28, 8.84E-05
P63254 (Cysteine-rich protein 1)	1.12, 1.11E-02
P45376 (Aldose reductase)	1.04, 3.60E-04
Q9QWG7 (Sulfotransferase family cytosolic 1B member 1)	-1.45, 2.99E-05
Q9QWG7-2 (Isoform 2 of Sulfotransferase family cytosolic 1B member 1)	-1.45, 2.99E-05
Q80ST9 (Lebercilin)	-1.08, 3.56E-03
Q80ST9-2 (Isoform 2 of Lebercilin)	-1.08, 3.56E-03
Q9DBT9 (Dimethylglycine dehydrogenase, mitochondrial)	-1.28, 4.04E-07
Q91WG0 (Acylcarnitine hydrolase)	-2.45, 2.18E-05
P07759 (Serine protease inhibitor A3K)	-1.02, 5.08E-06
Q91VA0-2 (Isoform 2 of Acyl-coenzyme A synthetase ACSM1, mitochondrial)	-1.06, 1.28E-06
P43006 (Excitatory amino acid transporter 2)	-1.78, 1.22E-04
P43006-2 (Isoform Glt-1A of Excitatory amino acid transporter 2)	-1.78, 1.22E-04
P43006-3 (Isoform Glt-1B of Excitatory amino acid transporter 2)	-1.78, 1.22E-04
O35400 (Sulfotransferase family cytosolic 2B member 1)	-1.19, 1.88E-04
O35400-2 (Isoform 2 of Sulfotransferase family cytosolic 2B member 1)	-1.19, 1.88E-04
Q91VA0 (Acyl-coenzyme A synthetase ACSM1, mitochondrial)	-1.07, 1.15E-06
P50236 (Bile salt sulfotransferase 2)	-2.61, 2.48E-03
P52843 (Bile salt sulfotransferase 1)	-2.61, 2.48E-03
P49710 (Hematopoietic lineage cell-specific protein)	2.17, 2.05E-04
Q8VBT2 (L-serine dehydratase/L-threonine deaminase)	1.36, 1.89E-05
Q07797 (Galectin-3-binding protein)	1.29, 7.71E-04
P29699 (Alpha-2-HS-glycoprotein)	1.21, 1.05E-04
O89086 (RNA-binding protein 3)	1.20, 2.03E-04
Q6IME9 (Keratin, type II cytoskeletal 72)	1.15, 1.99E-03
P05201 (Aspartate amino-transferase, cytoplasmic)	1.14, 2.40E-05
P28798 (Granulins)	1.13, 2.57E-03
P11688 (Integrin alpha-5)	1.12, 1.76E-03
Q64339 (Ubiquitin-like protein ISG15)	1.11, 1.28E-02
Q9CQU0(Thioredoxin domain-containing protein 12)	1.11, 1.71E-03
Q9CR51 (V-type proton ATPase subunit G 1)	1.11, 6.36E-05
Q6IRU2 (Tropomyosin alpha-4 chain)	1.10, 3.88E-05
Q99M73 (Keratin, type II cuticular Hb4)	1.08, 5.47E-04
Q8BGG9 (Acyl-coenzyme A amino acid N acyltransferase 2)	1.07, 1.58E-03
Q8VDD5 (Myosin-9)	1.06, 1.96E-04
P10605 (Cathepsin B)	1.05, 8.08E-07
O55111 (Desmoglein-2)	1.04, 6.63E-03
Q9D020 (Cytosolic 5'-nucleotidase 3A)	1.04, 3.45E-06
Q9D020-1 (Isoform 1 of Cytosolic 5'-	1.04, 3.45E-06

nucleotidase 3A)	
Q6P069 (Sorcin)	1.04, 7.19E-04
Q6P069-2 (Isoform 2 of Sorcin)	1.04, 7.19E-04
P15864 (Histone H1.2)	1.03, 3.45E-05
Q9WTM5 (RuvB-like 2)	1.03, 3.22E-02
Q7TMM9 (Tubulin beta-2A chain)	1.03, 1.09E-02
Q8R0W0 (Epiplakin)	1.03, 5.73E-04
P61226 (Ras-related protein Rap-2b)	1.02, 2.24E-03
P25688 (Uricase)	1.00, 1.47E-04
Q9R013 (Cathepsin F)	-1.01, 2.32E-03
P52430 (Serum paraoxonase/arylesterase 1)	-1.02, 2.05E-04
Q8BFP9 ([Pyruvate dehydrogenase (acetyl-transferring)] kinase isozyme 1, mitochondrial)	-1.02, 1.16E-04
Q64374 (Regucalcin)	-1.03, 5.46E-05
P50431 (Serine hydroxy-methyltransferase, cytosolic)	-1.04, 4.63E-06
Q8JZZ0 (UDP-glucurono-syltransferase 3A2)	-1.06, 4.96E-04
Q3UJU9 (Regulator of microtubule dynamics protein 3)	-1.07, 2.30E-05
Q63886 (UDP-glucuronosyltransferase 1-1)	-1.07, 1.40E-04
O88587 (Catechol O-methyl-transferase)	-1.09, 2.88E-05
O88587-2 (Isoform Soluble of Catechol O-methyltransferase)	-1.09, 2.88E-05
Q9D6Y9 (1,4-alpha-glucan-branching enzyme)	-1.10, 2.23E-05
Q8BSE0 (Regulator of microtubule dynamics protein 2)	-1.11, 8.69E-05
Q91W52 (Transmembrane protein 19)	-1.12, 4.70E-03
Q91W52-2(Isoform 2 of Transmembrane protein 19)	-1.12, 4.70E-03
O08756 (3-hydroxyacyl-CoA dehydrogenase type-2)	-1.12, 2.77E-07
Q05421 (Cytochrome P450 2E1)	-1.26, 1.25E-04
P20852 (Cytochrome P450 2A5)	-1.36, 9.97E-03
E9Q816 (Cytochrome P450 2W1)	-1.37, 7.17E-04

Supplemental Table 3: Summary of effects of PCB exposures on liver, and blood biomarkers in chronic PCB exposure study.

Target	Effects		Aroclor1260	PCB126	Ar1260/PCB126
Liver	Cytochrome P450s induction	Cyp 1a2	↔	↑	↑*
		Cyp 2b10	↑↑	↔	↑
		Cyp 3a11	↑	↔	↑
	Steatosis		↑↑	↑	↑
	Injury		↑	↔	↔
	Lipid uptake gene mRNA levels		↑	↑	↑
	Fatty acid β-oxidation gene mRNA levels		↔	?	?
	Fatty acid synthesis gene mRNA levels		↔	↓	↓
	Inflammation		↑↑	↔	↔
Blood	Insulin		↔	↔	↔
	Triglycerides		↔	↓	↓

Notes:

1. ↔ indicates no change; ↑ indicates increase; ↓ indicates decrease *versus* vehicle control;

2. * indicates interaction between Aroclor 1260 and PCB 126.

Supplemental Table 4: Summary of effects of PCB exposure and Ahr^{-/-} on liver, and blood biomarkers in acute AhR knockout study

Target	Effects		WT PCB126	Ahr^{-/-} Vehicle	Ahr^{-/-} PCB126
Liver	Cytochrome P450s induction	Cyp 1a1	↑	↓	↓*
		Cyp 1a2	↑	↓	↓*
		Cyp 2b10	↔	↑	↑
		Cyp 3a11	↔	↑	↑
	Steatosis		↑	↑↑↑	↑↑↑
	Injury		↔	↑↑	↑↑
	Lipid uptake gene mRNA levels		↔	↑	↑
	Lipolytic gene mRNA levels		↔	↓	↓
	Hepatic triglycerides		↔	↑	↑
	Hepatic FFA		↔	↑	↑
Blood	Glucose		↔	↓	↓
	Triglycerides		↔	↔	↔
	Cholesterol		↔	↓	↓

Notes:

1. ↔ indicates no change; ↑ indicates increase; ↓ indicates decrease *versus* vehicle control;

2. * indicates interaction between PCB126 and Ahr^{-/-}.

ABBREVIATIONS

ACHS   Anniston Community Health Survey

AhR   Aryl hydrocarbon receptor

AK3L1   Adenylate kinase isoenzyme

Alb   Albumin

ALT   Alanine aminotransferase

AML1   Acute myeloid leukemia 1

ANOVA   Analysis variation

ASL   Angiosarcoma of the liver

AST   Aspartate aminotransferase

ATF4   Activating transcription factor 4

BMI   Body mass index

BW   Body weight

CAR   Constitutive androstane receptor

Cd68   Cluster of differentiation 68

c-FOS   Cellular oncogene FOS

CREB	CAMP responsive element binding protein 1
CYP	Cytochrome P450
DCE	Dichloroethylene
EPA	Environment Protection Agency
ER	Endoplasmic reticulum
FASN	Fatty acid synthase
FFA	Free fatty acid
GCK	Glucokinase
GLUT4	Glucose transporter 4
GSK3b	Glycogen synthase kinase 3b
H&E	Hematoxylin and eosin
HCC	Hepatocellular carcinoma
HFD	High-fat diet
IHC	Immunohistochemistry
KEAP1	Kelch-like ECH-associated protein 1
LC3	Light chain 3
LFD	Low-fat control
LIX	Lipopolysaccharide-induced CXC chemokine

MDA	Malondialdehyde
NAFLD	Non-alcoholic fatty liver disease
NASH	Non-alcoholic steatohepatitis
NEFA	Non-essential fatty acid
Nrf2	Nuclear factor-like 2
OCRs	Oxygen consumption rates
OGTT	Glucose tolerance test
ORO	Oil Red-O
OSHA	Occupational Safety and Health Association
p62	Sequestosome 1
PAI-1	Plasminogen activator inhibitor 1
PAS	Periodic Acid-Schiff
PCK1	Phosphoenolpyruvate carboxykinase 1
PINK1	PTEN-induced kinase 1
PPARγ	Peroxisome proliferated-activated receptor γ
Ppm	Parts per million
ROS	Reactive oxygen species
SREBP-1c	Sterol regulatory element-binding protein-1c
TASH	Toxicant-associated steatohepatitis

TBARS   Thiobarbituric acid reactive substances

TCE   Trichloroethene

TG   Triglyceride

TNF-α   Tumor necrosis factor-α

CURRICULUM VITAE

Jian Jin

505 South Hancock Street

Louisville, KY 40202

Phone: 502-654-3415

Email: j0jin005@louisville.edu

Education

07/2006	M.D. in Clinical Medicine	
	Wenzhou Medical University, China	
11/2020	Ph.D. in Pharmacology and Toxicology	
	University of Louisville, Louisville, KY	

Publications

1. **Jin J**, et al., AhR activation plays a pivotal role in PCB-induced Steatosis (in preparation)

2. **Jin J**, Wahlang B, Shi H, Hardesty JE, Falkner KC, Head KZ, Srivastava S, Merchant ML, Rai SN, Cave MC, Prough RA. Dioxin-like and non-dioxin-like PCBs differentially regulate the hepatic proteome and modify diet-induced nonalcoholic fatty liver disease severity. Medicinal Chemistry Research. 2020;29(7):1247-63. doi: 10.1007/s00044-020-02581-w.

3. Shi H, **Jin J**, Hardesty JE, Falkner KC, Prough RA, Balamurugan AN, Mokshagundam SP, Chari ST, Cave MC. Polychlorinated biphenyl exposures differentially regulate hepatic metabolism and pancreatic function: Implications for nonalcoholic steatohepatitis and diabetes. Toxicology and applied pharmacology. 2019;363:22-33. Epub 2018/10/13. doi: 10.1016/j.taap.2018.10.011. PubMed PMID: 30312631. (First Co-author)

4. Wahlang B, **Jin J**, Hardesty JE, Head KZ, Shi H, Falkner KC, Prough RA, Klinge CM, Cave MC. Identifying sex differences arising from polychlorinated biphenyl exposures in toxicant-associated liver disease. Food and chemical toxicology : an international journal published for the British Industrial Biological Research Association. 2019;129:64-76. Epub 2019/04/27. doi: 10.1016/j.fct.2019.04.007. PubMed PMID: 31026535.

5. Wahlang B, **Jin J**, Beier J, Hardesty J, Daly E, Schnegelberger R, Falkner K, Prough R, Kirpich I, Cave M. Mechanisms of Environmental Contributions to Fatty Liver Disease. Current Environmental Health Reports. 2019;6. doi: 10.1007/s40572-019-00232-w.

6. Hardesty JE, Wahlang B, Falkner KC, Shi H, **Jin J**, Zhou Y, Wilkey DW, Merchant ML, Watson CT, Feng W, Morris AJ, Hennig B, Prough RA, Cave MC. Proteomic Analysis Reveals Novel Mechanisms by Which Polychlorinated Biphenyls Compromise the Liver Promoting Diet-Induced Steatohepatitis. Journal of proteome research. 2019;18(4):1582-94. Epub 2019/02/27. doi: 10.1021/acs.jproteome.8b00886. PubMed PMID: 30807179.

7. Hardesty JE, Wahlang B, Falkner KC, Shi H, **Jin J,** Wilkey D, Merchant M, Watson C, Prough RA, Cave MC. Hepatic signalling disruption by pollutant Polychlorinated biphenyls in steatohepatitis. Cellular signalling. 2019;53:132-9. Epub 2018/10/10. doi: 10.1016/j.cellsig.2018.10.004. PubMed PMID: 30300668; PMCID: PMC6289731.

8. Hardesty JE, Al-Eryani L, Wahlang B, Falkner KC, Shi H, **Jin J**, Vivace BJ, Ceresa BP, Prough RA, Cave MC. Epidermal Growth Factor Receptor Signaling Disruption by Endocrine and Metabolic Disrupting Chemicals. Toxicological sciences : an official journal of the Society of Toxicology. 2018;162(2):622-34. Epub 2018/01/13. doi: 10.1093/toxsci/kfy004. PubMed PMID: 29329451; PMCID: PMC5888991.